INHIBITION OF THE MITOCHONDRIAL CALCIUM UNIPORTER COMPLEX (MCU$_{CX}$) AS A NEUROPROTECTIVE STRATEGY FOR ISCHEMIC STROKE

by

Robyn Julia Novorolsky

Submitted in partial fulfillment of the requirements
for the degree of Doctor of Philosophy

at

Dalhousie University
Halifax, Nova Scotia
July, 2023

Dalhousie University is located in Mi'kma'ki, the
ancestral and unceded territory of the Mi'kmaq.
We are all Treaty people.

Dedicated to my family, for fostering my curiosity and always
believing in me.
My childhood self would have never thought I could be a scientist,
but you did, and because of that,
this is for you.

Table of Contents

List of Tables

List of Figures

Abstract

Ischemic stroke, typically caused by a clot that blocks a major cerebral artery, is a leading cause of death and disability. Despite intense effort, a viable protective strategy has yet to emerge. Mitochondrial dysfunction, resulting in metabolic collapse and the initiation of numerous cell death pathways, is considered to play a pivotal role in ischemic brain injury. Ischemia deprives mitochondria of oxygen and glucose necessary to manufacture adenosine triphosphate that fuels ion pumping. This causes a massive rise of cytosolic calcium (Ca^{2+}) levels that triggers toxic mitochondrial Ca^{2+} overloading. The mitochondrial Ca^{2+} uniporter complex (MCU_{cx}) mediates high-capacity mitochondrial Ca^{2+} uptake responsible for ischemic cell death. This thesis therefore examined the protective effects of the MCU_{cx} inhibitor Ru265 in models of ischemic stroke. Ru265 protected cortical neuron and astrocyte cultures from death by a lethal period of oxygen-glucose deprivation (OGD). In cortical neuron cultures, this was accompanied by preserved mitochondrial respiration and the prevention of changes in MCU_{cx} subunit expression. Ru265 also elevated anti-inflammatory cytokine mRNA levels in astrocyte cultures and suppressed lipopolysaccharide-induced pro-inflammatory cytokine mRNA expression in astrocyte and endothelial cell cultures. In mice subjected to hypoxic/ischemic (HI) brain injury, intraperitoneal injection of Ru265 (3 mg/kg) reduced sensorimotor deficits and infarct volumes. However, Ru265 (10 and 30 mg/kg) produced convulsions by a non-MCU_{cx} mechanism, perhaps involving P/Q-type Ca^{2+} channel inhibition. To reduce the pro-convulsant effects of Ru265, two strategies were tested. The first employed structural analogues of Ru265 termed Os245 and Os245'. Although these compounds preserved cell viability and mitochondrial function in the OGD model, they still caused convulsions. The second strategy utilized the phosphodiesterase 2A inhibitor PF-05180999 to oppose mitochondrial Ca^{2+} overloading by increasing mitochondrial Ca^{2+} extrusion. Combining low concentrations of Ru265 and PF-05180999 that by themselves are not neuroprotective, synergistically protected and markedly preserved mitochondrial respiration in cortical neuron cultures subjected to a lethal period of OGD. Alternative strategies to further improve the safety and efficacy of Ru265 are also discussed. These findings support the strong neuroprotective potential of Ru265 for ischemic stroke and provide methods by which to improve the safety of this promising MCU_{cx} inhibitor.

List of Abbreviations and Symbols Used

AAV	Adeno-associated virus
ATCC	American tissue culture collection
ATP	Adenosine triphosphate
BBB	Blood rain barrier
BSA	Bovine serum albumin
CBF	Cerebral blood flow
Ca^{2+}	Calcium
cAMP	Cyclic adenosine monophosphate
CCAC	Canadian council on animal care
CCL2	Chemokine ligand 2
cDNA	Complementary deoxyribonucleic acid
cm	centimetre
CNS	Central nervous system
CO_2	Carbon dioxide
DALY	Disability adjusted life years
DAMP	Damage associated nuclear patterns
DIV	days *in vitro*
DMEM	Dulbecos modified eagle's medium
DMEM:F12	Dulbecos modified eagle's medium/Nutrient mixture F-12
DMSO	Dimethyl sulfoxide
DNA	Deoxyribonucleic acid
DRP1	Dynamin-related protein 1
EC_{50}	Half maximal effective concentration
ECAR	Extracellular acidification rate
ECGS	Endothelial growth supplement
EMRE	Essential MCU_{cx} regulator
ETC	Electron transport chain
FBS	Fetal bovine serum

FCCP	carbonyl cyanide – 4 – (trifluoromethoxy) - phenylhydrazone
g	grams
GAPDH	Glyceraldehyde-3-phosphate dehydrogenase
GBSS	Glucose-free balanced salt solution
H_2O	Water
HBSS	Hank's balanced salt solution
HBEC-5i	Human brain endothelial cells
HEK293	Human embryonic kidney cells
HI	Hypoxic/Ischemia
HPRT1	Hypoxanthine phosphoribosyltransferase 1
hr	Hours
Hu	Human
IC_{50}	Half maximal inhibitory concentration
ICa	Presynaptic voltage-gated calcium current
ICAM-1	Intercellular adhesion molecule 1
ICP-MS	Inductively coupled plasma mass spectrometry
IL-1β	Interleukin 1 beta
IL-6	Interleukin 6
IL-8	Interleukin 8
IL-10	Interleukin 10
i.p.	Intraperitoneal
K^+	Potassium
kg	Kilogram
k_{obs}	Observed rate constant
L	Litre
LDH	Lactate dehydrogenase
Li^+	Lithium
LPS	Lipopolysaccharide
MCAO	Middle cerebral artery occlusion
MCU	Mitochondrial calcium uniporter subunit
MCUb	MCU_{cx} dominant-negative beta subunit

MCU_{cx}	Mitochondrial calcium uniporter complex
$MCU^{fl/fl}$	MCU-floxed
MCUR1	MCU_{cx} regulator subunit
mg	Milligrams
MICU1	Mitochondrial calcium uptake 1
MICU2	Mitochondrial calcium uptake 2
MICU3	Mitochondrial calcium uptake 3
min	Minutes
ml	Millilitres
mm	Millimetres
mM	Milimolar
mPTP	Mitochondria permeability transition pore
mRNA	Messenger ribonucleic acid
MTT	3-(4,5-dimethylthiazol-2-yl)-2,5-diphenyltetrazolium bromide
Mu	Mouse
mV	milivolts
n	Number of samples
Na^+	Sodium
NADH	Nicotinamide adenine dinucleotide
NCX	Mitochondrial sodium/calcium exchanger
NCLX	Mitochondrial sodium/calcium/lithium exchanger
Ndufs2	NADH dehydrogenase [ubiquinone] iron-sulfur protein 2
NF-κB	Nuclear factor-kappa-B
ng	Nanograms
NLRP3	Nucleotide-binding domain, leucine-rich–containing family, pyrin domain–containing-3
nm	Nanometers
nM	Nanomolar
NMDA	N-methyl-D-aspartate
NVU	Neurovascular unit
OCR	Oxygen consumption rate

OCT3	Organic cation transporter 3
OGD	Oxygen-glucose deprivation
Oligo	Oligomycin
Os	Osmium
Os245	Osmium 245
Os245'	Osmium 245 prime
OsOAd	Osmium adamantane analogue
PBS	Phosphate buffered saline
PDE	Phosphodiesterase
PDE2A	Phosphodiesterase 2A
PDL	Poly-D-lysine hydrobromide
PINK1	PTEN-induced putative kinase 1
PKA	Protein kinase A
POLR2F	RNA polymerase II, I And III subunit F
RIPA	radioimmunoprecipitation assay
RNA	Ribonucleic acid
ROS	Reactive oxygen species
Rot	Rotenone
rpm	Revolutions per minute
RT-qPCR	Reverse transcription quantitate polymerase chain reaction
Ru	Ruthenium
Ru265	Ruthenium 265
Ru360	Ruthenium 360
RuOAd	Ruthenium adamantane analogue
RuRed	Ruthenium Red
SD	Standard deviation
sec	Seconds
SEM	Standard error of mean
siRNA	Small interfering RNA
SRC	Spare respiratory capacity
TGFβ	Transforming growth factor beta

TLR4	Toll 4-like receptor
TNFα	Tumor necrosis factor alpha
t-PA	Tissue plasma activator
TrpLe™	Trypsin solution
TTC	2,3,5-triphenyltetrazolium chloride
UCLA	University committee on laboratory animals
µg	Micrograms
µl	Microlitres
µm	Micrometers
µM	Micromolar
Uqcrc2	Cytochrome b-c1 complex subunit 2
VCAM-1	Vascular cell adhesion molecule 1
VDAC	Voltage dependant anion channel
WT	Wild Type
xg	Relative centrifugal force
α	Alpha
~	Approximately
β	Beta
β-Actin	Beta-actin
°C	Degrees Celsius
>	Greater than
<	Less than
$\Delta\Psi_m$	Mitochondrial membrane potential
$\Delta\Delta$Cq	Delta delta quantification cycle
%	Percent
±	Plus-minus

Acknowledgements

After five years I think I could write an acknowledgements section that would rival the length of this thesis, but sadly I don't have the space, so I'll try my best to be concise. First and foremost, thank you to my supervisor, Dr. George Robertson. George, it has been such a joy to work with you these past five years, and I can't thank you enough for taking me on as a student. Your steadfast commitment to your work and your students is inspiring, especially throughout the uncertainty of the last few years. I have learned so much about research, science, and myself, and will be forever grateful for your guidance, mentorship, and how much you care. Thank you to all the past members of the lab, especially Arul, Aurelio, and Scott, for your support and friendships, and being so welcoming when I first started. Elizabeth, I can't thank you enough for teaching me just about everything I know. I often found myself saying 'what would Elizabeth do' whenever I had a problem in need of solving. Jude, I'm very grateful for all your support and everything you do behind the scenes to keep the lab running. Gabriel, thank you for all your help and support and making the final stretch of my thesis so much easier.

Thank you to my committee members, Dr. Denis Dupré and Dr. Matthew Herder, for their great advice and creating such a comfortable environment for me to share my progress with them. Thank you to Justin Wilson, and Josh and Nick from the Wilson Lab, for your collaborations and sending me all the compounds I could ever need. A special thank you to my examining committee, Dr. Sean Cregan, Dr. John Frampton, and Dr. Jim Fawcett for agreeing to be part of this process and taking the time to read my thesis.

Prachi, Bella, Basmah, Nick, Kaitlyn, Adam, and Gracious, first off and most importantly, thank you all for your friendship and encouragement, especially during the final stages of this thesis. Prachi, Bella, and Basmah, your enthusiasm and eagerness to learn has been contagious and has kept me going. Basmah especially, thank you for reading so many early drafts of this thesis and for figuring out how to add citations into EndNote for me. Nick, thank you for your easy nature and being so quick to learn things. It was always a good day if you were around to chat with. Kaitlyn, thank you for being such a great sounding board and for always getting it. Adam, you never fail to make me smile in the best possible way. Thank you for reading my books and talking to me about them. Gracious, I don't have the space to thank you for everything I need to so I won't even try, but arguably the most valuable thing to come from this degree is you in my life. It has been so reassuring to know I can always trust and rely on you, and like it or not, you're one of my forever friends now, so you're stuck with me!

Finally, a HUGE thank you to all my family and friends outside of the science world, I'm sure you all know way more about mitochondria than you ever though you would! Hopefully you kept reading past the title page to see these thanks because you were all so integral to me getting through this degree. Nicole and Nicole, thank you for being my constant cheerleaders and always knowing when to send the perfect message to make me smile or provide words of encouragement. Lizzy, there are so many things to thank you for, but ultimately, thank you for your forever friendship, for being able to read my mind, and for knowing me better than I know myself sometimes. Catherine, thank you for always lending an ear to listen to me ramble on about anything and always providing excellent opinions and perspective. Mom and Dad, thank you for everything. I would not have been able to do any of this without your unconditional love and support. Your unwavering belief in me has let me believe in myself. It's so much easier to jump into something when I know you think I'll succeed, but will still be there if I stumble.

Chapter 1: Introduction

Portions of this thesis appear in the following papers:

Novorolsky, R.J., Nichols, M., Kim, J.S., Pavlov, E.V., Woods, J.J., Wilson, J.J., & Robertson, G.S. (2020). The cell-permeable mitochondrial calcium uniporter inhibitor Ru265 preserves cortical neuron respiration after lethal oxygen glucose deprivation and reduces hypoxic/ischemic brain injury. *J Cereb Blood Flow Metab*, 40(6), 1172-1181. https://doi.org/10.1177/0271678X20908523

Woods, J.J., Novorolsky, R.J., Bigham, N.P., Robertson, G.S., & Wilson, J.J. (2023). Dinuclear nitrido-bridged osmium complexes inhibit the mitochondrial calcium uniporter and protect cortical neurons against lethal oxygen-glucose deprivation. *RSC Chem Biol*, 4(1), 84-93. https://doi.org/10.1039/d2cb00189f

Student contributions to the papers: RJN performed the cell viability studies, neuronal cell uptake studies, Seahorse XF24 studies, mouse seizure studies, statistical analysis, and assisted in the writing of the manuscripts along with George S. Robertson, Justin J. Wilson, and Joshua J. Woods.

1.1 The Disease Burden of Stroke

Stroke is the second leading cause of death and a leading cause of disability in the world (Feigin et al., 2022). Most strokes (85%) are ischemic and typically caused by a blood clot that blocks a major artery in the brain (Writing Group et al., 2016). The remaining strokes (15%) are hemorrhagic and result from the rupture of blood vessels in the brain (Writing Group et al., 2016). The brain is a highly energetic organ that requires large amounts of oxygen and glucose to operate properly. As a result, the brain is very susceptible to damage by impaired cerebral blood flow (CBF). This causes neurological deficits which, depending on injury severity, may be permanent. Those afflicted by stroke experience a reduced quality of life, and also a higher dependence on others for assistance with daily living tasks, which places a heavy burden on our society and healthcare networks (Anderson et al., 2004; Feigin et al., 2014). In developed

countries, stroke is the most common cause of acute hospitalization in neurology departments, and in individuals over 40 years of age, stroke is the greatest contributor to disability adjusted life years (DALY) worldwide (Grefkes & Fink, 2020). Despite improvements in the prevention of cardiovascular diseases and treatment of acute stroke, the absolute number of stroke deaths and DALY are still rising due to higher life expectancies and increased population growth (Grefkes & Fink, 2020).

Based on data from a sample of high-, middle- and low-income countries around the world, the annual treatment, rehabilitation, and indirect costs of stroke have been estimated to exceed $700 billion US dollars, and as the population continues to age, these costs are expected to be over $1 trillion US dollars by 2030 (Feigin et al., 2014). In addition, data suggests that by 2050 one out of three stroke patients will be 85 or older, suggesting there will be a much greater need for higher capacities in stroke care and neurorehabilitation, especially for older patients (Howard & Goff, 2012).

In the case of ischemic stroke, the current treatment options include thrombolysis with a thrombolytic agent such as tissue plasminogen activator (t-PA) to break down the blood clot, and/or endovascular thrombectomy to physically remove the blood clot (Casaubon et al., 2016). These treatments are highly effective at reducing stroke-related morbidity and mortality, however, only a relatively small number of patients meet the treatment eligibility criteria, and treatment must

begin within 4.5 and 6 hours (hr), respectively, from the onset of stroke symptoms (Grefkes & Fink, 2020; Parker & Ali, 2015). Although these treatments reduce mortality, the majority (>50%) of patients are still left with disabling neurological deficits (Grefkes & Fink, 2020). Hence, there is an urgent need for new stroke therapies that protect the brain from damage and facilitate repair necessary for functional recovery. The development of such therapies would be enabled by an improved understanding of the mechanisms responsible for brain injury and repair after a stroke.

1.2 Mitochondria are Key Players in Energy Production and Calcium (Ca^{2+}) Handling

Mitochondria are organelles that play a vital role in numerous cell processes, including energy production, calcium (Ca^{2+}) homeostasis, and regulating cell death signalling pathways (Walters & Usachev, 2023). These highly specialized organelles are comprised of an outer mitochondrial membrane and an inner mitochondrial membrane that creates two compartments known as the intermembrane space and mitochondrial matrix (Rizzuto et al., 2012). The outer mitochondrial membrane is permeable to all low-molecular-weight solutes, whereas the inner mitochondrial membrane is impermeable except by way of specific transporters (Rizzuto et al., 2012; Walters & Usachev, 2023). Embedded in the inner mitochondrial membrane are the respiratory Complexes I-V that constitute the electron transport chain (ETC) (Figure 1.1). These Complexes generate a powerful electrochemical gradient known as the mitochondrial

membrane potential ($\Delta\Psi_m$) by pumping protons from the matrix to the intermembrane space (Nunnari & Suomalainen, 2012; Zhao et al., 2019). The $\Delta\Psi_m$ is harvested by Complex V, or adenosine triphosphate (ATP) synthase, to produce cellular energy in the form of ATP)(Figure 1.1) (Nunnari & Suomalainen, 2012). Mitochondria are also a major source of reactive oxygen species (ROS) in cells (Yang et al., 2018). Electrons that escape from the ETC react with oxygen to form ROS that participate in cell signaling pathways which regulate proliferation, metabolism, differentiation, and survival (An et al., 2021). However, high levels of ROS can be detrimental, resulting in oxidative damage to critical cell components, including deoxyribonucleic acids (DNA), proteins, and lipids (Lin & Beal, 2006). Under normal physiological conditions in which ATP production is efficient, ROS generation is minimal and endogenous antioxidant systems are sufficient to prevent injurious ROS accumulation (An et al., 2021). Under pathological conditions that compromise mitochondrial function, excessive ROS production is thought to overwhelm endogenous antioxidant systems resulting in irreversible cell damage (Lin & Beal, 2006). However, anti-oxidant therapies have proven to be ineffective in the treatment of stroke, suggesting that ROS overproduction is not the primary cause of brain damage (Gilgun-Sherki, 2002).

Mitochondria also play an important role in cellular Ca^{2+} handling. Ca^{2+} is essential for several cellular processes, including neurotransmission, energy metabolism, and intracellular signalling (Rizzuto et al., 2012; Walters & Usachev, 2023). Mitochondria rapidly buffer cytosolic Ca^{2+} levels associated with a rise in

neuronal activity (Rizzuto et al., 2012; Walters & Usachev, 2023). High-capacity

mitochondrial Ca^{2+} uptake is mediated by the mitochondrial Ca^{2+} uniporter

complex (MCU_{cx}) (Baughman et al., 2011; Rizzuto et al., 2012). The increased

entry of Ca^{2+} into the mitochondrial matrix stimulates dehydrogenases that

generate reducing equivalents which drive ETC activity responsible for ATP

synthesis (Denton, 2009; Rizzuto et al., 2012). Elevated matrix Ca^{2+}

concentrations also increase ATP synthesis by directly activating Complex V

(Territo et al., 2000). Lastly, increased mitochondrial Ca^{2+} uptake by the MCU_{cx}

positions mitochondria at active synaptic sites in urgent need of metabolic

support by undocking these dynamic organelles from cytoskeletal motor proteins

(Chang et al., 2011; Niescier et al., 2013).

Outer Mitochondrial Membrane

Intermembrane Space

H⁺ → H^+

H^+ H^+ H^+ H^+ H^+ H^+ H^+ H^+ H^+ H^+

Inner Mitochondrial Membrane

Q

I II III Cyt c IV ATP Synthase

NADH FADH₂ → FAD ADP + P_i ATP

$NAD^+ + H^+$

2 e⁻

½ O₂ + 2H⁺ H₂O H^+

Mitochondrial Matrix
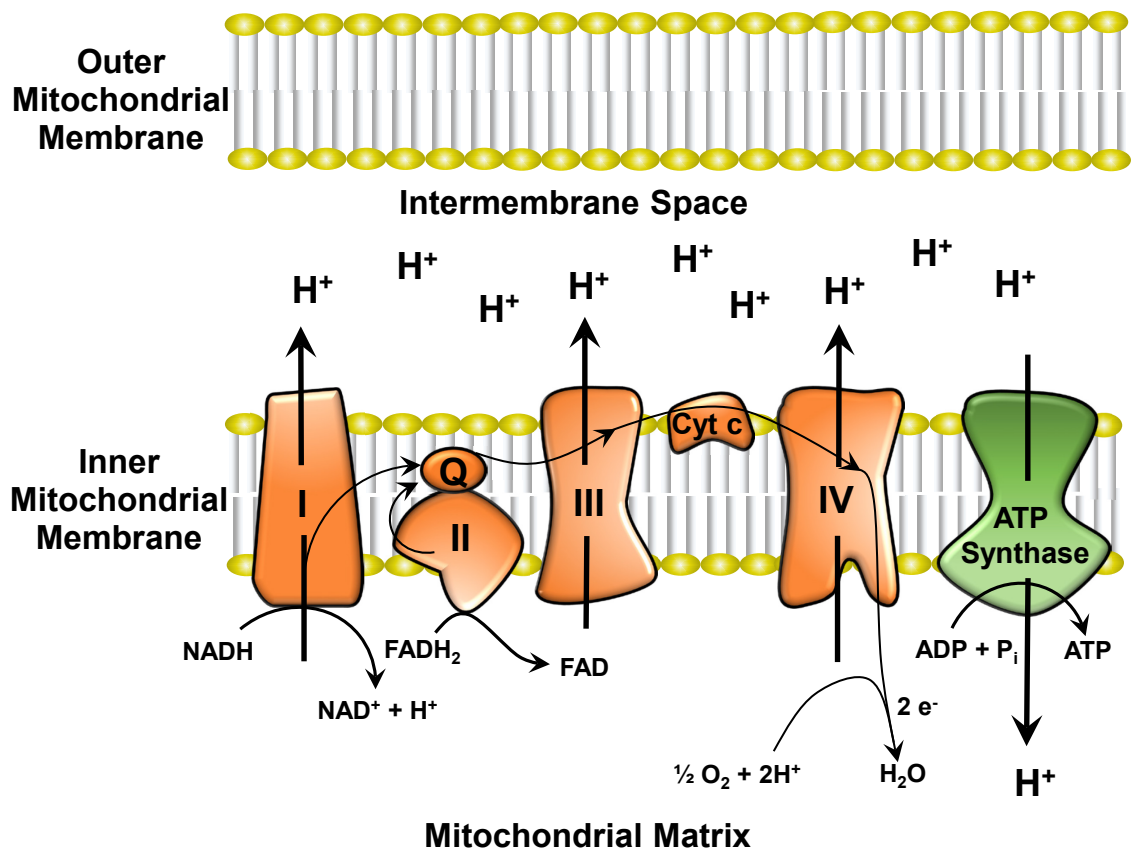
Figure 1.1. Schematic of the Electron Transport Chain (ETC) and ATP Synthase

The electron transport chain consists of complexes embedded in the inner mitochondrial membrane that couple redox reactions with the transfer of protons (H^+) into the intermembrane space, which creates an electrochemical proton gradient called the mitochondrial membrane potential ($\Delta\Psi_m$). The $\Delta\Psi_m$ is then harvested by ATP synthase to produce energy for the cell in the form of ATP.

1.3 Contributions of Mitochondria to Neuronal Injury in Stroke

The brain is one of the most energy-demanding organs in the body, rendering it highly dependent on optimal mitochondrial function to operate properly (An et al., 2021; Harris et al., 2012). Neurotransmission requires vast amounts of energy, mainly to fuel ATP-dependent sodium (Na^+)/potassium (K^+) pumping and vesicle recycling (Harris et al., 2012). To sustain these processes, mitochondria must consume high amounts of oxygen and glucose to produce the prodigious amounts of ATP required to sustain increased synaptic activity (Harris et al., 2012). This reliance on oxidative phosphorylation for ATP synthesis renders neurons highly susceptible to injury by mitochondrial dysfunction during periods of cerebral ischemia (Harris et al., 2012; Vakifahmetoglu-Norberg et al., 2017). During ischemic conditions, the lack of oxygen and glucose leads to metabolic collapse resulting in depolarization of the neuronal plasma membrane. This triggers excessive glutamate release, causing excitotoxicity and the discharge of numerous pro-death factors from damaged mitochondria which rapidly destroy neurons (Vakifahmetoglu-Norberg et al., 2017; Yang et al., 2018; Zhou et al., 2021). Furthermore, mitochondrial damage is one of the earliest neuropathological events in stroke (Barsoum et al., 2006). These findings highlight the importance of preserving mitochondrial function to effectively treat stroke.

Impaired mitochondrial dynamics, such as increased mitochondrial fission, have been implicated in the initiation of ischemic cell death (Zhou et al., 2021). Also,

the disruption of ETC activity due to inadequate oxygen and glucose levels leads to reduced ATP production and excessive ROS generation by mitochondria (An et al., 2021; Yang et al., 2018). Excessive ROS production results in oxidative stress and damage to lipids, proteins, and DNA, which can stimulate apoptosis (An et al., 2021). During cerebral ischemia, there is also a sustained dysregulation of plasma membrane and endoplasmic reticulum handling of Ca^{2+}, which leads to a toxic rise in cytosolic Ca^{2+} levels (Kristián & Siesjö, 1998). In an attempt to buffer cytosolic Ca^{2+}, excessive mitochondrial Ca^{2+} uptake occurs, leading to toxic mitochondrial Ca^{2+} overloading that irreversibly damages these organelles. Mitochondrial Ca^{2+} overloading also results in the activation of many Ca^{2+}-dependent proteases, lipases, and deoxyribonucleases, which further exacerbate ischemic cell death (Kristián & Siesjö, 1998; Zhou et al., 2021). Additionally, excessive mitochondrial Ca^{2+} uptake triggers mitochondrial-mediated cell death by opening the mitochondrial permeability transition pore (mPTP) (Vakifahmetoglu-Norberg et al., 2017; Yang et al., 2018). This increases the permeability of the inner mitochondrial membrane and suppresses ATP synthesis by depleting the $\Delta\Psi_m$ and activating the release of pro-death factors into the cytoplasm (Zhou et al., 2021). These pro-death factors include cytochrome c, which activates caspase-9 resulting in intrinsic cell death, and apoptosis inducing factor, which damages neurons by fragmenting DNA (Vakifahmetoglu-Norberg et al., 2017). The opening of the mPTP is predominately controlled by Ca^{2+} overloading, but can be enhanced by oxidative stress and ATP depletion during cerebral ischemia (Vakifahmetoglu-Norberg et

al., 2017; Zhou et al., 2021). Mitochondrial dysfunction therefore initiates multiple cell death pathways implicated in ischemic cell death (Green et al., 2014).

1.4 Structure and Function of the MCU$_{cx}$

Mitochondrial Ca^{2+} overloading is considered to be a pivotal event in ischemic cell death (Duchen, 2012). As mentioned earlier, high capacity mitochondrial Ca^{2+} uptake is mediated by the MCU$_{cx}$, located in the inner mitochondrial membrane (Figure 1.2). Ca^{2+} first passes through the outer mitochondrial membrane via voltage dependent anion channels (VDAC), which are the most abundant proteins on the outer mitochondrial membrane (Rizzuto et al., 2012). Lethal amounts of Ca^{2+} are then transported across the inner mitochondrial membrane and into the matrix via the MCU$_{cx}$ (Figure 1.2B) (Stefani et al., 2011). The MCU$_{cx}$ is a dynamic structure consisting of pore-forming subunits and regulatory subunits that work together to respond to increases in cytosolic Ca^{2+} levels by efficiently transporting high amounts of Ca^{2+} into mitochondria (Figure 1.2B). Since discovery of the mitochondrial Ca^{2+} uniporter subunit (MCU) that creates the MCU$_{cx}$ channel pore (Baughman et al., 2011; Stefani et al., 2011), six additional subunits have been identified. These include MCU$_{cx}$ dominant-negative beta subunit (MCUb), mitochondrial Ca^{2+} uptake 1, 2, and 3 (MICU1, MICU2, and MICU3), essential MCU$_{cx}$ regulator (EMRE), and MCU$_{cx}$ regulator 1 (MCUR1) (Figure 1.2). How these subunits interact to gate the MCU$_{cx}$ is a rapidly evolving area of research that is still not fully elucidated, and is complicated by differences in the tissue-dependent expression and activity of certain MCU$_{cx}$

subunits, as well as evidence that some subunits appear to have broad actions on mitochondrial function (Garbincius & Elrod, 2022; Walters & Usachev, 2023). Nonetheless, through the utilization of cryogenic microscopy images and experimentation with cells and mice lacking different subunits of the MCU_{cx}, a general framework has been established for how these subunits are arranged and function to control mitochondrial Ca^{2+} uptake.

The pore of the MCU_{cx} is made up of four transmembrane MCU subunits (Baradaran et al., 2018; Fan et al., 2018; Nguyen et al., 2018; Yoo et al., 2018) (Figure 1.2). Each MCU subunit has two coiled coil domains and two transmembrane domains separated by a short hydrophilic acid linker composed of a DIME motif, which consists of carboxylate groups that are strategically located at the pore entrance and appear to mediate the highly selective gating of Ca^{2+} by the MCU_{cx} (Baughman et al., 2011; Cao et al., 2017; Oxenoid et al., 2016; Stefani et al., 2011; Yoo et al., 2018). MCUb is considered to be the dominant negative subunit of the MCU_{cx}. This transmembrane subunit reduces Ca^{2+} conductance by displacing one or more MCU subunits from the channel pore (Lambert et al., 2019; Raffaello et al., 2013) (Figure 1.2). EMRE, found only in metazoans, is a protein with a single transmembrane domain (Kovacs-Bogdan et al., 2014; Sancak et al., 2013) (Figure 1.2). In the brain, the majority of MCU tetramers appear to associate with two EMREs (Watanabe et al., 2022). Importantly, EMRE is essential for *in vivo* MCU_{cx} activity and MCU oligomers alone are not sufficient for *in vivo* uniporter activity (Sancak et al., 2013). MCUR1

is another regulator of the MCU_{cx}, that when present further facilitates mitochondrial Ca^{2+} uptake (Mallilankaraman et al., 2012; Tsai et al., 2016) (Figure 1.2).

MICU1, MICU2, and MICU3 each have similar mass and two canonical Ca^{2+} binding EF hands (Csordas et al., 2013; Sancak et al., 2013). MICU1 forms homodimers or heterodimers with MICU2 or MICU3 that interact with the rest of the MCU_{cx} (Patron et al., 2019; Sancak et al., 2013; Wang et al., 2014) (Figure 1.2). These proteins are involved in enhancing channel activity by modifying the gating properties of the MCU_{cx} to favour the open confirmation of the channel in response to a rise in intracellular Ca^{2+} levels (Fan et al., 2020; Garbincius & Elrod, 2022; Walters & Usachev, 2023) (Figure 1.2). MICU3, expressed predominately in brain and skeletal muscles, has a greater affinity for Ca^{2+} than MICU2. This enables MICU1/3 dimers to become activated at lower cytosolic Ca^{2+} concentrations than MICU1/1 or MICU1/2 dimers (Kamer et al., 2017; Patron et al., 2014; Patron et al., 2019). MICU3 therefore supports the high metabolic needs of neurons by allowing small and fast increases of cytosolic Ca^{2+} concentrations associated with enhanced glutamatergic signaling to increase MCU_{cx} activity (Ashrafi et al., 2020; Patron et al., 2019). However, the ability of MICU3 to lower the Ca^{2+} threshold for MCU_{cx} activation comes at the cost of increasing the risk of injurious mitochondrial Ca^{2+} overloading.

Although there is still much to uncover regarding the functions of these subunits, especially in the brain, multiple studies have demonstrated that disrupting the function of several MCU$_{cx}$ subunits can lead to neurodegenerative and neurodevelopmental disorders (Llorente-Folch et al., 2015; Logan et al., 2014; Shamseldin et al., 2017; Singh et al., 2022). Mutations that result in the loss of function or regulation of subunits such as MICU1, MICU2, or EMRE, have been associated with impaired mitochondrial function, muscle weakness, cognitive deficits, and abnormal involuntary movements in humans (Konig et al., 2016; Logan et al., 2014; Shamseldin et al., 2017; Singh et al., 2022). These findings emphasize the importance of the presence and proper functioning of various MCU$_{cx}$ subunits for mitochondrial function and Ca^{2+} homeostasis, and provide insights into how aberrant MCU$_{cx}$ activity may contribute to neuronal injury.
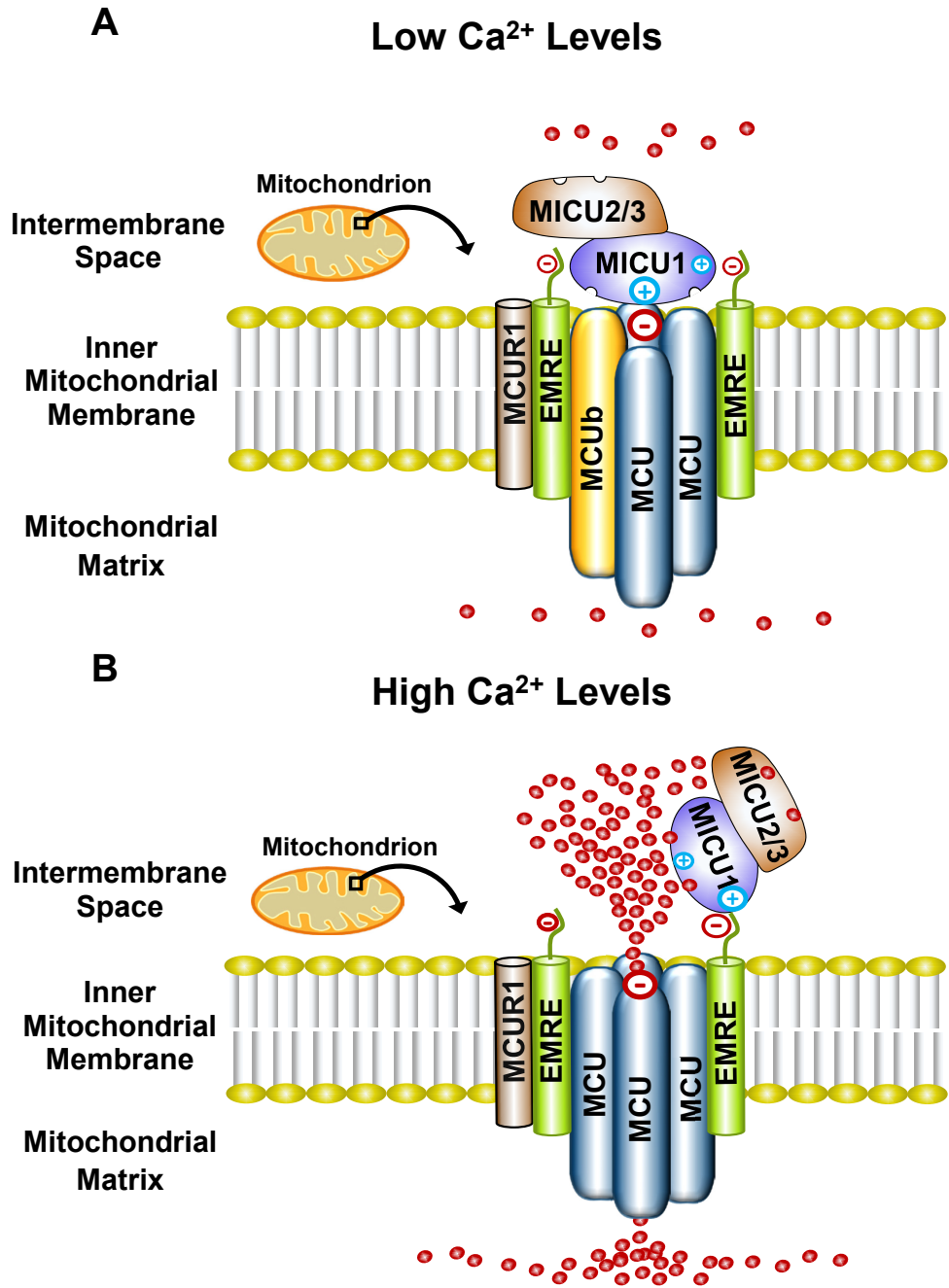
Figure 1.2. Functional architecture of the MCU_{cx}

The MCU_{cx} is located in the inner mitochondrial membrane and is comprised of transmembrane pore forming subunits (MCU and MCUb) and regulatory subunits (MCUR1, EMRE, MICU1, MICU2, and MICU3) (A). Elevated Ca^{2+} levels increase Ca^{2+} binding to MICU1/1, MICU1/2, or MICU1/3 dimers that exposes positively charged amino acids in MICU1 (B). This strengthens the association of MICU1 with negatively charged amino acids in EMRE, which displaces the dimer from the channel pore, resulting in increased Ca^{2+} influx into the mitochondrial matrix.

1.5 Mitochondrial Ca^{2+} Efflux

Mitochondrial Ca^{2+} efflux occurs through the mitochondrial Na$^+$/Ca^{2+}/lithium (Li$^+$) exchanger (NCLX) (Figure 1.3). The NCLX is a member of the plasma membrane Na$^+$/Ca^{2+} exchanger (NCX) superfamily, but exhibits some distinguishing features that contribute to its mitochondrial Ca^{2+} efflux activity (Palty et al., 2010). The NCLX is localized to the inner mitochondrial membrane and although structurally similar to NCX, operates under different ionic conditions and membrane potentials (Palty et al., 2010). As its name suggests, the NCLX has the unique ability to transport Na$^+$ or Li$^+$ in exchange for Ca^{2+}. The NCLX appears to import 3 Na$^+$ or Li$^+$ ions in exchange for the export of 1 Ca^{2+} ion, making the NCLX an electrogenic pump that utilizes the $\Delta\Psi_m$ to drive cation exchange (Islam et al., 2020; Lytton, 2007; Roy et al., 2017) (Figure 1.3). The NCLX also exhibits unique characteristics in its regulatory domain. Unlike the regulatory domain of NCX which harbours an allosteric Ca^{2+} binding site (Khananshvili, 2017), the NCLX regulatory domain contains several phosphorylation sites, notably protein kinase A (PKA) and Ca^{2+}/calmodulin-dependent kinase 2 sites, that control NCLX activity (Katoshevski et al., 2021) (Figure 1.3). PKA activity increases NCLX activity through phosphorylation at these sites (Katoshevski et al., 2022; Kostic et al., 2018; Kostic et al., 2015). The PKA site is also controlled by other players, most notably phosphodiesterases (PDE). PKA is allosterically activated by a rise in cyclic adenosine monophosphate (cAMP), which in turn is degraded by PDEs (Acin-Perez et al., 2009; Conti & Beavo, 2007). Inhibition of PDEs therefore causes PKA activation

by increasing cAMP levels, which in turn enhances NCLX activity by increasing phosphorylation of its regulatory domain (Kostic et al., 2018; Kostic et al., 2015; Rozenfeld et al., 2022). In addition, the NCLX regulatory domain contains a cluster of positively charged residues that are thought to act like a channel voltage sensor, which might allow this cluster to adjust NCLX activity in response to changes in the $\Delta\Psi_m$ (Kostic et al., 2018) (Figure 1.3).

A reduction in NCLX activity can also contribute to mitochondrial Ca^{2+} overloading through a decrease in mitochondrial Ca^{2+} efflux. The electrogenic nature of NCLX exchanger activity renders it susceptible to inhibition by depolarization of the $\Delta\Psi_m$ during cerebral ischemia. Depolarization of the $\Delta\Psi_m$ thus increases the risk of toxic mitochondrial Ca^{2+} overloading by suppressing NCLX activity (Giorgio et al., 2018; Kostic et al., 2018). Hence, loss of NCLX activity is another potential mechanism by which toxic mitochondrial Ca^{2+} overloading may occur in ischemic stroke.
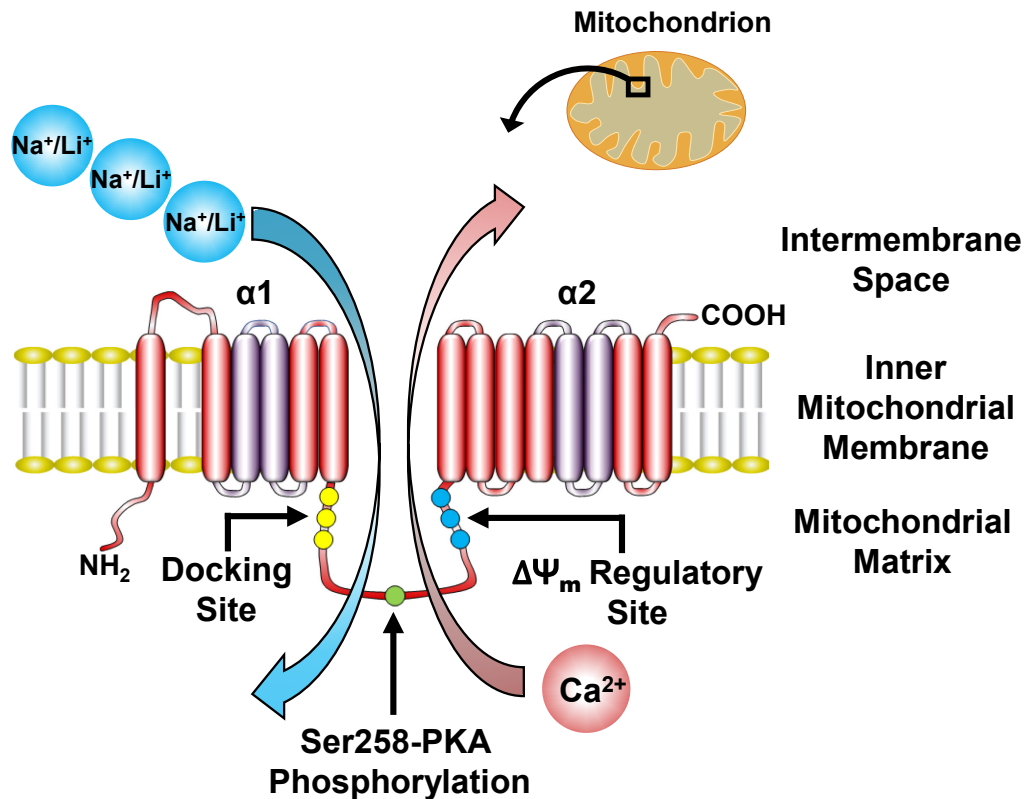
Figure 1.3. Representative model of the NCLX showing the regulatory domains and sites

The NCLX regulatory loop is located between the two catalytic α1 and α2 domains. NCLX has a $\Delta\Psi_m$ sensing allosteric site as well as a PKA-dependent phosphorylation site Ser258. The $\Delta\Psi_m$ provides the driving force for the electrogenic transport of three Na^+ or Li^+ ions for one Ca^{2+} ion. Phosphorylation of Ser258 by PKA increases NCLX activity.

1.6 The Neurovascular Unit (NVU)

The neurovascular unit (NVU) is the basic component of the blood brain barrier (BBB). This intricate structure is comprised of vascular cells (smooth muscle cells, endothelial cells, and pericytes), glia (astrocytes, oligodendrocytes, and microglia), and neurons that communicate with each other to regulate CBF (Iadecola, 2004; Kugler et al., 2021) (Figure 1.4). Historically, research surrounding neurodegenerative disorders and stroke has predominately focused on neuronal cell death and the destruction of other components of the NVU has been largely ignored (Lo et al., 2003). Recent evidence suggests that damage to these other components of the NVU further exacerbates injury during stroke, and failure to preserve the functions of this intricate structure contributes to poor outcomes and recovery post-stroke (Cai et al., 2017; Lo et al., 2003). In addition to neurons, this thesis will therefore address the role of mitochondrial Ca^{2+} overloading in two other major components of the NVU, astrocytes and endothelial cells.

Endothelial cells form the wall of cerebral blood vessels (Iadecola, 2004) (Figure 1.4). Tight junctions between endothelial cells create a physical barrier that impedes the paracellular diffusion of ions, macromolecules, and other polar solutes (Stamatovic et al., 2008) (Figure 1.4). Endothelial cells also act as a biochemical barrier by selectively transporting nutrients into the brain from the blood and exporting solutes and metabolite waste products out of the brain and into the blood (Iadecola, 2004; Stamatovic et al., 2008). This is achieved by

transporters, receptors, and ion channels situated on the luminal and/or abluminal membranes of endothelial cells (Iadecola, 2017; Loscher & Potschka, 2005). Endothelial cells also secrete a rich repertoire of cytokines and trophic factors in response to different stimuli such as dysregulation of the BBB and tissue damage (Lo et al., 2003; Verma et al., 2006).

Astrocytes are a type of glial cell that serve a variety of functions within the brain, including providing energy to neurons, communicating with other cell types, maintaining BBB integrity, and supporting neurogenesis (Bantle et al., 2021; Lo et al., 2003; Sofroniew & Vinters, 2010). Astrocytes extend endfoot processes that cover the entire abluminal surface of cerebral blood vessels (Mathiisen et al., 2010) (Figure 1.4). This configuration allows for bidirectional signalling between astrocyte endfeet and endothelial cells, which is essential for the regulation of cerebral vascular function and maintenance of NVU integrity (Gordon et al., 2007; Muoio et al., 2014; Petzold & Murthy, 2011).

Given the many important functions and the exquisite sensitivity of the NVU to ischemic damage, it is critical that we learn how to protect this intricate structure in order to effectively treat ischemic stroke. (Schaeffer & Iadecola, 2021). The NVU responds to the dynamic metabolic demands required for brain activity by rapidly altering CBF. The phenomenon, known as neurovascular coupling, depends heavily on mitochondrial Ca^{2+} uptake to rapidly buffer cytosolic Ca^{2+} and stimulate energy production in major cellular components of the NVU, such as

neurons, astrocytes, and endothelial cells (Iadecola, 2004, 2017). However, this also results in the NVU being highly susceptible to the lethal mitochondrial Ca^{2+} overloading during an ischemic stroke (Duchen, 2012; Halestrap, 2006). In addition, many of the activities of the NVU are energetically demanding, so reductions in ATP production and oxidative stress during ischemia can result in diminished function and damage of this complex structure (Cai et al., 2017; Grubb et al., 2021; Lo et al., 2003). Breakdown of the BBB also occurs during ischemic conditions, which contributes to a dysregulation of ion homeostasis, and the increased entry of injurious metabolites and proteins into the brain (Cai et al., 2017; Verma et al., 2006). Furthermore, aging, a risk factor for poor stroke outcomes, is known to suppress NVU repair (Cai et al., 2017; Shin et al., 2022). The intricacy and importance of the NVU to overall brain health, and its susceptibility to damage, highlights how preserving this structure is paramount for the effective treatment of stroke.
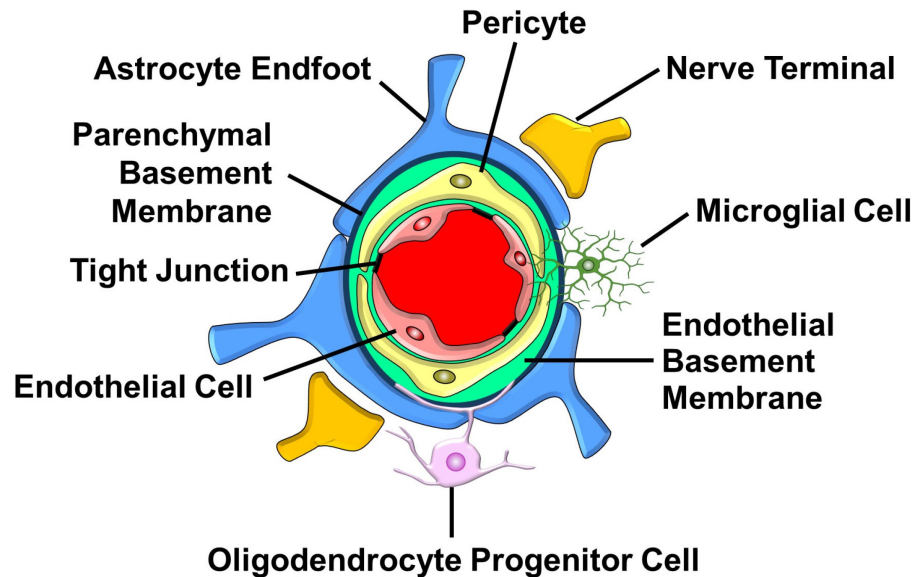
Figure 1.4. Schematic of the major structural and cellular components of the NVU

The NVU is an intricate structure comprised of vascular cells (endothelial cells, and pericytes), glia (astrocytes, oligodendrocytes, and microglia), and neurons that communicate with each other to regulate CBF. Endothelial cells that line the capillary lumen form tight junctions which oppose the movement of metabolites and proteins into the brain. Astrocytes extend endfoot processes that cover the abluminal surface of cerebral blood vessels, sense changes in neuronal activity, and communicate with other components of the NVU through the release of signalling molecules.

1.7 Exacerbation of Brain Injury in Stroke by Inflammation

One characteristic common to neuronal injury is the presence of neuroinflammation. High levels of inflammation in the brain are associated with many different neurodegenerative disorders (Bantle et al., 2021; González-Reyes et al., 2017; Jayaraj et al., 2019; Li et al., 2019). A key feature of both endothelial cells and astrocytes is their ability to release cytokines upon activation (Choi et al., 2014; Verma et al., 2006). Depending on the stimuli, these cell types release pro-inflammatory cytokines that exacerbate NVU damage, or anti-inflammatory cytokines and trophic factors that promote NVU repair (Choi et al., 2014; Li et al., 2019; Verma et al., 2006). During an ischemic stroke, reduced CBF, oxidative stress, and mitochondria damage stimulates the release of pro-inflammatory cytokines from astrocytes and endothelial cells that fosters a pro-inflammatory environment, which contributes to brain damage (Anrather & Iadecola, 2016; Crack & Wong, 2008; Jurcau & Simion, 2022). Inflammation-induced cell death is thought to cause secondary injury, which occurs during the acute phase of recovery (first 7 days) following the reestablishment of CBF after an ischemic stroke (Grefkes & Fink, 2020; Jayaraj et al., 2019).

The inflammatory cascade in an ischemic stroke is initiated after vessel occlusion due to stagnant blood flow, activation of intravascular leukocytes, and the release of pro-inflammatory mediators from the ischemic tissues (Anrather & Iadecola, 2016; Jurcau & Simion, 2022). Stagnant blood flow induces shear stress on vascular endothelium, leading to the release of molecules that recruit leukocytes

which initiate an inflammatory response in neighbouring cell types (Anrather & Iadecola, 2016; Jurcau & Simion, 2022). This also contributes to the breakdown of the BBB, which increases immune cell infiltration into the brain. The unique location of brain endothelial cells also allows them to secrete cytokines into both the brain and the blood circulation, and therefore exert inflammatory effects in both the brain and periphery (Verma et al., 2006). Mitochondrial Ca^{2+} overloading during ischemia can also trigger the release of mitochondrial damage-associated molecular patterns (DAMPs) from injured and dying neurons that stimulate microglia and astrocytes to release pro-inflammatory cytokines, which promote neuroinflammation and cell death (Anrather & Iadecola, 2016).

The restoration of blood flow after cerebral ischemia can trigger reperfusion injury (Al-Mufti et al., 2018). Immune activation is thought to worsen reperfusion injury following endovascular therapy by damaging the NVU (Iadecola et al., 2020). Although the precise mechanisms are not clear, excessive ROS production by dysfunctional mitochondria appears to exacerbate inflammation by activating the redox sensitive transcription factor, nuclear factor-kappa-B (NF-κB), and the NLRP3-inflammasome pathway (Blaser et al., 2016; Song et al., 2017; Vallabhapurapu & Karin, 2009). This triggers the increased production of numerous pro-inflammatory cytokines by astrocytes and endothelial cells, and elevates the expression of cellular adhesion molecules on the surface of endothelial cells (Shi et al., 2019). Mitochondrial damage generates DAMPs that further increase injurious pro-inflammatory signalling (Bantle et al., 2021; Joshi et

al., 2019). These findings suggest that mitochondrial dysfunction and damage also contribute to brain injury after a stroke by driving inflammation. Drugs that preserve mitochondrial function may therefore further improve clinical stroke outcomes by suppressing inflammation.

1.8 Inhibitors of the MCU$_{cx}$ as Neuroprotective Agents

Mitochondrial dysfunction and mitochondrial Ca^{2+} overloading are widely accepted as early pathological events in ischemic injury that trigger multiple cell death pathways (Duchen, 2012; Halestrap, 2006). Therefore, preserving mitochondrial function by inhibiting the MCU$_{cx}$ to prevent mitochondrial Ca^{2+} overloading has emerged as an attractive therapeutic approach for the treatment of ischemic stroke. This therapeutic approach is supported by evidence that selective deletion of the MCU in cardiac myocytes and Thy-1 expressing neurons at sexual maturity protects mice from ischemic/reperfusion injury in the heart and brain, respectively (Kwong et al., 2015; Luongo et al., 2015; Nichols et al., 2018). Based on these findings, compounds that inhibit the MCU$_{cx}$ should confer similar protective benefits.

The ruthenium (Ru)-based complex Ru360, found in Ruthenium Red (RuRed), has been used for decades to study the effects of MCU$_{cx}$ inhibition (Broekemeier et al., 1994; Moore, 1971). Although Ru360 and RuRed are effective MCU$_{cx}$ inhibitors in isolated mitochondria and permeabilized cells, their use in intact cells and animals is limited by poor cell permeability, toxicity, and low-yielding and

challenging chemical synthesis (Nathan & Wilson, 2017; Velasco et al., 1995; Woods et al., 2020). In 2019, the Wilson laboratory developed a novel Ru-based inhibitor, termed Ru265, by introducing structural modifications to Ru360 (Woods et al., 2019)(see Figure 3.1 in Chapter 3). Ru265 demonstrated superior cell-permeability and greater MCU_{cx} inhibitory potency relative to Ru360 in human embryonic kidney (HEK293) cells and can be synthesized without a strenuous purification process (Woods et al., 2019). This compound also prevented the loss of the $\Delta\Psi_m$ in neonatal ventricular myocytes subjected to hypoxia/reoxygenation injury through suppression of mitochondrial Ca^{2+} overloading (Woods et al., 2019).

These findings suggest Ru265 should also be an effective neuroprotective agent in ischemic stroke by suppressing MCU_{cx}-mediated mitochondrial Ca^{2+} overloading. Therefore, the ability of Ru265 to protect neurons and the brain from ischemic injury was investigated in this thesis. To obtain insights into how certain structural properties contribute to the biological activities of Ru265, additional compounds were generated by introducing structural modifications to Ru265. These compounds include the nitro-bridged osmium (Os) analogues Os245, Os245', and the adamantane containing analogues RuOAd, and OsOAd (see Figure 6.1 in Chapter 6). The ability of these analogues to protect against ischemic injury was also examined in this thesis.

1.9 Models of Injury

In this thesis, an *in vitro* model of ischemic/reperfusion injury, an *in vitro* model of inflammation, and an *in vivo* model of hypoxia/ischemia were employed to assess the therapeutic potential of MCU_{cx} inhibition for ischemic stroke. For the *in vitro* experiments, primary cortical neuron cultures, primary cortical astrocyte cultures, and the human brain endothelial cell line termed HBEC-5i were used to assess the neuroprotective and anti-inflammatory effects of the different MCU_{cx} inhibitors. Adult male C57Bl/6 mice were used in the *in vivo* experiments.

Oxygen-glucose deprivation (OGD) was used to model ischemic/reperfusion injury in cultured cells. The OGD method consists of placing cell cultures into glucose-free media bubbled with an anaerobic gas mixture to remove oxygen, and then placing the cultures into a sealed hypoxic chamber containing anaerobic gas for a set time at physiological temperatures (Zeiger et al., 2011). Cultures exposed to OGD experience many of the key features implicated in ischemic/reperfusion brain injury (Zeiger et al., 2011). These pathological events include a rapid energetic decline, excessive glutamate release, ROS overproduction, ionic dysfunction, mitochondrial swelling, and signalling cascades associated with both apoptotic and necrotic cell death (Zeiger et al., 2011).

Treatment with lipopolysaccharide (LPS) was used as an *in vitro* model of inflammation. LPS is a component of the cell membrane of gram-negative

bacteria that stimulates pro-inflammatory signalling by activating the Toll 4-like receptor (TLR4) (Skrzypczak-Wiercioch & Sałat, 2022). TLR4 activation stimulates pro-inflammatory cytokine expression by astrocytes and endothelial cells (Skrzypczak-Wiercioch & Sałat, 2022). LPS treatment is therefore a useful model to examine how these cellular components of the NVU contribute to neuroinflammation (Park et al., 2017; Skrzypczak-Wiercioch & Sałat, 2022).

To examine the protective potential of Ru265 *in vivo*, a mouse model of hypoxia/ischemia (HI) brain injury was employed. This model involves unilateral occlusion of the common carotid artery, followed by subjecting animals to hypoxia for a set time, and then returning them to normoxic conditions (Adhami et al., 2006; Nichols et al., 2018). This combination of carotid occlusion and hypoxia diminishes CBF and causes brain infarction (Adhami et al., 2006). Studies using this model have observed partial cerebral reperfusion with complete systemic re-oxygenation resulting in necrosis, autophagy, and apoptosis in the affected hemisphere (Adhami et al., 2006; Wang et al., 2009; Zhu et al., 2005). Hence, this brain injury model activates neuronal cell death mechanisms implicated in ischemic stroke (Davoli et al., 2002; Liu et al., 2010).

1.10 Central Hypothesis and Research Aims

The central hypothesis guiding these studies was that compounds which effectively block MCU_{cx}-mediated mitochondrial Ca^{2+} overloading would prevent ischemic cell death by preserving mitochondrial function. This central hypothesis was tested by completing the following research aims:

1. Assessment of the effects of the MCU_{cx} inhibitor Ru265 on cell viability and mitochondrial function in mouse primary cortical neuron and astrocyte cultures subjected to a lethal period of OGD.

2. Examination of the effects of Ru265 on pro-inflammatory and anti-inflammatory cytokine expression in astrocytes and endothelial cells treated with vehicle or LPS.

3. Determination of the effectiveness and safety of Ru265 in a mouse model of hypoxic/ischemic brain injury.

4. Assessment of the neuroprotective effects of different analogues of Ru265 in mouse primary cortical neuron cultures subjected to a lethal period of OGD.

5. Examination of the effects of combining MCU_{cx} inhibition with NCLX activation on mitochondrial function and cell viability in mouse primary cortical neuron cultures subjected to a lethal period of OGD.

Chapter 2: Materials and Methods

2.1 Animal Care

All studies using animals in this thesis were approved by the University Committee on Laboratory Animals (UCLA) ethics committee at Dalhousie University and conducted according to the Canadian Council on Animal Care (CCAC) guidelines. Mice were housed in the Life Sciences Research Institute Animal Care Facility on a 12 hr light/dark cycle and had *ad libitum* access to food and water.

2.2 Mouse Primary Cortical Neuron Cultures

For all experiments using primary cortical neuron cultures, E16 embryos were harvested from time-pregnant CD1 mice (Charles Rivers). Embryonic brains were aseptically removed and placed in Neurobasal media (Life Technologies) containing 10% fetal bovine serum (FBS; GE Healthcare Life Sciences) on ice. The cortices were isolated and the meninges were then peeled off. The cortices from all embryos were placed in a 35 mm petri dish containing Hanks Basic Salt Solution (HBSS; Life Technologies). Cortices were treated with 2 ml of Stem-Pro Accutase cell dissociation reagent (Life Technologies) and gently aspirated once to slightly break down cortices before they were left to incubate in the accutase for 15 minutes (min) at 37°C. After incubation, protease activity was inhibited by adding 1 ml of FBS, and the cortical tissue was transferred to a 15 ml conical tube containing 2 ml of complete neurobasal media (Neurobasal medium + B-27

supplement + 500 µM glutamine + 20 µg/ml gentamycin; Life Technologies). The cortical tissue was aspirated 7 times using a fire polished pipette to further break apart the tissue, and then was left for a couple minutes to allow for larger tissue pieces to settle before the supernatant was collected and passed through a pre-wetted 40 micron filter cell strainer. This procedure was repeated with the remaining cortical tissue solution to further break apart some of the larger pieces of cortical tissue. After the entire cortical tissue solution was filtered, the cell strainer was washed twice with 5 ml of complete neurobasal media. The neurons were then centrifuged at 800 rpm for 7 min, the supernatant was removed, and the cells were resuspended in complete neurobasal media. Next, the cells were stained with Trypan Blue and counted using the countess automated cell counter (Invitrogen). Cells were plated at a density of 150,000 cells/well in-48 well plates, 200,000 cells/well in 24-well plates, 1,000,000 cells/well in 6-well plates, 100,000 cells/well in 24-well Seahorse plates, 60,000 cells/well in 96-well Seahorse plates, and 250,000 cells/well in 35 mm imaging dishes. All plates were coated with 50 µg/ml of Poly-D-lysine hydrobromide (PDL, molecular weight 70,000-150,000; Sigma-Aldrich) and left overnight in the 37°C, 5% carbon dioxide (CO_2) incubator, and then washed 2x with Type 1 sterile water (H_2O) and left to dry overnight before cells were plated. Media changes occurred on the fourth, seventh, and tenth day after plating, where half of the media was removed and replaced with fresh complete neurobasal media. Neuron cultures were used after 10-13 days *in vitro* (DIV) for all experiments.

2.3 Mouse Primary Astrocyte Cultures

Primary astrocyte cultures were prepared using cortical tissues harvested from CD1 pups (postnatal day 0). The pups were anesthetized and decapitated, and the heads were placed in HBSS on ice. The brains were aseptically removed and placed in HBSS on ice, the cortices were dissected and isolated, and the meninges were peeled off. All cortices were placed together in a 65 mm petri dish containing HBSS, and the cortices were diced into very tiny pieces (about 1 mm) using a scalpel blade. The cortical tissue was then transferred into a 15 ml conical tube, the supernatant was removed, and 4 ml of Trypsin solution (CTS™ TrypLE™; ThemoFisher) was added. To promote trypsinization, the 15 ml tube was placed in a 37°C hot water bath for a total of 15 min. During this period, the solution was pipetted up and down a few times every few minutes to promote break down of the larger tissue pieces. After the 15 min incubation, enzyme activity was inhibited by adding 1 ml of FBS, and the solution was passed through a 40 micron filter cell strainer. The cell strainer was then washed twice with 5 ml of astrocyte media (Dulbecos Modified Eagle's Medium (DMEM) High glucose + 10% FBS + 20 µg/ml gentamycin; Life Technologies). The cells were centrifuged at 800 rpm for 5 min and then the supernatant was removed and the cells were resuspended in astrocyte media. This step was repeated two more times, and the cellular debris was discarded after every spin. After the third spin, the cells were resuspended in astrocyte media and then plated on T75cm^2 flasks with each flask receiving cells derived from 1.5 pups. About an hour after plating, a complete media change was performed to further remove any cellular debris.

Subsequent media changes were performed every three days. Once flasks reached confluency (about DIV 7-9), they were passed and the astrocytes were plated for experiments. To pass the astrocytes, the flasks were first placed on an orbital shaker in a 37°C incubator and shaken at 210 rpm for 2 hr to shake off any microglia or other non-adherent cells. The media was then removed and the astrocytes were washed with phosphate buffered saline (PBS; Life Technologies) to further remove any remaining non-adherent cells from the astrocyte monolayer. Astrocytes were then trypsinized with 5 ml of TrpLe™ for 5 min. Enzyme activity was inhibited by adding astrocyte media and the cells from all the flasks were pooled into a 50 ml conical tube. The cells were centrifuged at 800 rpm for 5 min and then the supernatant was removed, and the cells were resuspended with astrocyte media and plated for experimentation. About 1 hr after plating, a complete media change was done to remove any cellular debris, and subsequent media changes were performed every three days. Experiments were performed 9-11 days after passage, once the astrocytes reached a suitable confluency in the cell plate wells.

2.4 HBEC-5i Cell Cultures

HBEC-5i cells were obtained from the American Tissue Culture Collection (ATCC). HBEC-5i cells are a *Homo sapiens* cerebral microvascular endothelial cell line derived from human cerebral cortex tissue. Cells were maintained at 37°C, 5% CO_2 and grown in Dulbecos Modified Eagle's Medium/Nutrient Mixture F-12 (DMEM:F12; Life Technologies) supplemented with 10% FBS, 40 µg/ml

endothelial growth supplement (ECGS; VWR), and 25µg/ml gentamycin. Cells were maintained in T75cm^2 tissue culture flasks coated with 0.1% gelatin and passaged when 80% confluency was reached. For experimentation, cells were seeded into 12-well plates at a density of 75,000 cells/well the day prior to the start of the experiment.

2.5 OGD Experiments

Primary cortical neuron cultures were seeded in 48-well plates at a density of 150,000 cells/well for all OGD experiments. Primary astrocyte cultures were seeded in 24-well plates and used for OGD experiments once cells reached a suitable confluency in the wells. Glucose-free balanced salt solution (GBSS; 0.15 M NaCl, 2.8 mM KCl, 1 mM CaCl$_2$, 10 mM Hepes, pH 7.4) was prepared by bubbling a gas mixture of 90% nitrogen, 5% CO$_2$ and 5% hydrogen through the solution to remove oxygen. The cultures were washed twice with this oxygen free GBSS and placed in an air-tight container that was flushed with a gas mixture of 90% nitrogen, 5% CO$_2$ and 5% hydrogen for 3 min to remove any oxygen from the chamber. This air-tight chamber was then placed in a 37°C incubator for the duration of the OGD (90 min for cortical neurons; 4 hr for astrocytes). The OGD was terminated by the removal of the GBSS and reintroduction of complete neurobasal media to the neuron cultures and astrocyte media to the astrocyte cultures. Cells were returned to incubation at 37°C, 5% CO$_2$ until the end of the experiment (24 hr for cell viability and toxicity assays, 24 hr or 4 hr for ribonucleic acid (RNA) extraction, 1 hr for Seahorse assays).

2.6 Treatment with Neuroprotective Agents

Stock concentrations of the MCU_{cx} inhibitors Ru360, Ru265, Os245, Os245' RuOAd, and OsOAd were prepared in sterile Type 1 H_2O, and stock concentrations of the phosphodiesterase 2A (PDE2A) inhibitor, PF-05180999 (MedChemExpress) were prepared in Dimethyl sulfoxide (DMSO; Sigma-Aldrich). To treat cultures, first media was prepared with 2x the final desired concentration of the compound. Half of the media in the wells was then removed and replaced with an equal volume of media with the compound of interest at 2x concentration, resulting in the desired final concentration in the wells. Unless otherwise indicated, compounds were added to culture media at the specified time before the OGD treatment, were present in the GBSS during the OGD, and remained in the culture media after OGD (reperfusion). For LPS-induced cytokine expression experiments described in Chapter 4, Ru265 was added to the culture media at the specified time before the LPS treatment and was present in the culture media during the time the LPS was present.

2.7 Measurement of Mitochondrial Ca^{2+} Uptake

Primary cortical neuron cultures were seeded onto 35 mm glass bottom imaging dishes at a density of 250,000 cells/dish. At DIV 5, the neurons were transduced with an adeno-associated virus (AAV9) viral vector encoding the mitochondria-targeted low affinity Ca^{2+} indicator, Mito-LAR-GECO1.2 (generously provided by Dr. Robert Rendon, University of Nevada, Reno, USA). The cultures were left for 5 additional days to allow for sufficient transduction before experimentation, and

imaging took place on DIV 10. Imaging was performed using a Zeiss cell observer spinning-disk confocal microscope equipped with a 488 nm Argon laser. Prior to imaging, cultures were treated with either vehicle or 10 µM Ru265 for 4 hr, and then imaged to determine the baseline fluorescence signal. After capturing the baseline images, 20 µM of Kaempferol (prepared in DMSO; Cayman Chemicals) was added to the cultures, and images were captured every 30 seconds (sec) for 12 min at different locations within each dish. The fluorescence intensity of each image was quantified using the Zeiss Zen (blue edition) imaging software, with an increase in fluorescence intensity representing an elevation in mitochondrial Ca^{2+} levels. The percent increase in fluorescence intensity was calculated by dividing the average fluorescence intensity of the cells at the specific time point by the baseline average fluorescence intensity of the cells and multiplying by 100.

2.8 Cellular Uptake

Primary cortical neuron cultures were seeded in 24-well plates at a density of 200,000 cells/well for cellular uptake studies. At DIV 10-13, neurons were treated with the compound of interest for varying periods of time. After the treatment period, the media was removed, and the cells were washed three times with 500 µl of cold PBS followed by the addition of 75 µl of radioimmunoprecipitation assay (RIPA; 150mM NaCl, 25mM Tris pH 7.4, 0.1% Na deoxycholate, 0.1% Triton-X, 0.1% Sodium Dodecyl Sulfate) cell lysis buffer. Plates were then placed on an orbital shaker for 30 min and then the cell lysates were collected and

centrifuged at 13,000 rpm for 15 min. The amount of Ru or Os in each of the

samples was measured using Inductively Coupled Plasma Mass Spectrometry

(ICP-MS). The protein concentrations in each of the samples were determined

using the Bradford protein assay (Bio-Rad). These measurements enabled

normalization of Ru or Os concentrations based on the protein content of each

sample, and samples are reported as ng amounts of Ru or Os per μg of protein.

2.9 ICP-MS

The concentrations of Ru or Os in microwave-assisted digested cell lysate

samples was quantified using an iCAP Q ICP-MS (Thermo Fisher Scientific)

paired with an ESI SC-4DXS autosampler (Elemental Scientific) in Kinetic Energy

Discrimination mode using high purity helium (99.999%) as the collision gas. A

seven-point calibration curve (0.05, 0.1, 0.5, 1, 5, 10, and 50 μg/l Ru or Os in 2%

nitric acid) was used to determine unknown concentrations in the samples. An

online internal standard addition was performed to correct for any instrumental

drift using 50 μg/l scandium in 2% nitric acid delivered with an SC FAST Valve

(Elemental Scientific). ICP-MS analysis was carried out with a dwell time of 0.01

sec and 25 sweeps. A minimum of 3 main runs with a maximum relative standard

deviation (SD) of 5.0% were taken for each sample. Since each Ru360 and

Ru265 molecule contains two Ru atoms, and each Os245 and Os245' molecule

contains two Os atoms, Ru and Os values were divided by half to estimate

compound concentrations.

2.10 3-(4,5-dimethylthiazol-2-yl)-2,5-diphenyltetrazolium bromide (MTT) assay

Cell viability was assessed using the 3-(4,5-dimethylthiazol-2-yl)-2,5-diphenyltetrazolium bromide (MTT) assay. This assay determines cell viability by measuring Nicotinamide adenine dinucleotide (NADH)-dependent dehydrogenase activity indicative of cell viability (Huet et al., 1992). For this assay, 5 mg/ml of MTT (dissolved in PBS; Sigma-Aldrich) was added to wells so the final concentration of MTT in the wells was 0.5mg/ml. For example, for a well containing 500 µl of media, 50 µl of MTT was added. Plates were incubated at 37°C, 5% CO_2 for 1 hr (neuron cultures) or 3 hr (astrocyte cultures), and then the supernatant was removed, and the formazan crystals were dissolved with DMSO (250 µl per well). The absorbance of each well was measured at 550 nm using the spectrostar nano absorbance plate reader (BMG Labtech). The absorbance of control (No OGD) wells was defined as 100% cell viability. Percent viability was calculated by dividing the absorbance value of the treatment group by the average absorbance value of the No OGD group and multiplying by 100.

2.11 Lactate Dehydrogenase (LDH) Cell Cytotoxicity Assay

Cell cytotoxicity was assessed 24 hr after OGD using the CytoTox-ONE™ Homogenous Membrane Integrity Assay (Promega). This assay measures the amount of lactate dehydrogenase (LDH) in the culture media resulting from the release of this intracellular enzyme upon plasma membrane damage. Prior to the start of the assay, the cell plate was removed from the 37°C incubator and

allowed to equilibrate to 22°C. To determine maximal LDH release, lysis solution

supplied with the assay kit was added for 10 min to a few wells which served as

maximal LDH release controls. For each well, 100 µl of media was collected and

transferred to a well in a black-wall 96 well plate, and then 100 µl of CytoTox-

ONE™ Reagent was added to the wells. This plate was shaken for 30 sec and

then left for 10 min at 22°C. At the end of the incubation time, 50µl of the reaction

stop solution was added to the wells. The fluorescence was then measured using

the FLUOstar Omega microplate reader (BMG Labtech) with the

excitation/emission set to 560nm/590nm. The percent cytotoxicity for each

treatment was calculated by dividing the fluorescence value for the experimental

group by the fluorescence value for the maximum LDH release control group and

then multiplying by 100.

2.12 Assessment of Mitochondrial Respiration and Glycolysis

Primary cortical neuron cultures were seeded at a density of 100,000 cells/well in

seahorse XFe24 well plates and a density of 60,000 cells/well in Seahorse

XFe96 well plates for analysis of mitochondrial function. Oxygen consumption

rates (OCR) and extracellular acidification rates (ECAR) were measured using

the Seahorse XFe24 extracellular flux analyzer in Chapters 3 and 6, and the

Seahorse XFe96 extracellular flux analyzer in Chapter 7 (Agilent Technologies).

Preparation of the calibration plate for sensor calibration was performed

according to the manufacturer's protocol. For control plates, a media change was

performed, and for OGD plates, neurons were subjected to OGD as previously

described in Section 2.5 (30 min OGD in Chapters 3 and 6, and 90 min OGD in Chapter 7). After OGD, cultures were returned to complete neurobasal media for 1 hr. To allow cultures to equilibrate to the Seahorse assay conditions, the culture media was replaced with artificial cerebral spinal fluid [NaCl (120 mM), KCl (3.5 mM), $CaCl_2$ (1.3 mM), KH_2PO_4 (0.4 mM), $MgCl_2$ (1 mM), HEPES (20 mM), glucose (15 mM), sodium pyruvate (2 mM), and fatty acid free bovine serum albumin (BSA, Thermo Fisher; 4 mg/ml)] and placed in a 37°C incubator 1 hr prior to running the assay. Mitochondrial function was determined by measuring OCR and ECAR at baseline and after the sequential addition of oligomycin (Oligo; 2 µM), [carbonyl cyanide 4-(trifluoromethoxy) phenylhydrazone] (FCCP; 2 µM for XFe24 analyzer, 1 µM for XFe96 analyzer), Rotenone (Rot; 300 nM), and Antimycin (5 µM). Three measurements were acquired at each condition, providing an analysis of mitochondrial respiration and glycolysis for the cortical neuron cultures.

2.13 LPS-induced Cytokine Expression

Primary astrocyte cultures were seeded in 6-well plates and HBEC-5i cells were seeded in 12-well plates for LPS-induced cytokine expression experiments. Cells were first treated with Ru265 for 24 hr as described in Section 2.6. At the time of LPS treatment, half of the culture media was removed from the wells and replaced with an equal volume of fresh culture media containing 200 ng/ml of LPS (Sigma-Aldrich), resulting in a final concentration of 100 ng/ml of LPS in the wells. Cultures were incubated for with LPS for either 4 or 24 hr for astrocyte

cultures and 24 hr for HBEC-5i cells, and then treated with total RNA lysis

solution (Bio-Rad) followed by RNA extraction.

2.14 Reverse Transcription Quantitative Polymerase Chain Reaction (RT-qPCR)

Primary cortical neuron cultures and primary astrocyte cultures were seeded in 6-

well plates, and HBEC-5i cells were seeded in 12-well plates. RNA was extracted

from the cells using the Aurum total RNA minikit (Bio-Rad, cat# 732-6820)

following the spin protocol according to the manufacturer's instructions. After

elution of the RNA, the concentration and purity of RNA was estimated using the

SPECTROstar Nano spectrophotometer (BMG Labtech), and the quality and

overall integrity of the RNA was assessed using the Experion bioanalyzer along

with the RNA StdSens Analysis Kit (Bio-Rad). Only samples with RNA integrity

values of 7.5 or above were used for further analysis. Reverse transcription was

performed with the iScript complementary DNA (cDNA) synthesis kit (Bio-Rad)

using 600 ng (astrocytes), 750 ng (HBEC-5i cells), or 850 ng (neurons) of

template RNA for each sample. No template controls (without RNA template

present) and no reverse transcriptase controls (without reverse transcriptase

present) were run with every cDNA synthesis reaction. Reverse transcription

quantitative polymerase chain reaction (RT-qPCR) was performed with the

SsoFast EvaGreen Supermix kit (Bio-Rad) with GAPDH, HPRT1, and POLR2F

evaluated as reference genes for astrocytes and neurons, and β-actin and

GAPDH evaluated as reference genes for HBEC-5i cells. The annealing

temperature was optimized for each of the genes by running a melt curve

program, and a standard curve analysis was run to determine the ideal sample

concentration to be used in the RT-qPCR runs. All RT-qPCR runs were

performed with the Bio-Rad CFX96 real-time system C1000 touch thermal cycler.

The RT-qPCR protocol conditions were as follows: 95°C × 30 sec + [95°C × 5

sec + (optimal annealing temp of primer pair; usually 55°C or 60°C) × 5 sec +

plate reading] × 40 cycles + melting curve. The melting curve programme was a

2 sec stop with plate reading for every 0.5°C increase from 65 to 95°C. Data

analysis was performed with CFX Maestro software (Bio-Rad) using the ΔΔCq

method. Target genes used in RT-qPCR analysis and the primer sequences are

shown in Table 1.

Table 1. Primer sequences of target genes in RT-qPCR

Gene	Forward Primer	Reverse Primer
Hu. CCL2	CAGCCAGATGCAATCAATGCC	TGGAATCCTGAACCCACTTCT
Mu. EMRE	TTTTGCCCAAGCCGGTGAAA	TGTTAATCGTCGTCGTCGTCA
Hu. ICAM-1	GCAGACAGTGACCATCTACAGCTT	CTTCTGAGACCTCTGGCTTCGT
Hu. IL-1β	AAAGCTTGGTGATGTCTGGTC	GGACATGGAGAACACCACTTG
Mu. IL-1β	AAATGCCACCTTTTGACAGTG	CTGGATGCTCTCATCAGGACA
Hu. IL-6	ACTCACCTCTTCAGAACGAATTG	CCATCTTTGGAAGGTTCAGGTTG
Mu. IL-6	CTGCAAGAGACTTCCATCCAG	AGTGGTATAGACAGGTCTGTTGG
Hu. IL-8	ATGACTTCCAAGCTGGCCGTGGCT	TCTCAGCCCTCTTCAAAAACTTCT
Mu. IL-10	GCTCTTACTGACTGGCATGAG	CGCAGCTCTAGGAGCATGTG
Mu. MCU	CGCCAGGAATATGTTTATCCA	CTTGTAATGGGTCTCTCAGTCTCTT
Mu. MCUb	AGTTACCTTCTTCCTGTCGTTTGCG	CAGGGATTCTGTAGCCTCAGCAAGG
Mu. MCUR1	AGTTTTCAGCCCTCAGAGCAG	GGACTTTGGTCACTTCATCCATCA
Mu. MICU1	ACACCCTCAAGTCTGGCTTAT	TTCCCATCTTTGAAGTGCTTCTT
Mu. MICU2	TGGAGCACGACGGAGAGTAT	GCCAGCTTCTTGACCAGTGT
Mu. MICU3	CGACCTTCAAATCCTGCCTG	TCTGCGTGCTCTGACCTTAC
Mu. Ndufs2	CAGCCAGATATTGAATGGGCA	TGTTGGTCACCGCTTTTTCCT
Mu. TGFβ	AGCTGGTGAAACGGAAGCG	GCGAGCCTTAGTTTGGACAGG
Mu. TNFα	CAGGCGGTGCCTATGTCTC	CGATCACCCCGAAGTTCAGTAG
Mu. Uqcrc2	TGCTCCTCTGTCAAGAATCG	CAGTGTACGCCATGTTTTCC
Hu. VCAM-1	CAGTAAGGCAGGCTGTAAAAGA	TGGAGCTGGTAGACCCTCG
Hu. βActin	CCTGGCGTCGTGATTAGTGAT	AGACGTTCAGTCCTGTCCATAA
Hu. GAPDH	CACCATCTTCCAGGAGCGAGATC	GCAGGAGGCATTGCTGATGATC
Mu. GAPDH	AGGTCGGTGTGAACGGATTTG	GGGGTCGTTGATGGCAACA
Mu. HPRT1	TCAGTCAACGGGGGACATAAA	GGGGCTGTACTGCTTAACCAG
Mu. POLR2F	CGACGACTTTGATGACGTTG	GCTCACCAGATGGGAGAATC

2.15 Measurement of Ru Concentrations in Plasma and Forebrain

Adult male C57Bl/6 mice (12 weeks old) were given an intraperitoneal (i.p.) injection of saline, 1 mg/kg Ru265, or 10 mg/kg Ru265. One hour later, all animals were injected with an overdose of sodium pentobarbital (150 mg/kg, i.p.) and blood was collected by cardiac puncture. The animals were then perfused intracardially with 10 ml of normal saline to remove the blood from the brain. Forebrains were then harvested and dried at 99°C for 16 hr. Blood samples were centrifuged at 13 000 ×g for 10 min at 4°C, and plasma was collected and immediately stored at −80°C until analysis. Plasma (500 µl) and dried forebrains were placed in 3 ml of 70% nitric acid and homogenized in a microwave homogenizer. Both blood and forebrain samples were then diluted to a working nitric acid solution of 2% and analyzed by ICP-MS as described in Section 2.9 to measure Ru concentrations. Forebrain concentrations were estimated from dry weight by multiplying the ratio of wet to dry weight with 1 g of brain equalling 1 ml of water.

2.16 Hypoxic/ischemic (HI) Brain Damage

Adult male C57Bl/6 mice (8-12 weeks old) were injected i.p. with saline or 3mg/kg of Ru265 30 min prior to HI brain injury. To perform the HI injury model, mice were first anesthetized using isoflurane (3% with an oxygen flow rate of 1.5 l/min), and injected with 5 mg/kg of ketoprofen (i.p.; Cayman Chemicals) to alleviate pain following recovery. The ventral portion of the neck was shaved and

cleaned with soluprep (SoluMed Inc.) and betadiene (Purdue Frederick Inc.). A 1 cm incision was made with a scalpel to expose the sternohyoid and sternomastoid muscles, and the left carotid artery was isolated and removed from the vagus nerve by blunt dissection. The common carotid was then permanently occluded using a high temperature electrocautery pen (Bovine Instruments). Incomplete occlusions and/or animals displaying blood loss were immediately euthanized and excluded from the study. Following a 2-3 hr recovery period, animals were placed in a low oxygen chamber (8% oxygen balanced with nitrogen, flow rate 4 l/min) for 50 min, and then removed and individually housed to recover for 24 hr.

2.17 Assessment of Sensorimotor Behavioural Deficits using Neuroscores

A comprehensive behavioural assessment of sensorimotor deficits produced by HI brain injury was performed using a neuroscore scale developed by Dr. Ulrich Dirnagl (Charité – Universitätsmedizin Berlin, Germany). Scores ranged from 0 (healthy) to 56 (the worst performance in all categories) and represented the sum of scores for six general deficit categories and seven focal deficit categories. The general deficit categories included hair, ears, eyes, posture, spontaneous activity, and epileptic behaviour. The focal deficit categories included body symmetry, gait, climbing on an angled surface, circling behaviour, front limb symmetry, compulsory circling, and whisper response to light touch. Mice were scored 24 hr after HI injury by raters unaware of the treatment groups.

2.18 Measurement of Infarct Volume using 2,3,5-triphenyltetrazolium chloride (TTC) Staining

Infarct volume was evaluated using 2,3,5-triphenyltetrazolium chloride (TTC; Sigma-Aldrich) staining. Mice were euthanized 24 hr after HI injury by injection of sodium pentobarbital (150 mg/kg; i.p.) and perfused with PBS. The brain was removed and cut into 5 coronal sections (1 mm thick) spanning 1.5 to -2.5 mm from bregma. Sections were stained with PBS containing 2% TTC for 15 min at 37°C and then fixed in PBS containing 4% formaldehyde for 20 min and stored in PBS containing 1% formaldehyde until image analysis. Images were captured with a Canon PowerShot SD1400IS Digital ELPH 14.1 megapixel camera. The area encompassing the infarct for the 5 serial sections was calculated and converted into a volume using image J (version 1.48v).

2.19 Measurement of Seizure-like Behaviours

Adult male C57Bl/6 mice (10-12 weeks old) were administered an i.p. injection of either Ru265, Os245, or Os245' dissolved in saline. For the initial assessment of different doses of Ru265, animals were observed for 90 min by two raters unaware of the treatment conditions, and the duration of convulsions and frequency of seizure-like behaviours including whisker trembling, motionless staring, facial jerking, mild convulsions, and severe convulsions was recorded. When assessing the convulsive effects of Os245 and Os245', animals were observed continuously for 135 min, and the duration of convulsions observed throughout the test period was recorded. During this period, convulsions

progressed from shorter (30 sec-2 min) mild convulsions to longer (8-10 min) more severe convulsions. All mice were euthanized with an overdose of sodium pentobarbital (150 mg/kg, i.p.) at the completion of the experiments.

2.20 Assessment of Ru265-induced Convulsions in Thy1-MCU Deficient Mice

Thy1-cre/ERT2-eYFP mice (The Jackson Laboratory; Stock No: 012708) were crossed with C57Bl/6 MCU-floxed (MCU$^{fl/fl}$) mice (Dr. Jeffrey Molkentin, Philadelphia, OH, USA) to generate Thy1-creERT2-eYFP$^{+/-}$/MCU$^{fl/fl}$ mice. Mice (8-10 weeks old) received tamoxifen (80 mg/kg) once daily for 5 days by oral gavage, followed by a 3 week washout period to generate mice lacking the MCU in Thy1-expressing neurons. These Thy1-MCU deficient mice, along with Thy1-cre/ERT2-eYFP mice (Thy1 controls) were then injected with 10 mg/kg (i.p.) of Ru265, and the frequency of mild and severe convulsions was assessed over a 150 min period as previously described in Section 2.19.

2.21 Assessment of Synergism, Additivity, or Antagonism

Primary cortical neuron cultures were treated with varying concentrations of either Ru265 or PF-05180999 or both Ru265 and PF-05180999 to assess the potential synergistic interactions between these compounds. Briefly, cultures were treated with Ru265 (1, 2, 3, 5, or 10 µM) and PF-05180999 (10, 30, 50, 100, 300, or 500 nM) for 24 hr according to Section 2.6, and then subjected to OGD according to Section 2.5. Cell viability was assessed 24 hr after OGD using

the MTT assay as described in Section 2.10. The potential synergistic

interactions between the two treatments was assessed using the SynergyFinder

software (version 3.0), where the Bliss independence drug interactions model

was used (Ianevski et al., 2022). Drug combination responses were plotted as 3D

synergy maps to illustrate the potential synergistic, additive, or antagonistic

interactions of the combined treatment. This generated synergy scores for each

of the different concentrations of Ru265 + PF-05180999 that were tested. This

allowed for the assessment of the most effective co-treatment concentrations for

preserving cell viability after OGD. As per the SynergyFinder analysis, a synergy

score of < -10 was considered as antagonistic, a score from -10 to +10 as

additive, and a score > +10 as synergistic.

2.22 Statistical Analyses

A one-way ANOVA followed by group comparisons with the Tukey's post hoc test

was used to assess the effects of the various compounds used on cell viability,

cell cytotoxicity, and mRNA expression after OGD and after LPS treatment. A

two-way ANOVA followed by group comparisons with the Bonferroni's post-hoc

test was used to assess the differences in kaempferol-induced Ca^{2+} uptake with

and without Ru265 treatment. This analysis was also used to assess potential

differences in OCR and ECAR levels in cortical neuron cultures after treatment

with various compounds and subjection to OGD. Mann-Whitney U tests were

performed to assess potential differences between neuroscores and infarct

volume sizes of vehicle and Ru265 treated mice after HI injury. All statistical tests

were performed using GraphPad Prism (version 9.5.1; GraphPad Software) with

an alpha level set to 0.05. All bars represent the mean ± SD.

Chapter 3: The Cell-Permeable MCU$_{cx}$ Inhibitor Ru265 Protects Mouse Primary Cortical Neuron Cultures from OGD-induced Injury

3.1 Introduction

The inhibitory properties of Ru-based compounds on MCU$_{cx}$ activity has been well documented, and compounds such as RuRed and Ru360, the main MCU$_{cx}$ inhibitory component of RuRed, have traditionally been used to examine the effects of MCU$_{cx}$ inhibition on Ca^{2+} handling in various cell types (Broekemeier et al., 1994; Dray et al., 1990; Emerson et al., 2002; Garcia-Rivas et al., 2006). However, the use of these compounds as MCU$_{cx}$ inhibitors has been limited due to a number of drawbacks including the high number of impurities, low specificity, and neurotoxic actions of RuRed, and the challenging synthesis, and poor stability and cellular uptake of Ru360 (Cibulsky & Sather, 1999; Nathan et al., 2017; Velasco et al., 1995; Woods et al., 2019). Nevertheless, these MCU$_{cx}$ inhibitors have been useful tools to examine the effects of MCU$_{cx}$ inhibition in isolated mitochondria and permeabilized cell models. However, their ability to inhibit the MCU$_{cx}$ complex in intact cells is questionable. This has fueled the search for MCU$_{cx}$ inhibitors with improved cell-penetration.

3.2 Rationale

One recently developed MCU_{cx} inhibitor, Ru265, is a structural analogue of Ru360 (Woods et al., 2019)(Figure 3.1). MCU_{cx} inhibition by Ru265 has been well characterized in isolated mitochondria and permeabilized HEK293 cells (Woods et al., 2019). This compound has also been shown to prevent the loss of the $\Delta\Psi_m$ after hypoxia/reoxygenation in neonatal ventricular myocytes by suppressing mitochondrial Ca^{2+} overloading (Woods et al., 2019). Previous experimentation in our laboratory indicated that MCU_{cx} inhibition may be neuroprotective in cell-based and animal models of ischemic/reperfusion brain injury (Nichols et al., 2018). In the case of the former, MCU_{cx} silencing by small interfering RNA (siRNA) delivery in primary cortical neuron cultures mitigated mitochondrial respiratory deficits and viability loss after exposure to a lethal period of OGD, an *in vitro* model of ischemic/reperfusion brain injury (Nichols et al., 2018). Based on these findings, the abilities of Ru265 to inhibit mitochondrial Ca^{2+} uptake and protect primary cortical neuron cultures from OGD-induced cell death were examined.
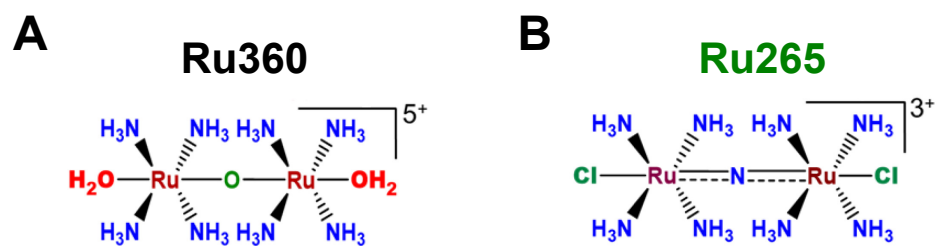
Figure 3.1. Chemical structures of Ru360 (A) and Ru265 (B)

3.3 Results

3.3.1 Ru265 Blocks Kaempferol-induced Mitochondrial Ca^{2+} Uptake

To measure mitochondrial Ca^{2+} levels, primary cultures of mouse cortical neurons were transduced on DIV5 with an AAV9 viral vector encoding the mitochondria-targeted low affinity Ca^{2+} indicator Mito-LAR-GECO1.2. After 5 days, cultures were treated with either vehicle (Type 1 sterile H$_2$O) or 10 µM of Ru265 for 4 hr before images were captured to determine the baseline level of fluorescence in the cultures (Figure 3.2A, C). The percent increase in fluorescence intensity was calculated by dividing the average fluorescence intensity of the cells observed each min from 0.5-12 min by the average baseline fluorescence intensity (0 min) and multiplying by 100 (Figure 3.2E). In control cultures pretreated with vehicle, addition of the MCU$_{cx}$ activator kaempferol (20 µM) resulted in a steady increase in fluorescent intensity that became maximal (66 ± 21.1%; mean ± SD) after 12 min (Figure 3.2B, E). Kaempferol thus produced a gradual elevation of mitochondrial Ca^{2+} uptake from 1-12 min. In contrast, Ru265 markedly suppressed the maximal rise in fluorescence intensity to 8.2 ± 5.7% (mean ± SD) at 12 min relative to that observed in vehicle-treated cells (Figure 3.2D-E). The MCU$_{cx}$ inhibitor Ru265 thus reached concentrations in cortical neuron cultures sufficient to block mitochondrial Ca^{2+} uptake.
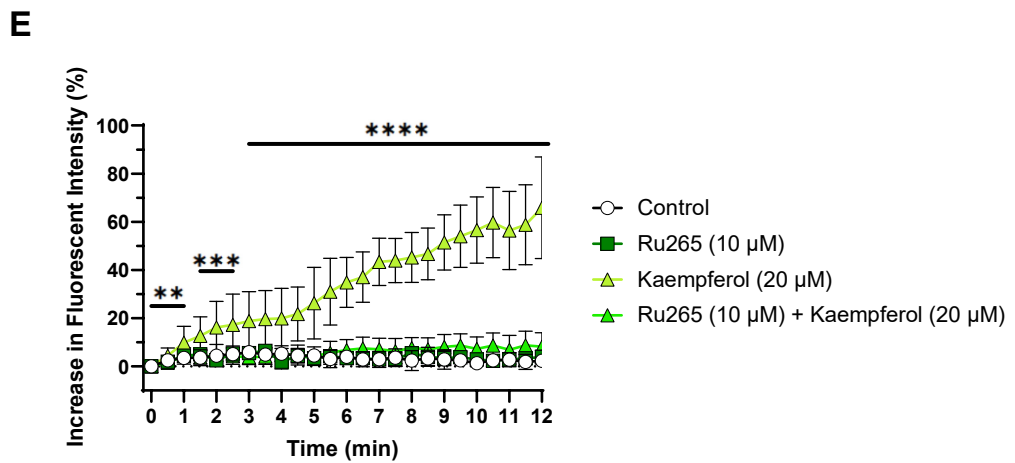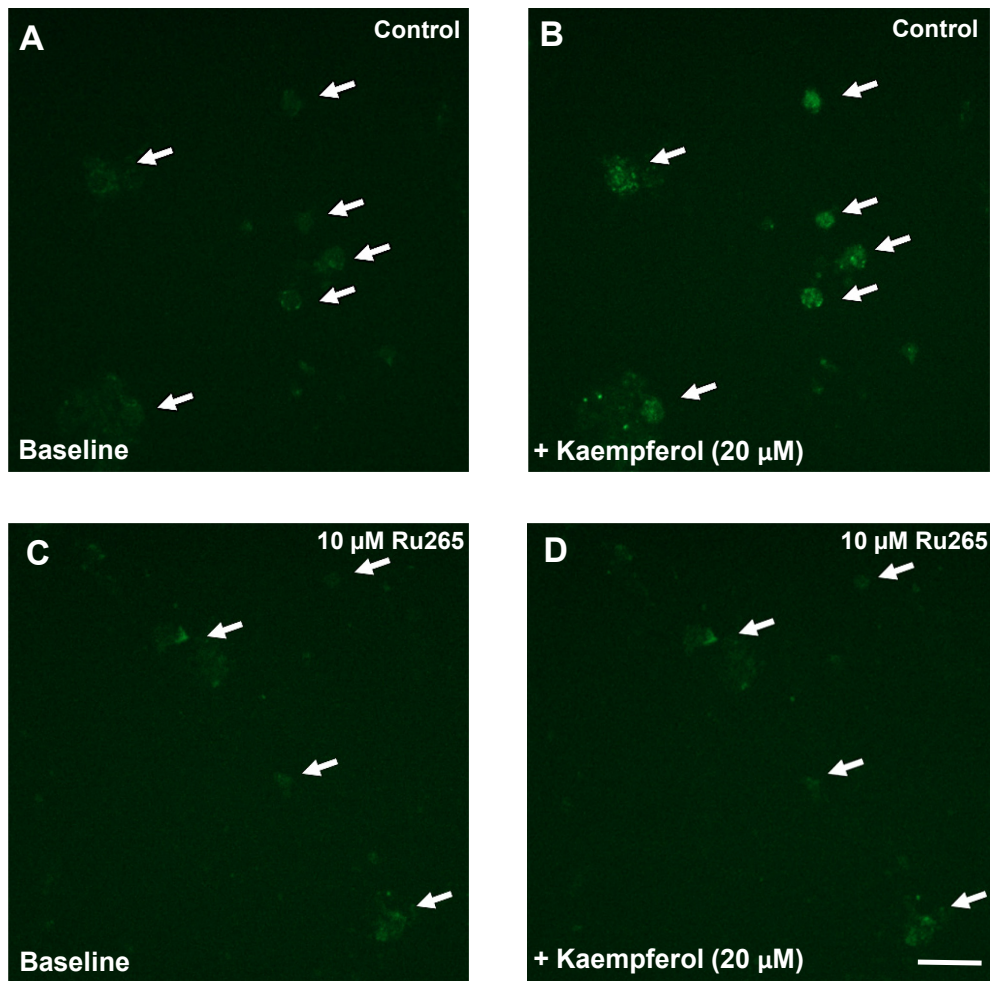
Figure 3.2. Ru265 blocks mitochondrial Ca^{2+} uptake in cortical neuron cultures

Fluorescence in primary cortical neuron cultures expressing the mitochondrial Ca^{2+} indicator Mito-LAR-GECO1.2. Representative images of cultures pretreated with vehicle or Ru265 (10 µM) for 4 hr at baseline (A and C, respectively) and 12 min after the addition of 20 µM of kaempferol (B and D, respectively). Percent increase in fluorescence intensity from 0.5-12 min relative to average baseline fluorescence intensity (0 min) (E). Each point represents the mean ± SD of data from 3 experiments, 8 images/group/experiment. **$p < 0.01$, ***$p < 0.001$ ****$p < 0.0001$; two-way ANOVA between Kaempferol (20 µM) treatment and Ru265 (10 µM) + Kaempferol (20 µM) treatment on data from 0-12 min followed by Bonferroni's post hoc test. Scale bar = 20 µm.

3.3.2 Ru265 has Superior Cellular Uptake Relative to Ru360 in Primary Cortical Neuron Cultures

Cortical neuron cultures were treated with Ru360 or Ru265 at concentrations of 2, 10, or 50 µM for 30 min or 24 hr. The cellular uptake of Ru360 and Ru265 was estimated by measuring Ru concentrations in the cell lysates with ICP-MS. Since Ru360 and Ru265 each have two Ru atoms, Ru values were divided by 2 and normalized with respect to protein concentrations to obtain ng of Ru/µg of protein. Ru265 produced concentration and time dependent increases in intracellular Ru levels (Figure 3.3A-B). The intracellular Ru levels produced by Ru265 were consistently greater than those generated by Ru360 at the equivalent concentrations and time points. Relative to Ru360 (10 µM), Ru265 (10 µM) produced intracellular Ru concentrations that were 2.5 and 8.4 times higher in the cell lysates at 30 min and 24 hr, respectively (Figure 3.3A-B). These findings indicate that Ru265 more readily enters neurons than Ru360.
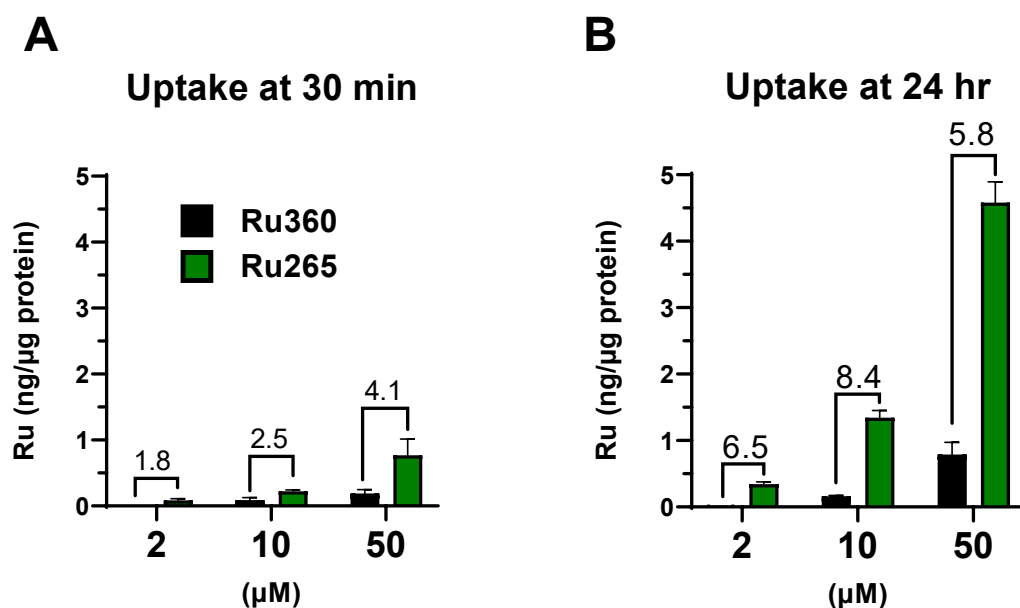
Figure 3.3. Cellular uptake of Ru265 and Ru360 in primary cortical neuron cultures

Ru concentrations in cell lysates of primary cortical neuron cultures 30 min (A) and 24 hr (B) after treatment with Ru360 (2, 10, or 50 μM) or Ru265 (2, 10, or 50 μM). Concentrations are expressed as ng of Ru per μg of protein. Bars shows the mean ± SD of data from 4 wells/group. Numbers above bars represent the fold increase in Ru265 relative to Ru360 uptake.

3.3.3 Ru265 Produces a Concentration-dependent Protection of Cortical Neurons against OGD

To assess the neuroprotective effects of MCU_{cx} inhibition by Ru265, primary cortical neuron cultures were treated with vehicle (Type 1 sterile H_2O) or increasing concentrations of Ru265 (1, 2, 3, 5, or 10 µM) for 24 hr before being subjected to 90 min of OGD. Cell viability was measured using the MTT assay and expressed as the percent relative to No OGD control cultures. In this experiment, OGD (90 min) reduced cortical neuron cell viability to 43.5 ± 9.4% (mean ± SD) according to the MTT assay (Figure 3.4A). Pre-treatment with Ru265 generated a concentration-dependent increase in cell viability at 24 hr after 90 min of OGD with near complete protection at a concentration of 10 µM (92 ± 7.9%; mean ± SD) (Figure 3.4A). Based on the log agonist versus response function in Prism (version 9.5.1), the concentration of Ru265 that produced half-maximal protection was 4.1 µM (EC_{50} = 4.1 µM). In stark contrast, even a high concentration of Ru360 (50 µM) failed to improve cortical neuron viability at 24 hr after OGD (Figure 3.4A). These findings are consistent with the considerably greater cell permeability of Ru265 compared to Ru360 (Figure 3.3). To further assess the ability of Ru265 to protect cortical neurons from OGD-induced cell death, the LDH release assay for cytotoxicity was employed. Percent cytotoxicity was calculated relative to maximal LDH release in control cultures generated by complete cell lysis. The average cytotoxicity observed 24 hr after OGD was 79 ± 3.9% (mean ± SD) in vehicle treated cells (Figure 3.4B). Pre-treatment for 24 hr before OGD with 10 µM of Ru265 reduced cytotoxicity to

26 ± 14.8% (mean ± SD) (Figure 3.4B). This suppression of LDH release further supports the neuroprotective effects of Ru265 in the OGD model.
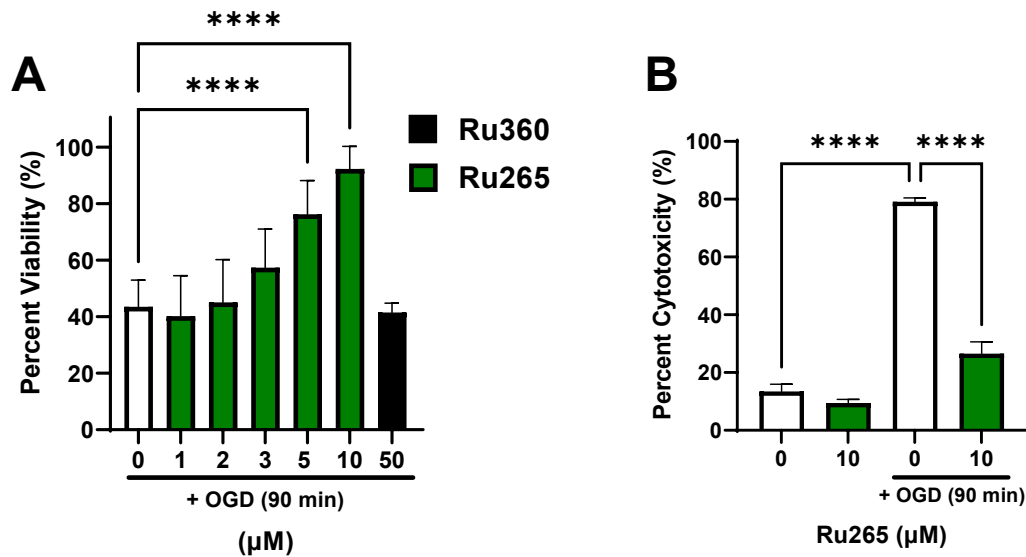
Figure 3.4. Ru265 protects cortical neuron cultures against OGD-induced cell death

The ability of Ru265 to protect cortical neuron cultures from OGD-induced cell death was measured using cell viability and cytotoxicity assays. Percent viability in cortical neuron cultures treated with vehicle (Type 1 H_2O), Ru265 (1, 2, 3, 5, or 10 µM), or Ru360 (50 µM) for 24 hr before OGD (90 min) was measured using the MTT assay 24h after OGD (A). Values represent viability relative to control (No OGD) cultures (100% cell viability). Each bar represents the mean ± SD of data from 5 experiments, 6 wells/experiment. Percent cytotoxicity in cortical neuron cultures treated with vehicle (Type 1 H_2O) or 10 µM of Ru265 for 24 hr that were left as control (No OGD) or then subjected to OGD (90 min). Cytotoxicity was measured 24 hr later by the detection of LDH levels in the media (B). Values represent cytotoxicity relative to maximal LDH release treatments (100% cell cytotoxicity). Bars represent the mean ± SD of data from 3 experiments, 4 wells/experiment. ****p<0.0001; ordinary one-way ANOVA followed by Tukey's multiple comparisons test.

3.3.4 Ru265 must be Present during OGD to Preserve the Cell Viability of Cortical Neurons

To determine when Ru265 had to be present in order to protect cortical neuron cultures subjected to OGD, the effects of seven different periods of Ru265 treatment were examined. This enabled assessment of the ability of Ru265 to protect cortical neurons against OGD injury when present: 1) 24 hr before OGD only, 2) during OGD only, 3) 24h following OGD only, 4) 24 hr before and during OGD only, 5) during and 24 hr after OGD, 6) 24 hr before OGD and 24 hr after OGD, but not during OGD, or 7) 24 hr before OGD, during OGD, and 24 hr after OGD (Figure 3.5). Treatment with Ru265 only during OGD produced near complete protection (over 90% cell viability). Extended pre-treatment or post-treatment periods did not generate additional protective benefits. However, neuroprotection failed to occur if cultures were only treated with Ru265 before or after OGD (Figure 3.5). The failure of pre-treatment alone to protect the cortical neuron cultures suggests that MCU_{cx} inhibition with Ru265 is reversible, while the ability of Ru265 to produce maximal protection when only present during OGD suggests that lethal mitochondrial Ca^{2+} overloading occurs during OGD. However, it is still possible that mitochondrial Ca^{2+} overloading may occur during the short interval (5-10 min) before Ru265 can be added to the cultures after OGD.
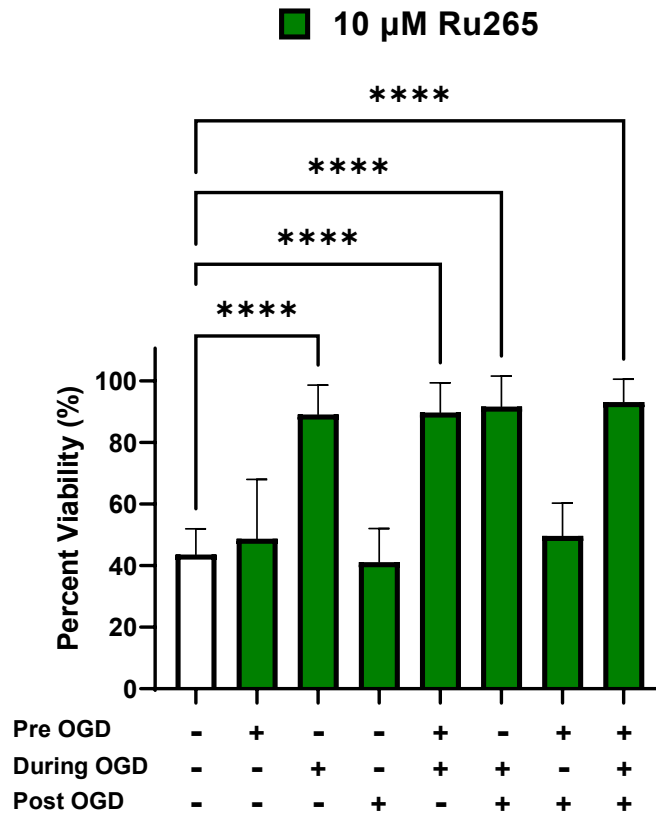
Figure 3.5. Effects of treatment with Ru265 at different time points on OGD-induced cell viability loss in cortical neuron cultures

Percent cell viability in cortical neuron cultures treated with Ru265 (10 μM) at different time points (pre OGD only, during OGD only, post OGD only, pre + during OGD, during + post OGD, pre + post OGD, or pre + during + post OGD) on OGD-induced cell viability loss. Cell viability was measured using the MTT assay 24 hr after OGD (90 min). Values represent viability relative to control (No OGD) cortical neuron cultures. Bars represent the mean ± SD of data from 3 experiments, 6 wells/experiment. ****p<0.0001; ordinary one-way ANOVA followed by Tukey's multiple comparisons test.

3.3.5 Ru265 Preserves OCR and ECAR after Exposure to OGD

The Seahorse XFe24 extracellular flux assay analyzer was used to compare the effects of vehicle (Type 1 sterile H_2O) and Ru265 on mitochondrial function by measuring OCR (Figure 3.6A-C), and glycolysis by measuring ECAR (Figure 3.7A-B) in control cortical neuron cultures (No OGD) and cultures subjected to OGD. The sequential addition of compounds that inhibit ATP synthase (oligomycin), uncouple mitochondrial respiration (FCCP), block Complex I activity (rotenone) or inhibit Complex III activity (antimycin) was performed to assess various aspects of mitochondrial function by measuring their effects on OCR. These included basal respiration, ATP production, maximal respiration, spare respiratory capacity (SRC) and proton leak (Figure 3.6A). Pilot experiments indicated that compared to the 48-well polystyrene cell culture plates used in the previous studies, a shorter period of OGD (30 min) was sufficient to produce a 50% loss of cell viability, while a higher concentration of Ru265 (50 µM) was required to suppress OGD-induced cell viability loss in the XF24 plates. Treatment of No OGD control cultures with Ru265 (50 µM) for 24 hr did not alter basal respiration, oligomycin sensitive ATP synthesis, FCCP-induced maximal respiration, or residual respiration (protein leak) observed after the sequential addition of rotenone and antimycin (Figure 3.6B). ECAR, indicative of glycolysis, was also unchanged by treatment with 50 µM of Ru265 for 24 hr (Figure 3.7A). In cultures subjected to 30 min of OGD, OCR (Figure 3.6C) and ECAR (Figure 3.7B) were markedly suppressed 2 hr later. Consistent with increased cortical

neuron viability after OGD, Ru265 completely preserved mitochondrial respiration

(Figure 3.6C) and glycolysis (Figure 3.7B) 2 hr after OGD.
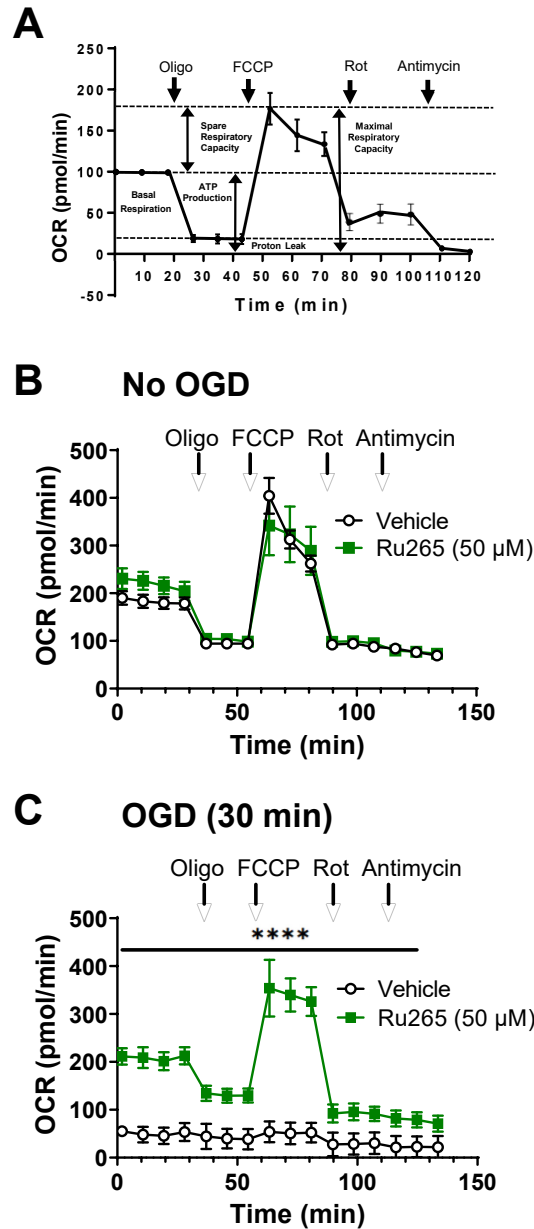
Figure 3.6. Ru265 preserves mitochondrial respiration in primary cortical neuron cultures subjected to OGD

The Seahorse XFe24 extracellular flux analyser was used to measure various aspects of mitochondrial function such as basal respiration, maximal respiration, spare respiratory, ATP production, and proton leak (A). OCR measurements in primary cortical neurons cultures after the sequential addition of Oligo (1 µM), FCCP (2 µM), Rot (300 nM) and Antimycin (5 µM) following treatment with vehicle (Type 1 H_2O) or Ru265 (50 µM) for 24 hr (B) and 2 hr after 30 min of OGD (C). Bars show the mean ± SD of data representative of 3 experiments, 5 wells/experiment. ****$p < 0.0001$; two-way ANOVA followed by Bonferroni's post hoc test.
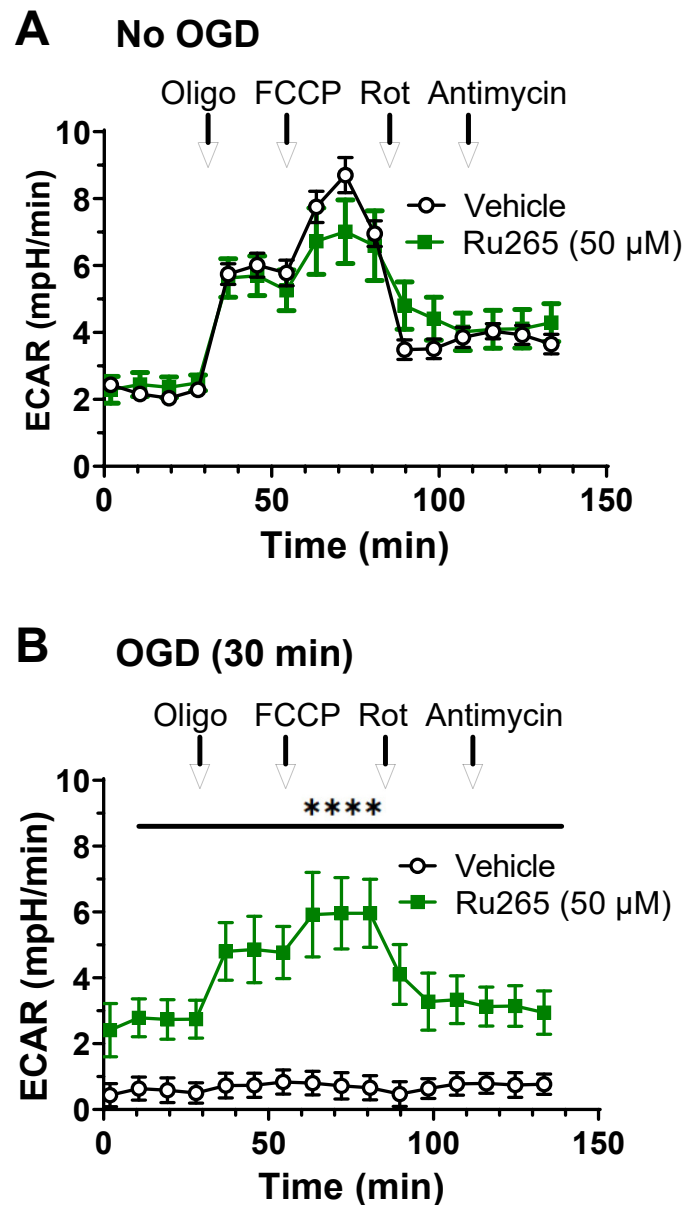
Figure 3.7. Ru265 preserves glycolysis in primary cortical neuron cultures subjected to OGD

Extracellular acidification rate (ECAR) measurements in primary cortical neurons cultures after the sequential addition of Oligo (1 µM), FCCP (2 µM), Rot (300 nM), and Antimycin (5 µM) following treatment with vehicle (Type 1 H_2O) or Ru265 (50 µM) for 24 h (A) and 2 hr after 30 min of OGD (B). Bars show the mean ± SD of data representative of 3 experiments, 5 wells/experiment. ****p <0.0001; two-way ANOVA followed by Bonferroni's post hoc test.

3.3.6 Ru265 Prevents OGD-induced Changes in MCU$_{cx}$ Subunit mRNA

Levels

RT-qPCR was used to measure the effects of OGD on relative mRNA levels of

the seven MCU$_{cx}$ subunits. Primary cortical neuron cultures were treated with

vehicle (Type 1 sterile H$_2$O) or Ru265 (10 µM) for 24 hr and either used as

control (No OGD) or subjected to OGD (90 min). RT-qPCR was performed 4 and

24 hr later. Relative to No OGD cultures, OGD reduced mRNA levels of the pore

forming subunit MCU at 24 hr (Figure 3.8A). Treatment with Ru265 (10 µM)

prevented this OGD-induced decrease in MCU mRNA levels (Figure 3.8A).

MCUb mRNA levels were also higher in Ru265 than vehicle treated cultures 4 hr

after OGD (Figure 3.8B). Ru265 also altered mRNA levels of the regulatory

subunits of the MCU$_{cx}$ in neurons subjected to OGD. MCUR1 mRNA levels were

lower in Ru265 than vehicle treated cultures at 4 and 24 hr after OGD (Figure

3.8C). OGD produced a small elevation of EMRE mRNA levels at 24 hr after

OGD that was also reversed by Ru265 (Figure 3.8D). By comparison, mRNA

levels for the gate-keeping proteins were impacted to a lesser extent by OGD

(Figure 3.9A-C). OGD did not change mRNA levels for MICU1 (Figure 3.9A) or

MICU2 (Figure 3.9B) but did reduce MICU3 mRNA levels at 24 hr (Figure 3.9C).

In keeping with the inhibitory effects of Ru265 on OGD-induced changes in

MCU$_{cx}$ subunit mRNA levels, Ru265 prevented this reduction in MICU3 mRNA

levels 24 hr after OGD (Figure 3.9C). These findings indicate that Ru265

prevents OGD-induced changes in mRNA levels for various subunits of the

MCU$_{cx}$. Although OGD did not alter MICU2 expression, MICU2 mRNA levels in

vehicle and Ru265 cultures were different at 24 hr after OGD (Figure 3.9B). This difference reflected the combined effects of a small rise in MICU2 mRNA levels in vehicle treated cultures and a minor decrease in MICU2 levels in Ru265 treated cultures.
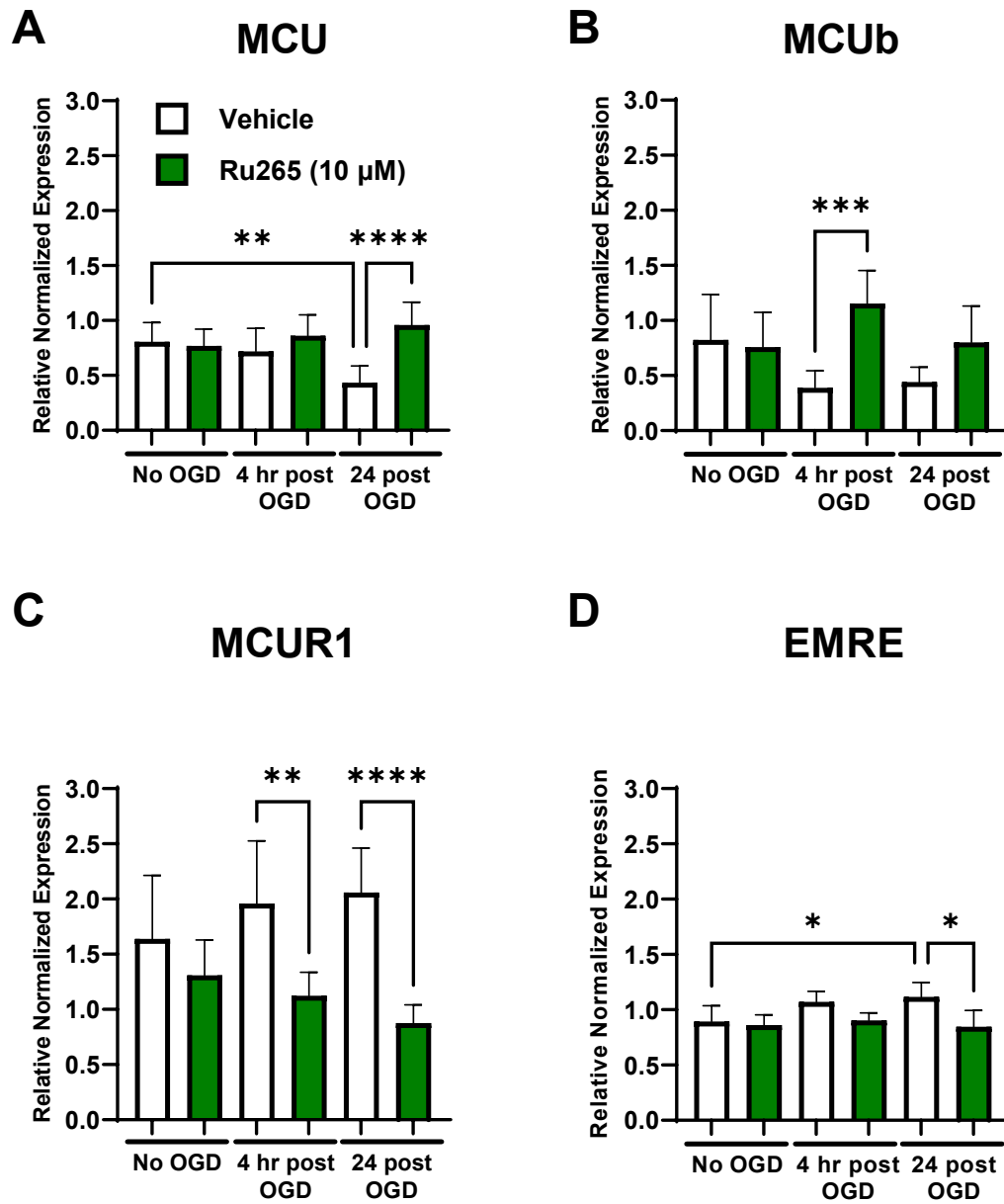
Figure 3.8. Ru265 prevents OGD-induced changes in MCU$_{cx}$ pore forming subunit and regulatory subunit mRNA levels in primary cultures of mouse cortical neurons

Primary cortical neuron cultures were treated with vehicle (Type 1 H$_2$0) or Ru265 (10 μM) for 24 hr, and mRNA levels of the subunits MCU (A), MCUb (B), MCUR1 (C), and EMRE (D) were measured using RT-qPCR in control (No OGD) cultures or cultures subjected to OGD (90 min) 4 hr or 24 hr after OGD. Bars show the mean ± SD of data from 2 experiments, 4 wells/experiment. *p<0.05, **p<0.01, ***p<0.001, ****p<0.0001; ordinary one-way ANOVA followed by Tukey's multiple comparisons test.
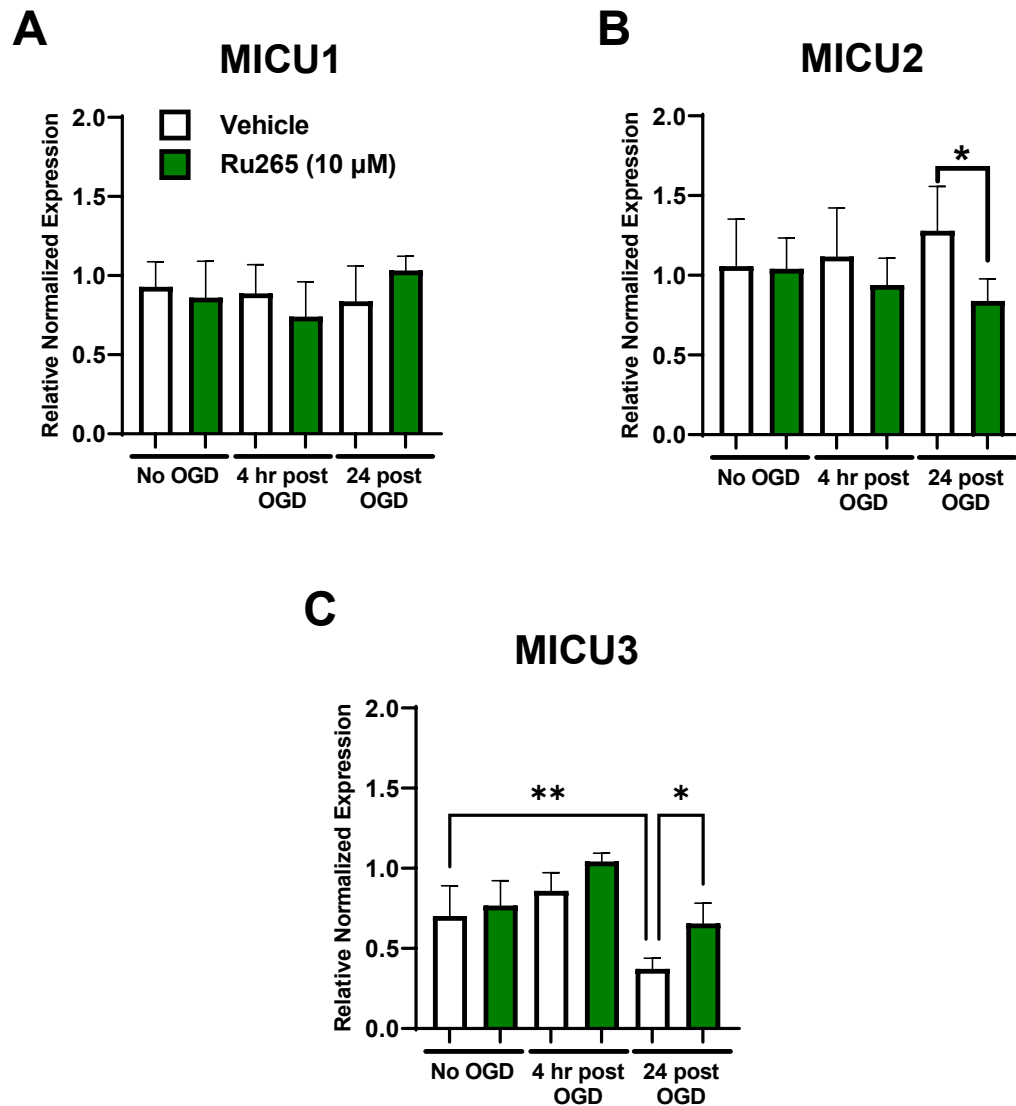
Figure 3.9. Ru265 reduces OGD-induced changes in MICU subunit mRNA levels in primary cultures of mouse cortical neurons

Primary cortical neuron cultures were treated with vehicle (Type 1 H_2O) or Ru265 (10 µM) for 24 hr and mRNA levels of the subunits MICU1 (A), MICU2 (B), and MICU3 (C) were measured in control (No OGD) cultures or cultures subjected to OGD (90 min). RT-qPCR was performed 4 hr or 24 hr after OGD. Bars show the mean ± SD of data from 2 experiments, 4 wells/experiment. $*p<0.05$, $**p<0.01$; ordinary one-way ANOVA followed by Tukey's multiple comparisons test.

3.3.7 Ru265 Preserved Complex III Subunit 2 mRNA Levels in Mouse Cortical Neuron Cultures Subjected to OGD

RT-qPCR was used to measure the effects of OGD on the relative mRNA levels of subunit 2 of Complex I NADH dehydrogenase (Figure 3.10A) and subunit 2 of Complex III Cytochrome b-c1 (Figure 3.10B). Primary cortical neuron cultures were treated with vehicle (Type 1 sterile H_2O) or Ru265 (10 µM) and left as control (No OGD) or subjected to OGD (90 min) 24 hrs later. Levels of NADH dehydrogenase and Cytochrome b-c1 mRNAs were measured 4 hr and 24 hr post OGD and at the corresponding time points for No OGD cultures. Relative to No OGD cultures, OGD did not alter the mRNA levels of Complex I subunit 2 (Figure 3.10A) at 4 and 24 hrs, but reduced mRNA levels of Complex III subunit 2 (Figure 3.10B) 24 hr after OGD. Compared to No OGD cultures, Ru265 (10 µM) completely prevented OGD-induced reductions in Complex III subunit 2 mRNA levels (Figure 3.10B).

A **Complex I Subunit 2**

B **Complex III Subunit 2**
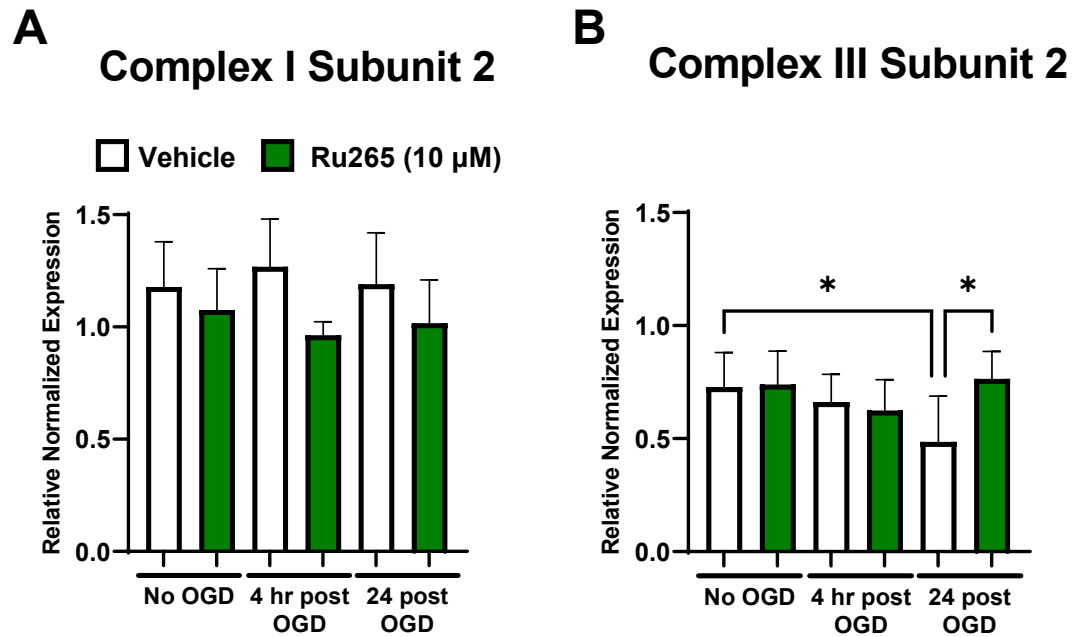
Figure 3.10. Effects of Ru265 on ETC complex subunit mRNA levels in cortical neuron cultures exposed to OGD

Primary cortical neuron cultures were treated with vehicle (Type 1 H_2O) or Ru265 (10 µM) for 24 hr and mRNA levels of subunit 2 of complex I of the ETC (A) and subunit 2 of complex III of the ETC (B) were measured using RT-qPCR in control (No OGD) cultures or cultures subjected to OGD (90 min) 4 hr or 24 hr after OGD. Bars show the mean ± SD of data from 2 experiments, 4 wells/experiment. *$p < 0.05$; ordinary one-way ANOVA followed by Tukey's multiple comparisons test.

3.4 Discussion

3.4.1 Inhibition of Mitochondrial Ca^{2+} Uptake with Ru265

Genetically encoded fluorescent Ca^{2+} indicators are useful tools for imaging changes in the concentration of Ca^{2+} associated with intracellular signalling pathways (Wu et al., 2014). The Ca^{2+} indicator, Mito-LAR-GECO1.2, has been optimized for the detection of mitochondria Ca^{2+} levels (Wu et al., 2014). The quantification of fluorescence in primary cortical neuron cultures treated with an AAV9 viral vector encoding this indicator was used to measure mitochondrial Ca^{2+} levels (Wu et al., 2014). In these cultures, mitochondrial Ca^{2+} uptake via the MCU_{cx} was stimulated through the addition of the dietary flavonoid Kaempferol. Kaempferol has been shown to directly stimulate MCU_{cx} activity (Montero et al., 2004). Kaempferol produced a rapid increase of fluorescent intensity in these cultures, indicating an increase in mitochondrial Ca^{2+} uptake via the MCU_{cx}. Treatment with Ru265 resulted in a near complete absence of kaempferol-induced fluorescence. This finding indicates that Ru265 blocks mitochondrial Ca^{2+} uptake in cortical neurons by inhibiting the MCU_{cx}.

3.4.2 Ru265 has Superior Cellular Uptake Relative to Ru360 in Primary Cortical Neuron Cultures

Ru265 produced concentration- and time-dependent increases in intracellular Ru levels that were greater than those generated by Ru360 at the equivalent concentrations and time points. Assuming protein and water respectively account for about 20% and 70% of cortical neuron mass, it was estimated that cortical

neurons exposed to Ru265 (10 µM) for 30 min generated intracellular

concentrations that approached 100 nM. These findings both confirm and extend

previous data demonstrating the superior uptake of Ru265 over Ru360 in HeLa

and HEK293 cells, and demonstrates that the modifications made to Ru360,

such as substituting the oxygen atom that bridges the two Ru molecules with a

nitrogen atom and exchanging the two carboxyl ligands for chloride ligands,

improved its cellular uptake by neurons (Woods et al., 2019). By comparison to

HeLa and HEK293 cells treated with Ru265 (50 µM) for 24 hr (Woods et al.,

2019), intracellular Ru concentrations were over 90 times higher in cortical

neurons. It is possible that the methodological differences of using graphite

furnace absorption spectroscopy instead of ICP-MS to measure Ru in the cell

lysates may have accounted for these differing findings. Alternatively, the high

metabolic demands imposed by excitatory neurotransmission in cortical neurons

after 12 days in culture (Zeiger et al., 2011) may have enhanced Ru265 uptake

by multiple mechanisms, such as organic anion transporters, calcium

exchangers, and voltage-gated calcium channels (Charuk et al., 1990; Puckett et

al., 2010; Tapia & Velasco, 1997). The supra-linear increases in intracellular Ru

concentrations generated by 10 µM of Ru265 compared to 10 µM of Ru360 from

30 min to 24 hr may reflect multiple uptake mechanisms for Ru265 relative to

Ru360.

3.4.3 Ru265 Produces Concentration-dependent and Time-dependent Protection against OGD Injury

Primary cortical neuron cultures subjected to OGD were used to model neuronal cell death resulting from ischemic reperfusion injury (Zeiger et al., 2011). In these cultures, a 90 min period of OGD was determined to produce a consistent and sufficient cell death (~50%) in neuron cultures. Treatment with Ru265 ($\geq$ 5 µM) during OGD prevented cell death 24 hr after OGD. By contrast, Ru360 (1-50 µM) was unable to improve cortical neuron viability 24 hr after OGD. These results further support the superior potency and improved cell permeability of Ru265 over Ru360. The cellular uptake studies suggest that Ru360 fails to protect against OGD-induced cell viability loss because it does not reach sufficient intracellular concentrations to block the MCU_{cx}. This likely explains why Ru630 is ineffective at preventing mitochondrial Ca^{2+} overloading and preserving cell viability in intact cells.

Next, the effects of adding Ru265 at different time points on OGD-induced cell viability loss was examined to gain a better understanding of the temporal effects of MCU_{cx} inhibition on cell survival. Ru265 only protected against OGD-induced cell death when this MCU_{cx} inhibitor was present during OGD. When present before and/or after OGD only, Ru265 was completely ineffective at protecting neuron cultures. This demonstrates that Ru265 reversibly inhibits the MCU_{cx} since there is no protection observed when cultures are pretreated with Ru265 and then washed and placed in Ru265-free GBSS during OGD. This also

suggests that toxic mitochondrial Ca^{2+} overloading by the MCU_{cx} occurs primarily during OGD and not reperfusion. Given that mitochondrial Ca^{2+} overloading is an early trigger of multiple cell death effectors, these findings provide a potential explanation for the repeated failure of putative neuroprotectants in the clinic (Gladstone et al., 2002).

3.4.4 Ru265 Preserves OCR and ECAR after Exposure to OGD

The effects of OGD and Ru265 treatment on key parameters of mitochondrial function were assessed in cortical neuron cultures using the Seahorse XFe24 extracellular flux analyser. This assay creates a transient microchamber just above the cell monolayer enabling the measurement of oxygen concentrations associated with respiring neurons in real time (Brand & Nicholls, 2011). The XFe24 allows for the sequential addition of different ETC inhibitors to assess different aspects of mitochondrial function as determined by changes in OCR (Brand & Nicholls, 2011). ECAR is also measured by the XFe24 and provides a readout of glycolysis. Oligomycin (ATP synthase inhibitor; 2 µM) blocks oxidative phosphorylation, providing a measure of cellular ATP production (Brand & Nicholls, 2011). The remaining OCR after the addition of oligomycin indicates the proton leak across the mitochondrial membrane (Brand & Nicholls, 2011; Divakaruni & Brand, 2011). To determine the maximal OCR that cells can sustain, the proton uncoupler FCCP (2 µM) was injected (Brand & Nicholls, 2011). Finally, the addition of rotenone (complex I inhibitor; 300nM) and antimycin (complex III inhibitor; 5 µM) was performed to completely inhibit

mitochondria respiration (Brand & Nicholls, 2011). The difference between basal

and maximal OCR is referred to as spare respiratory capacity (SRC). This is a

measure of overall mitochondria integrity and function because SRC enables

neurons to respond rapidly to the increased metabolic demands associated with

neurotransmission (Brand & Nicholls, 2011; Desler et al., 2012). Treatment with

Ru265 for 24 hr had no effect on any of the mitochondrial respiration parameters

in No OGD cultures. In cultures exposed to OGD, OCR and ECAR were

markedly suppressed. Consistent with the protection from OGD-induced cell

death seen in earlier experiments, Ru265 completely preserved mitochondrial

respiration and glycolysis 2 hr after OGD. Ru265 also prevented the OGD-

induced loss of SRC, signifying that the neurons were still functioning well and

had maintained mitochondrial integrity and health. These findings indicate that

MCU_{cx}-mediated mitochondrial Ca^{2+} overloading is a pivotal pathological event in

the collapse of mitochondrial function after OGD.

3.4.5 Ru265 Prevents OGD-induced Changes in MCU_{cx} Subunit mRNA Levels

The MCU_{cx} is a transmembrane multi-protein complex that mediates high-

capacity mitochondrial Ca^{2+} uptake. Briefly, this complex is a dynamic structure

consisting of pore forming subunits and regulatory subunits that work together

and play an integral role in the formation of the channel and its response to

changes in intracellular Ca^{2+} levels. The pore of the complex is formed by a

homo-oligomer of four MCU subunits (Baradaran et al., 2018; Fan et al., 2020;

Nguyen et al., 2018; Yoo et al., 2018). Each MCU subunit has a short hydrophilic acid linker composed of a DIME motif that separates the two transmembrane domains of the subunit (Baughman et al., 2011; Cao et al., 2017; Stefani et al., 2011). This motif is strategically located on the pore entrance and appears to mediate the highly selective gating of Ca^{2+} by the MCU_{cx} (Cao et al., 2017; Oxenoid et al., 2016; Yoo et al., 2018). In some cases, one or more of the 4 MCU subunits is replaced by a MCUb transmembrane subunit, and this displacement has been shown to reduce Ca^{2+} conductance by the MCU_{cx} (Lambert et al., 2019; Raffaello et al., 2013). The regulatory subunit EMRE is a transmembrane protein that acts as an essential regulator and stabilizer of the MCU_{cx} (Garbincius & Elrod, 2022; Mallilankaraman et al., 2012; Tsai et al., 2016). MCUR1 is also a regulatory subunit of the MCU_{cx} that when absent reduces mitochondrial Ca^{2+} uptake, but does not appear to be essential for MCU_{cx} activity (Garbincius & Elrod, 2022; Mallilankaraman et al., 2012; Tsai et al., 2016).

The three MICU proteins, MICU1, MICU2, and MICU3, are involved in enhancing channel activity in response to a rise in intracellular Ca^{2+} levels (Garbincius & Elrod, 2022; Walters & Usachev, 2023). Recent studies suggest that these MICU proteins might modify the gating properties of the MCU_{cx} in such a way that it allows the channel to spend more time in the open state (Fan et al., 2020; Garg et al., 2021). Under normal conditions, MICU1 exists as a hexamer, but a rise in Ca^{2+} levels in the intermembrane space triggers these hexamers to dissociate (Gottschalk et al., 2019; Gottschalk et al., 2022). MICU1 then forms homodimers

76

or heterodimers with MICU2 or MICU3 that facilitates mitochondrial Ca^{2+} uptake by promoting a redistribution of other MCU_{cx} subunits to the inner boundary membrane compartment of the inner mitochondrial membrane (Gottschalk et al., 2019; Gottschalk et al., 2022). This redistribution and restructuring of subunits increases MCU_{cx} activity during high Ca^{2+} levels through promoting and maintaining the open conformation of the complex (Garg et al., 2021; Gottschalk et al., 2022). The intricacy of the interactions between these different subunits highlights the dynamic nature of this complex, and indicates how changes in the spatial relationships between these subunits allow the MCU_{cx} to adapt in response to environmental changes.

There is limited knowledge about the transcriptional regulation of MCU_{cx} subunits. However, it is clear that mRNA levels for the MCU, MCUb, EMRE, MCUR1,MICU1, MICU2, and MICU3 subunits vary between tissues and cell types, and that their expression is influenced by cell stress and changes in intracellular Ca^{2+} levels (Markus et al., 2016; Patel et al., 2023; Watanabe et al., 2022). In keeping with these findings, OGD also altered MCU_{cx} subunit mRNA levels in cortical neuron cultures. After OGD, mRNA levels for MCU, MCUb, and MICU3 decreased, EMRE increased and MCUR1, MICU1, and MICU2 remained relatively constant. These changes may reflect compensatory mechanisms designed to oppose the deleterious effects of an excessive rise in cytosolic Ca^{2+} levels produced by OGD. A reduction in MCU mRNA levels might therefore reflect an attempt to decrease injurious MCU_{cx} overactivity. Compared to

MICU1/MICU2 dimers, MICU1/MICU3 dimers have a lower Ca^{2+} threshold for MCU_{cx} activation (Patron et al., 2019). A reduction of MICU3 at 24 hr after OGD would therefore lower the risk of toxic mitochondrial Ca^{2+} overloading.

Expression of the dominant negative subunit MCUb has also been shown to increase 24 hr after heart failure and cardiac ischemia/reperfusion injury, perhaps as a protective mechanism against Ca^{2+} overloading (Lambert et al., 2019). However, MCUb levels did not increase after OGD signifying a possible difference in the regulation of this subunit in neurons relative to cardiac cells after ischemic injury. Less is known about the role of MCUb in neurons, but it has been reported that cortical neurons express relatively low levels of MCUb, suggesting that it does not play an important role in regulating MCU_{cx} activity in cortical neurons (Markus et al., 2016; Walters & Usachev, 2023). MCUR1 has been shown to regulate proper complex formation. However, there is conflicting data on how MCUR1 regulates mitochondrial Ca^{2+} uptake. For example, MCUR1 may increase mitochondrial Ca^{2+} uptake by secondary actions on the respiratory protein complexes that enhance the $\Delta\Psi_m$, which might provide the driving force for mitochondrial Ca^{2+} uptake rather than direct actions on the MCU_{cx} (Garbincius & Elrod, 2022; Mallilankaraman et al., 2012; Patel et al., 2023; Tomar et al., 2016).

Although it is not yet clear how variations in subunit mRNA expression occur after OGD, these changes emphasize the dynamic nature of the MCU_{cx}. In all

cases where there was a change in subunit expression after OGD, Ru265 completely prevented them. This suggests that Ru265 stabilizes MCU$_{cx}$ subunit expression by preventing mitochondrial Ca^{2+} overloading. The ability of Ru265 to prevent perturbations in MCU$_{cx}$ subunit expression may therefore contribute to the neuroprotective actions of this compound.

3.4.6 Ru265 Preserved Complex III Subunit mRNA Levels after Exposure to OGD

Complex I (NADH dehydrogenase) and Complex III (Cytochrome b-c1) are members of the ETC that pump protons into the intermembrane space, thus contributing to the generation of the $\Delta\Psi_m$, which drives ATP production (Zhao et al., 2019). There were no changes in the mRNA levels of subunit 2 of Complex I after OGD, and a modest reduction in subunit 2 of Complex III mRNA levels 24 hr after OGD. This suggests that the reduction in mitochondrial respiration seen in cortical neuron cultures 2 hr after OGD in the Seahorse assay is not simply due to a decrease in ETC complex levels, but also supressed ETC activity (Brand & Nicholls, 2011). Consistent with the preservation of MCU$_{cx}$ subunit expression after OGD, Ru265 also maintained complex III mRNA levels at normal levels 24 hr after OGD. This finding further supports the ability of Ru265 to protect cortical neurons from OGD-induced death by preserving mitochondrial function.

Chapter 4: OGD-induced Viability Loss and LPS-induced Cytokine Expression in Mouse Astrocyte Cultures and LPS-induced Cytokine Expression in Human Brain Endothelial Cell Cultures are Suppressed by Ru265

4.1 Introduction

In addition to neuronal cells, other cell types of the NVU are susceptible to ischemic damage by mitochondrial Ca^{2+} overloading. In particular, damage to multiple NVU components, such as endothelial cells, pericytes, microglia, and astrocytes is hallmark of stroke injury (Jayaraj et al., 2019). These cellular components of the NVU work in unison to rapidly adjust CBF in support of the dynamic metabolic demands required for neurotransmission (Longden et al., 2016; Muoio et al., 2014). As a result, the NVU relies heavily on mitochondria to rapidly sequester large amounts of Ca^{2+} and produce the massive amounts of ATP necessary for neurovascular coupling (Iadecola, 2017). This renders the NVU extremely vulnerable to injurious mitochondrial Ca^{2+} overloading by cerebral ischemia (An et al., 2021; Duchen, 2012; Reichard & Asosingh, 2019). Finding ways to protect the various cellular components of the NVU from injury is thus considered to be crucial for the effective treatment of stroke (Iadecola, 2017).

The importance of the NVU has encouraged experimentation in this thesis to assess the protective potential of Ru265 in other cell types, namely mouse

primary cortical astrocyte cultures and a human brain endothelial cell line (HBEC-5i). Astrocytes are glial cells found in the brain and spinal cord. They play a variety of roles critical for brain function such as providing energy to neurons, regulating ion homeostasis, maintaining BBB integrity, and supporting neurogenesis (Bantle et al., 2021; Lo et al., 2003; Sofroniew & Vinters, 2010). Endothelial cells comprise the wall of cerebral blood vessels and form tight junctions that create a physical barrier which impedes the paracellular diffusion of molecules, ions, and potentially harmful substances into the brain (Iadecola, 2004; Stamatovic et al., 2008). A wide variety of transports are expressed by endothelial cells that move nutrients into the brain and waste products out of the brain (Iadecola, 2004; Stamatovic et al., 2008). Endothelial cells in the brain are surrounded by astrocytes that extend endfeet which communicate with other cell types in the NVU through the release of growth and vasoactive factors that maintain integrity of the NVU and regulate CBF (Goldman & Chen, 2011; Muoio et al., 2014; Shen et al., 2003).

One characteristic of both astrocytes and endothelial cells is that they are able to release pro- and anti-inflammatory cytokines in response to dysregulation of the BBB and tissue damage (Choi et al., 2014; Verma et al., 2006). Astrocytes become activated in response to pathological changes by a process termed reactive astrogliosis, resulting in their release of different extracellular molecules, including neurotrophic factors, inflammatory factors, and cytotoxins (Li et al., 2019; Sofroniew & Vinters, 2010). Depending on the signals they receive from

the surrounding tissue, astrocytes can have pro-inflammatory effects that further exacerbate injury, or exert anti-inflammatory effects which facilitate recovery. These two astrocyte phenotypes are generally classified as A1 (pro-inflammatory) or A2 (anti-inflammatory). The balance between these two phenotypes tends to change from A1 to A2 with increasing time after an injury (Jayaraj et al., 2019; Li et al., 2019). For example, it is well documented that high levels of pro-inflammatory cytokines such as IL-1β, TNFα, and IL-6 are produced during the acute phase (first 7 days) after an ischemic stroke, which promote secondary injury in the brain (Grefkes & Fink, 2020; Jayaraj et al., 2019). This is followed by an increase in the production of TGFβ and IL-10 that reduces inflammation and promotes cell survival (Mayo et al., 2016; Norden et al., 2014). Brain endothelial cells also secrete pro-inflammatory cytokines and trophic factors that promote brain injury and repair, respectively (Smyth et al., 2018; Verma et al., 2006).

LPS, a component of the cell membrane of gram-negative bacteria, stimulates cytokine release from astrocytes and endothelial cell cultures by activating the TLR4 (Skrzypczak-Wiercioch & Sałat, 2022). LPS treatment has therefore been used to model the inflammatory response of cells to TLR4 stimulation implicated in ischemic brain injury (Skrzypczak-Wiercioch & Sałat, 2022). In this chapter, the ability of Ru265 to protect mouse primary cortical astrocytes from OGD-induced cell death and reduce LPS-induced cytokine release in astrocyte cultures and HBEC-5i cells were assessed. The studies were designed to determine whether

MCU$_{cx}$ inhibition protects these two major cellular components of the NVU, as well as to gain a better understanding of the potential anti-inflammatory benefits of Ru265 in the treatment of ischemic brain injury.

4.2 Results

4.2.1 Ru265 Protects Mouse Primary Astrocyte Cultures Against OGD-induced Injury

To examine the protective potential of Ru265 in a different neural cell subtype, primary cultures of mouse astrocytes were treated with vehicle (Type 1 sterile H$_2$O) or 5, 10, or 20 μM of Ru265 for 24 hr before OGD (4 hr). Cell viability was measured using the MTT assay 24 hr later (Figure 4.1). This longer (4 hr) period of OGD was necessary to achieve about a 50% reduction in the cell viability of astrocyte cultures. Percent viability was calculated relative to No OGD control cultures. Treatment with 5, 10, and 20 μM of Ru265 increased cell viability after OGD from 49.6 ± 4.7% to 68.7 ± 1.9%, 81.4 ± 6%, and 82.1 ± 5.8% (mean ± SD), respectively. Relative to cell viability values for vehicle-treated cultures after OGD, all of these values for Ru265-treated cells were greater (Figure 4.1). These findings extend the protective effects of Ru265 against OGD-induced injury to a second neural cell subtype.
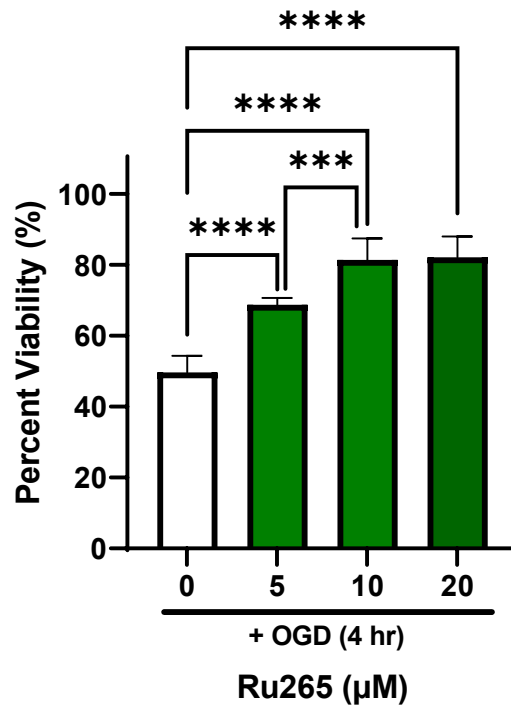
Figure 4.1. Ru265 preserves cell viability in primary astrocyte cultures subjected to OGD

The ability of Ru265 to protect primary astrocyte cultures from OGD-induced cell viability loss was measured using the MTT assay. Percent viability in astrocyte cultures treated with vehicle (Type 1 H_2O) or Ru265 (5, 10, or 20 µM) for 24 hr before OGD (4 hr) was measured 24 hr after OGD. Values represent viability relative to control (No OGD) cultures (100% cell viability). Bars represent the mean ± SD of data from 3 experiments, 5 wells/experiment. ***$p<0.001$, ****$p<0.0001$; ordinary one-way ANOVA followed by Tukey's multiple comparisons test.

4.2.2 Ru265 Suppressed LPS-induced Increases of Pro-inflammatory

Cytokine mRNA Levels in Primary Cultures of Mouse Astrocytes

RT-qPCR was used to measure LPS-induced increases of pro-inflammatory

cytokine mRNA levels in primary astrocyte cultures. Primary mouse astrocyte

cultures were treated with vehicle (Type 1 sterile H_2O) or Ru265 (10 or 20 µM)

for 24 hr before the addition of PBS (control) or LPS (100 ng/ml) followed by the

measurements of mRNA levels for the pro-inflammatory cytokines IL-1β, TNFα,

and IL-6 4 hr and 24 hr later (Figures 4.2A-F). At 4 and 24 hr post LPS treatment,

mRNA levels for these pro-inflammatory cytokines were elevated compared to

the control cultures (Figures 4.2A-F). Ru265 (10 and 20 µM) failed to suppress

LPS-induced increases in IL-1β or IL-6 expression at 4 hr (Figure 4.2A and E).

However, Ru265 reduced mRNA levels for IL-1β at a concentration of 10 µM

(Figure 4.2B) and IL-6 at concentrations of 10 and 20 µM 24 hr after LPS

compared to cultures treated with vehicle (Figure 4.2F). By contrast, LPS-

induced TNFα expression was only reduced by the higher concentration of

Ru265 (20 µM) 4 and 24 hr after LPS treatment (Figure 4.2C and D).

Nevertheless, there did appear to be a concentration dependent decrease in the

mRNA expression of TNFα with 10 and 20 µM of Ru265. These results suggest

that Ru265 may reduce inflammation by suppressing the induction of pro-

inflammatory cytokine gene expression in astrocytes.
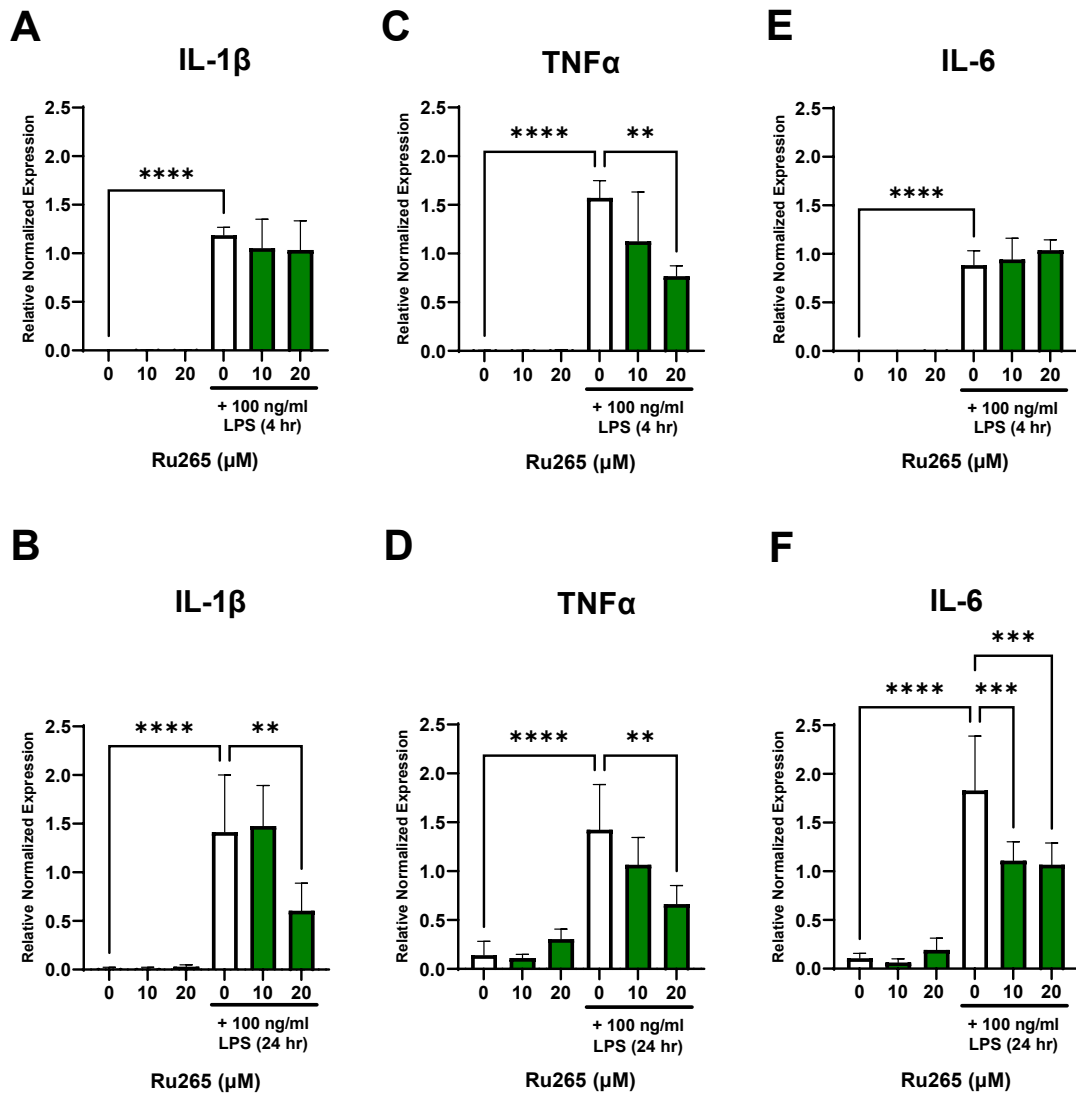
Figure 4.2. Effects of Ru265 on LPS-induced IL-1β, TNFα, and IL-6 mRNA levels in primary astrocyte cultures

Primary astrocyte cultures were treated with vehicle (Type 1 H$_2$0) or Ru265 (10 or 20 µM) for 24 hr before the addition of PBS (control) or LPS (100 ng/ml). The mRNA levels of IL-1β (A and B), TNFα (C and D), and IL-6 (E and F) were then measured 4 hr (A, C, and E), or 24 hr (B, D, and F) after the addition of PBS or LPS using RT-qPCR. Bars show the mean ± SD of data from 1 experiment (4 wells) for the 4 hr time point and 3 experiments (3 wells/experiment) for the 24 hr time points. **p<0.01, ***p<0.001, ****p<0.0001; ordinary one-way ANOVA followed by Tukey's multiple comparisons test.

4.2.3 Ru265 Increased TGFβ and IL-10 Gene Expression in Primary Cultures of Mouse Astrocytes

Using RT-qPCR, mRNA levels of the anti-inflammatory cytokines TGFβ and IL-10 were measured in primary cultures of mouse astrocytes that received vehicle (Type 1 sterile H_2O) or Ru265 (10 or 20 μM) for 24 hr before the addition of PBS (control) or LPS (100 ng/ml) (Figure 4.3A-D). After both 4 and 24 hr of LPS treatment there was an increase in TGFβ but not IL-10 mRNA levels (Figure 4.3A-D). Interestingly, TGFβ and IL-10 mRNA levels were increased 48 hr after the addition of Ru265 (20 μM) (Figure 4.3B and D). However, Ru265 (10 and 20 μM) mitigated the increases in TGFβ mRNA levels in LPS-treated cultures at 4 and 24 hr (Figure 4.3A and B). Compared to LPS-treated cultures, IL-10 mRNA levels were higher in LPS-treated cultures first treated with Ru265 (10 and 20 μM) at 4 hr (Figure 4.3C). Treatment with 20 μM of Ru265 also elevated IL-10 mRNA levels 24 hr after LPS treatment (Figure 4.3D). Hence, unlike the pro-inflammatory cytokines IL-1β, TNFα, and IL-6, Ru265 alone elevated mRNA levels of TFGβ and IL-10, cytokines known to have anti-inflammatory and neuroprotective properties.
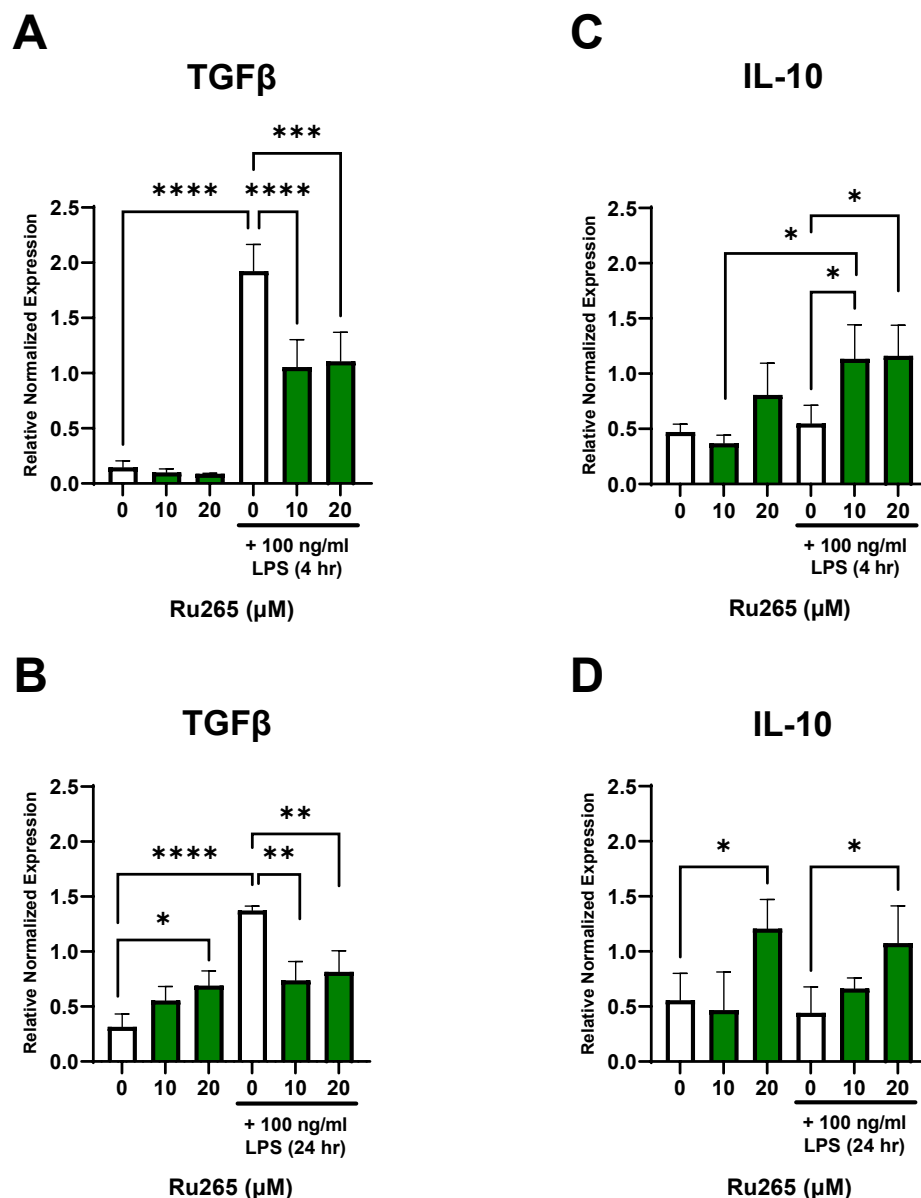
Figure 4.3. Effects of Ru265 on LPS-induced TFGβ and IL-10 mRNA levels in primary astrocyte cultures

Primary astrocyte cultures were treated with vehicle (Type 1 H_2O) or Ru265 (10 or 20 µM) for 24 hr before the addition of PBS (control) or LPS (100 ng/ml). TFGβ (A and B) and IL-10 (C and D) mRNA levels were measured 4 hr (A and C) or 24 hr (B and D) after the addition of PBS or LPS using RT-qPCR. Bars show the mean ± SD of data from 1 experiment (4 wells) for the 4 hr time point and 3 experiments (3 wells/experiment) for the 24 hr time point. *p<0.05, **p<0.01, ***p<0.001, ****p<0.0001; ordinary one-way ANOVA followed by Tukey's multiple comparisons test.

4.2.4 Ru265 Suppressed the Induction of Pro-inflammatory Cytokine and Adhesion Molecule mRNA Levels by LPS in HBEC-5i Cells

HBEC-5i cells, a human brain endothelial cell line, was used to further examine the anti-inflammatory effects of Ru265. HBEC-5i cells were treated with vehicle (Type 1 sterile H_2O) or increasing concentrations of Ru265 (3, 5, or 10 µM) for 24 hr before the addition of PBS (control) or LPS (100 ng/ml) for 24 hr (Figure 4.4A-F). Cells were then collected for RT-qPCR analysis of mRNA levels for the pro-inflammatory cytokines CCL2, IL-1β, IL-6, and IL-8, and the cell adhesion molecules VCAM-1 and ICAM-1. The expression of these genes was upregulated by LPS (Figure 4.4A-F). Ru265 (3-10 µM) failed to suppress induction of CCL2 gene expression by LPS (Figure 4.4A). However, Ru265 (3-10 µM) attenuated the rise in IL-1β mRNA levels produced by LPS (Figure 4.4B), while the highest concentration of Ru265 (10 µM) suppressed the induction of IL-6, IL-8, and VCAM-1 but not ICAM-1 by LPS (Figure 4.4C-F). These findings extend the anti-inflammatory effects of Ru265 by showing that this MCU$_{cx}$ inhibitor mitigated LPS-induced pro-inflammatory cytokine and cell adhesion molecule gene expression in a human brain endothelial cell line.
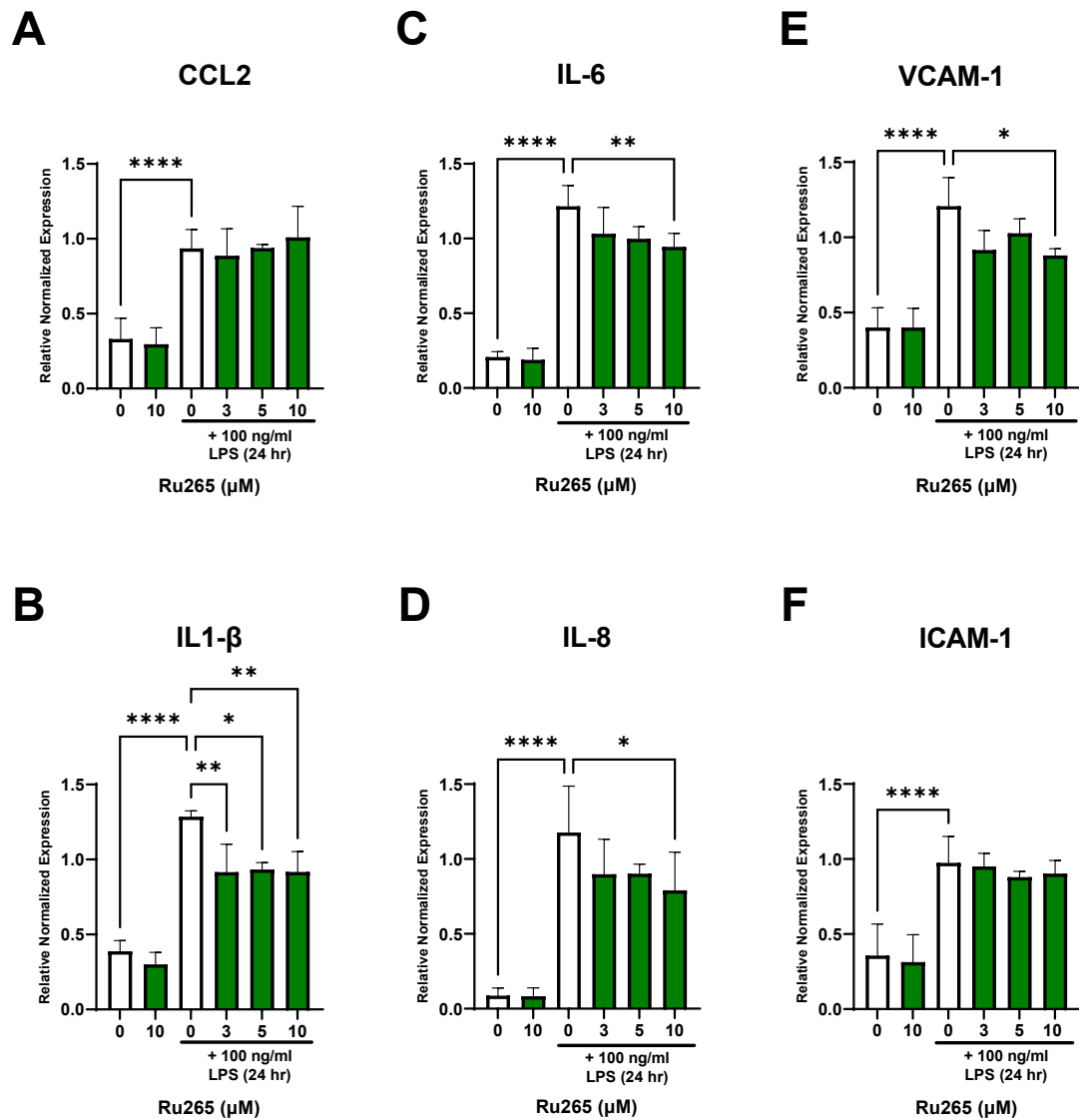
Figure 4.4. Effects of Ru265 on LPS-induced cytokine and cell adhesion molecule mRNA levels in HBEC-5i cells

HBEC-5i cells were treated with vehicle (Type 1 H₂0) or Ru265 (3, 5, or 10 µM) for 24 hr before the addition of PBS (control) or LPS (100 ng/ml) for 24 hr. Levels of mRNAs for CCL2 (A), IL-1β (B), IL-6 (C), IL-8 (D), VCAM-1 (E), and ICAM-1 (F) were then measured using RT-qPCR. Bars show the mean ± SD of data from 3 experiments, 3 wells/experiment. *p<0.05, **p<0.01, ****p<0.0001; ordinary one-way ANOVA followed by Tukey's multiple comparisons test.

4.3 Discussion

4.3.1 Ru265 Protects Mouse Primary Astrocyte Cultures against OGD-induced Injury

Astrocytes perform many functions important for neuronal survival and play a pivotal role in propagating signals between multiple cell types of the NVU necessary for the rapid adjustment of CBF to support the prodigious metabolic demands imposed by neurotransmission (Bantle et al., 2021; Iadecola, 2017; Zhang et al., 2020). Compared to neurons, astrocytes are more resistant to OGD because astrocytes have higher glycogen stores that slows ATP depletion in the absence of oxygen and glucose (Baldassarro et al., 2018; Rossi et al., 2007). It was therefore necessary to subject astrocyte cultures to a longer period of OGD (4 hr) to reliably produce a ~50% loss in cell viability. Similar to cortical neurons, Ru265 effectively preserved astrocyte viability after this period of OGD. These results indicate that preventing injurious mitochondrial Ca^{2+} overloading with Ru265 treatment also effectively protects astrocyte cultures from OGD-induced cell death. There is clear evidence that Ca^{2+} overloading and mitochondrial dysfunction contribute to astrocyte cell death after OGD. In astrocyte cultures exposed to OGD, mitochondrial Ca^{2+} overloading triggers caspase-mediated cell death (Huang et al., 2013; Mukda et al., 2019). Astrocyte cultures subjected to OGD display many of the hallmark features of mitochondrial dysfunction, including impaired Ca^{2+} homeostasis, elevated ROS levels, depolarization of the $\Delta\Psi_m$, and suppressed ATP synthesis (Guo et al., 2018; Guo et al., 2012; Kintner et al., 2007; Xu et al., 2005). Furthermore, treatments that preserve mitochondrial

bioenergetics reduce OGD-induced cell death in astrocyte cultures (Guo et al.,

2018; Guo et al., 2012; Kintner et al., 2007). This suggests that inhibition of the

MCU_{cx} with Ru265 may also protect the brain from ischemic injury by improving

astrocyte survival. Indeed, the preservation of astrocyte function has been found

to be beneficial for neurons and other brain cell subtypes during ischemic

conditions (Baldassarro et al., 2018; Rossi et al., 2007). Neurons co-cultured with

astrocytes fare much better after OGD and seem to be less susceptible to OGD-

induced injury (Baldassarro et al., 2018; Rossi et al., 2007). The shuttling of

nutrients such as glucose to neurons and the large glutamate uptake capacity by

astrocytes also supports neuronal survival during cerebral ischemia (Rossi et al.,

2007). The findings suggest that astrocyte protection may also contribute to the

therapeutic benefits of MCU_{cx} inhibition in the treatment of ischemic stroke.

**4.3.2 Ru265 Supresses the LPS-induced Inflammatory Response in Primary
Cultures of Mouse Astrocytes**

Astrocytes also play an important role in mounting the inflammatory response to

different stimuli associated with injury and neurodegenerative diseases, such as

oxidative stress, excitotoxicity, and pro-death signalling molecules (Bantle et al.,

2021; Choi et al., 2014; Jayaraj et al., 2019; Li et al., 2019). Astrocytes have

TLR4 receptors and can therefore be stimulated by LPS to release pro-

inflammatory cytokines, which provides a model to examine how astrocytes

contribute to neuroinflammation (Park et al., 2017; Skrzypczak-Wiercioch &

Sałat, 2022). Indeed, treatment with LPS induced the expression of the pro-

inflammatory cytokines IL-1β, TNFα, and IL-6 in primary astrocyte cultures. Furthermore, Ru265 treatment was able to supress this LPS-induced increase in pro-inflammatory cytokines. This suggests that Ru265 might possess anti-inflammatory properties by suppressing the induction of pro-inflammatory cytokine expression in astrocytes.

ROS production drives pro-inflammatory cytokine expression by activating the redox sensitive transcriptional factor NF-κB and the NLRP3-inflammasome pathway (Blaser et al., 2016; Song et al., 2017; Vallabhapurapu & Karin, 2009). Mitochondria in astrocytes are a major source of ROS production that drives ischemic brain injury (Chen et al., 2020). Furthermore, mitochondrial damage produces powerful pro-inflammatory signaling molecules that activate injurious A1 astrocytes (Joshi et al., 2019). Alterations in the balance of mitochondria fusion-fission dynamics, such as an increase in fission and phosphorylated dynamin-related protein 1 (DRP1), have also been shown to increase the inflammatory activation of astrocytes, resulting in neuroinflammation (Bantle et al., 2021; Joshi et al., 2019; Rahman & Suk, 2020). Conversely, treatment with an inhibitor of mitochondrial fission was shown to suppress glial activation and neuroinflammation, and transferring functional mitochondria to astrocyte cultures is neural protective (Joshi et al., 2019; Rahman & Suk, 2020). In addition, impaired Ca^{2+} signalling and homeostasis caused by mitochondrial dysfunction have been shown to drive the inflammatory response in astrocytes (Bantle et al., 2021; Hansson et al., 2016; Panattoni et al., 2021; Strokin et al., 2011).

Spontaneous Ca^{2+} spikes and Ca^{2+} transients in astrocytes that occur more frequently after central nervous system (CNS) injury and inflammation have been correlated with the polarization of astrocytes to an A1 pro-inflammatory phenotype (Hansson et al., 2016; Panattoni et al., 2021; Strokin et al., 2011). The resultant rise of cytosolic Ca^{2+} levels therefore increases the risk of excessive mitochondrial Ca^{2+} uptake known to trigger ROS overproduction and inflammation (Peng & Jou, 2010). It is therefore likely that by preserving mitochondrial function, which maintains Ca^{2+} homeostasis and opposes excessive ROS production, Ru265 suppresses astrocyte-mediated inflammation.

4.3.3 Ru265 Induced Anti-inflammatory Cytokines Gene Expression in Primary Cultures of Mouse Astrocytes

Astrocytes also resolve inflammation and promote cell survival by producing TGFβ and IL-10 (Dobolyi et al., 2012; Kwilasz et al., 2015; Lobo-Silva et al., 2016). Astrocytes cultured from IL-10 deficient mice release higher levels of pro-inflammatory cytokines and more readily polarize to a pro-inflammatory A1 phenotype after LPS stimulation (Zhang et al., 2020). In contrast, adding IL-10 to astrocyte cultures derived from these IL-10 deficient mice attenuates this pro-inflammatory A1 phenotype (Zhang et al., 2020). Astrocyte-derived IL-10 also improves neuronal survival after axotomy by reducing microglia activation (Villacampa et al., 2015). Mouse studies have also demonstrated that treatment with IL-10, or the induction of IL-10 synthesis and release, improves learning and memory, reduces neurodegeneration, and enhances recovery after brain injury

(Kwilasz et al., 2015; Mayo et al., 2016; Zhang et al., 2020). Lastly, reduced MCU_{cx} inhibition conferred by increased expression of the inhibitory MCUb subunit is associated with the polarization of macrophages from a pro-inflammatory M1 to an anti-inflammatory M2 phenotype (Feno et al., 2021). It is therefore tempting to speculate that by inhibiting the MCU_{cx} and suppressing mitochondrial ROS production, Ru265 also promoted the polarization of astrocytes to an anti-inflammatory A2 phenotype resulting in increased production of TGFβ and IL-10.

Another interesting characteristic of IL-10 is that it has been shown to increase astrocyte production of TGFβ. This pleiotropic cytokine has both pro- and anti-inflammatory activities depending on the context (Norden et al., 2014; Sanjabi et al., 2009). Experimentation with co-cultured astrocytes and microglia demonstrated that IL-10 stimulated the release of TGFβ from activated astrocytes, which in turn attenuated microglia activation and reduced inflammation (Norden et al., 2014). These findings are intriguing because TGFβ mRNA levels were not elevated in astrocyte cultures until 48 hr after treatment with Ru265. This delayed upregulation of TGFβ mRNA by Ru265 might therefore reflect TGFβ induction subsequent to the elevation of IL-10 levels. This finding further suggests that Ru265 promotes the polarization of astrocytes to an anti-inflammatory A2 phenotype. This is anticipated to add to the potential beneficial effects of Ru265 by reducing injurious brain inflammation.

The generation of IL-10 has also been linked to reduced infarct size in murine models of ischemic-reperfusion injury produced by transient middle cerebral artery occlusion (MCAO) (Frenkel et al., 2005; Tukhovskaya et al., 2014). IL-10 deficient mice demonstrated a significantly greater infarct size compared to wild type (WT) mice, while immune-mediated neuroprotection produced by the oral consumption of myelin oligodendrocyte glycoprotein before MCAO was conferred by regulatory T cells that release IL-10 (Frenkel et al., 2005). IL-10 administration also reduced infarct size after MCAO, and in primary hippocampal cultures, IL-10 reduced cell death after OGD (Tukhovskaya et al., 2014). Further, this reduction in cell death by IL-10 was associated with preservation of intracellular Ca^{2+} handling likely involving mitochondria (Tukhovskaya et al., 2014). This suggests that the ability of Ru265 to increase IL-10 expression might contribute to the neuroprotective potential of this compound in the treatment of ischemic stroke by maintaining Ca^{2+} handling and reducing inflammation. Furthermore, the induction of TGFβ and IL-10 mRNA levels by Ru265 in astrocytes may also protect and repair the NVU after an ischemic stroke.

4.3.4 Ru265 Suppressed LPS-induced Pro-inflammatory Cytokine and Adhesion Molecule Gene Expression in HBEC-5i Cells

Endothelial cells, important components of the NVU that form the wall of cerebral blood vessels, also play a key role in neuroinflammation (Iadecola, 2004; Verma et al., 2006). Brain endothelial cells are crucial for the maintenance and function of the BBB, which ensures a healthy microenvironment in the brain (Smyth et al.,

2018). Breakdown of the BBB that often occurs in numerous inflammatory and neurodegenerative conditions can exacerbate injury (Verma et al., 2006). Brain endothelial cells can play dual roles in these disorders by releasing pro-inflammatory cytokines that worsen brain injury or various anti-inflammatory cytokines and trophic factors which protect and promote the repair of the brain (Shen et al., 2004; Smyth et al., 2018; Verma et al., 2006). The unique location of brain endothelial cells allows them to secrete cytokines into both the brain and the blood circulation, thus influencing both the brain and periphery (Verma et al., 2006). With respect to the former, there is strong evidence indicating that brain endothelial cells contribute to neuroinflammation by secreting pro-inflammatory cytokines (Smyth et al., 2018; Verma et al., 2006). Ru265 was found to suppress the expression of pro-inflammatory cytokines and cellular adhesion molecules in HBEC-5i cells treated with LPS. Cellular adhesion molecules (ICAM-1 and VCAM-1) promote brain inflammation by enabling immune cell infiltration. Binding to ICAM-1 and VCAM-1 induces pro-inflammatory signaling in immune cells and initiates their movement into the brain parenchyma (Smyth et al., 2018). Ru265 suppressed the induction of IL-1β, IL-6, IL-8, and VCAM-1 mRNA levels by LPS in HBEC-5i cells. This finding extends the anti-inflammatory effects of Ru265 from astrocytes to human brain endothelial cells. Taken together, Ru265 should therefore further maintain NVU homeostasis after an ischemic stroke by reducing the inflammation. Hence, the abilities of Ru265 to not only protect neurons and astrocytes but also suppress pro-inflammatory signaling in astrocytes and brain endothelial cells and promote anti-inflammatory cytokine expression in astrocytes

indicate that this compound has strong potential for the treatment of ischemic

stroke by acting on various cellular components of the NVU.

Chapter 5: Ru265 Reduces Hypoxic/Ischemic (HI) Brain Injury but also Promotes Seizure Activity in Mice

5.1 Introduction

The previous chapters demonstrated that the MCU_{cx} inhibitor Ru265 blocked mitochondrial Ca^{2+} uptake in cortical neuron cultures, suppressed OGD-induced cell death in primary mouse cortical neuron and astrocyte cultures, increased anti-inflammatory cytokine gene expression in astrocyte cultures, and reduced pro-inflammatory cytokine gene expression in LPS-treated astrocyte and HBEC-5i cultures. These cell based findings support the neural protective potential of Ru265. However, to assess the safety and better characterize the neural protective potential of Ru265 for stroke, it is necessary to employ a suitable animal model.

The genetic identification of the MCU subunit in 2011 enabled the generation of inducible cell specific MCU deficient mice (Baughman et al., 2011; Stefani et al., 2011). Experimentation with these mice has shown that ablation of the MCU in cardiac myocytes at adulthood reduces ischemic/reperfusion injury in the heart (Kwong et al., 2015; Luongo et al., 2015). Furthermore, our laboratory has shown that deletion of the MCU in Thy-1 expressing neurons at sexual maturity mitigates sensorimotor deficits and preserves the integrity of mitochondria and neurons in the forebrain of mice subjected to HI brain injury (Nichols et al., 2018). These studies suggest that inhibition of the MCU_{cx} with Ru265 should also be

protective in mice subjected to HI brain injury. HI brain injury is produced by occlusion of a common carotid artery, followed by placing the animal in a low oxygen chamber that results in unilateral HI brain injury. The degree of injury can then be determined by measuring the infarct size in the affected hemisphere. The primary aims for these experiments were to assess if Ru265: (1) reaches concentrations in the brain that suppress OGD-induced cell death in primary cultures of mouse cortical neurons and (2) reduces sensorimotor deficits and infarct volumes in mice subjected to HI brain injury. While completing these studies, it was observed that Ru265 produced motor convulsions in mice when injected i.p. at doses of 10 and 30 mg/kg. To determine if Ru265-induced convulsions were mediated by the MCU_{cx}, convulsions were measured in Thy 1 control mice with an intact MCU_{cx} and Thy1-MCU deficient mice injected with Ru265 at a dose of 10 mg/kg (i.p.).

5.2 Results

5.2.1 Ru265 Reduces Sensorimotor Deficits and Infarct Volumes in Mice Subjected to HI Brain Injury

Injection of Ru265 (1 and 10 mg/kg, i.p.) produced a dose-dependent elevation of plasma and forebrain Ru concentrations in adult (20 g) male C57Bl/6 mice (Table 2). The neuroprotective potential of Ru265 was then examined in adult male mice subjected to HI brain injury. Relative to mice that received saline (8 ml/kg, i.p.) 30 min before being subjected to HI brain injury, Ru265 (3 mg/kg, i.p.) reduced sensorimotor deficits and infarct volumes 24 hr after HI (Figure 5.1A-C).

Interestingly, measurements of forebrain Ru concentrations indicated that even at a dose of 10 mg/kg (i.p.), Ru265 forebrain concentrations (0.315 ± 0.007 μM; mean ± standard error of mean (SEM); Table 2) were less than 10% of the EC_{50} (4.1 μM; Figure 3.3A) for elevating the viability of cortical neurons exposed to OGD.

Table 2. Plasma and forebrain concentrations of Ru265

Treatment	Plasma (μM ± SEM)	Forebrain (μM ± SEM)
Saline (8 ml/kg, i.p.)	ND	ND
Ru265 (1 mg/kg, i.p.)	0.771 ± 0.009	0.026 ± 0.004
Ru265 (10 mg/kg, i.p.)	6.123 ± 0.012	0.315 ± 0.007

Note: Plasma and forebrain concentrations of Ru265 1 hr after the injection of saline (8 ml/kg, i.p.) or Ru265 (1 or 10 mg/kg, i.p.) determined by measuring Ru levels with ICP-MS.
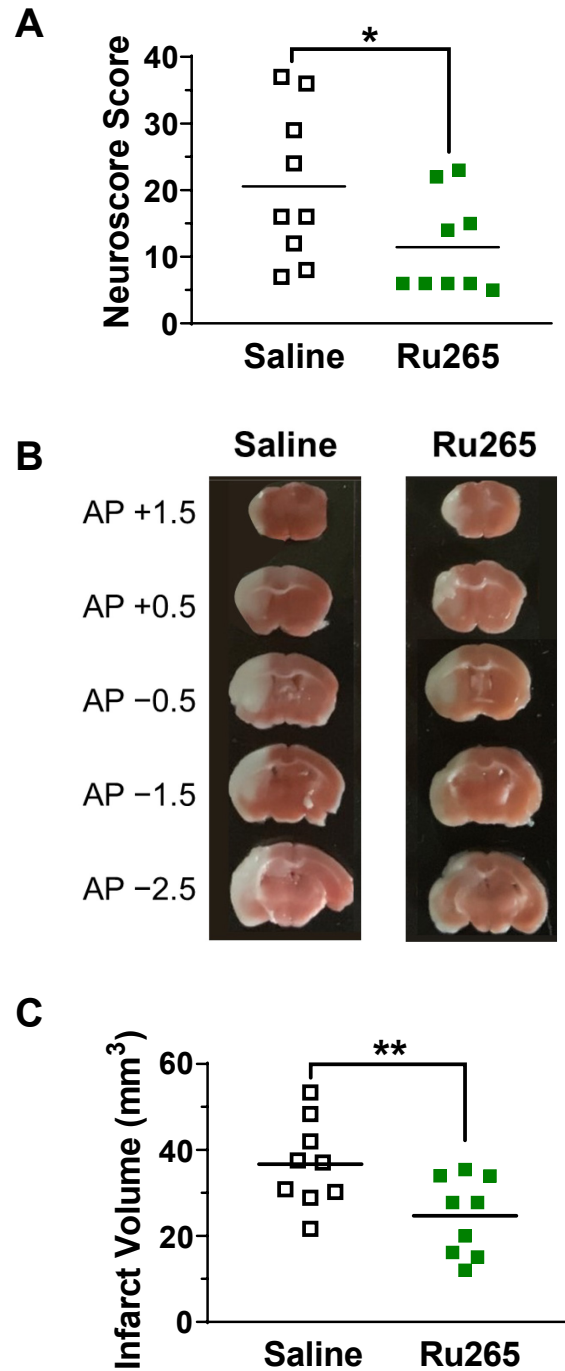
Figure 5.1. Ru265 reduces sensorimotor deficits and infarct volumes in mice subjected to HI brain injury

Adult male C57Bl/6 mice were injected with saline (8 ml/kg, i.p.) or Ru265 (3 mg/kg, i.p.) 30 min before HI injury. Neuroscores (A) and infarct volumes (C) were measured 24 hr later. Representative TTC stained sections 24 hr after HI injury of mice injected with saline or Ru265 (B). The lines in A and C represents the average value of data for 9 mice. *p<0.05, **p<0.01; Mann-Whitney U tests.

5.2.2 Ru265 Produced Dose-dependent Increases in the Frequency and Duration of Seizure-like Behaviours

During these studies, it was observed that Ru265 produced seizure-like behaviours similar to those observed in rodents and cats injected with RuRed, which contains Ru360 (Garcia-Ugalde & Tapia, 1991; Tapia, 1982; Tapia et al., 1976). The dose- and time-dependent effects of Ru265 on a variety seizure-like behaviours were therefore measured in male C57Bl/6 mice. Mice were injected with increasing doses of Ru265 and observed for 90 min. The frequency and duration of seizure-like behaviours were recorded by raters unaware of the treatment conditions. At a dose of 3 mg/kg (i.p.), Ru265 caused bouts of motionless staring, typical of absence seizures, within 30 min of the injection, that occurred more frequently during the remaining 60 min of the test period (Figure 5.2A). By comparison, the frequency of motionless staring did not increase at doses of 10 or 30 mg/kg (i.p.). Facial jerking was also observed at a dose of 3 mg/kg (i.p.) and became more frequent at 10 mg/kg (i.p.) but declined at a higher dose of 30 mg/kg (i.p.) because the animals were incapacitated by severe convulsions lasting over 10 min that were characterized by muscle contractions and repeated jerking movements of the limbs on both sides of the body (Figure 5.2A-B). By contrast, 3 mg/kg (i.p.) did not produce convulsions during the 90 min test-period (Figure 5.2A-B). Whisker trembling at a dose of 10 mg/kg (i.p.) of Ru265 was associated with the induction of mild absence seizures. Ru265 (30 mg/kg; i.p.) produced severe convulsions that lasted for 15 min (Figure 5.2B). The onset of convulsions was also more rapid for 30 mg/kg (i.p.) compared to 10

mg/kg (i.p.) of Ru265 (Figure 5.2B). The severity of these Ru265-induced convulsions increased over time. By 2 and 4 hr all animals injected with 30 and 10 mg/kg (i.p.) respectively had to be humanely euthanized.
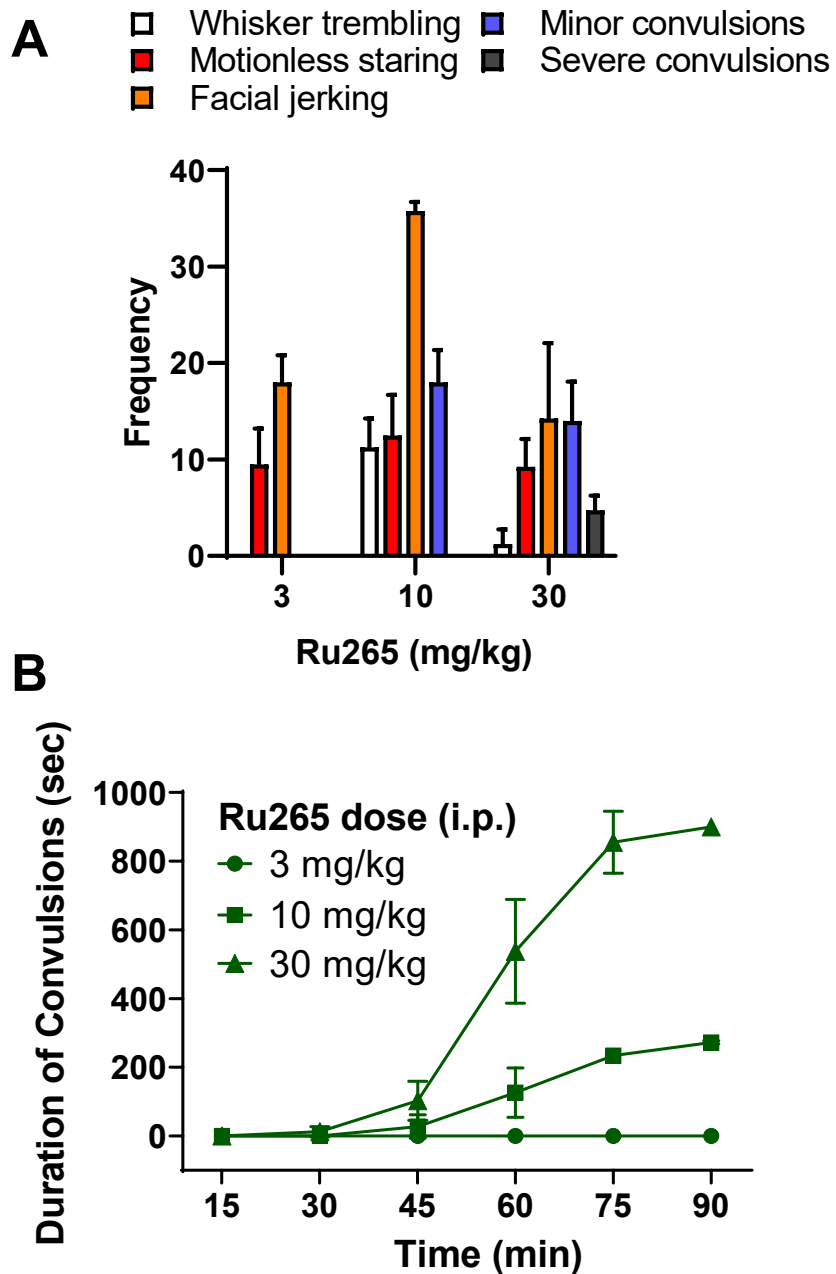
Figure 5.2. The frequency and duration of seizure-like behaviours after Ru265 injections

Adult male C57Bl/6 mice were injected with 3, 10, or 30 mg/kg (i.p.) of Ru265 and observed over a 90 min period. The frequency of seizure-like behaviours (A) and duration of convulsions (B) were recorded over a 90 min period by raters unaware of the treatment conditions. Data represent the mean ± SD; n = 4 mice/group.

5.2.3 Ru265-induced Convulsions are Not Mediated by MCU$_{cx}$ Inhibition

Thy1-MCU deficient mice were used to determine if Ru265-induced convulsions were mediated by the MCU$_{cx}$. Thy1 and Thy1-MCU deficient mice were injected i.p. with 10 mg/kg of Ru265, a dose that induced convulsions about 1 hr post injection (Figure 5.2B). There were no differences in the frequency or duration of Ru265-induced convulsions between Thy1 controls and Thy1-MCU deficient mice (Figure 5.3). This suggests that the pro-convulsant effects of Ru265 are more likely caused by an off-target activity rather than inhibition of the MCU$_{cx}$.
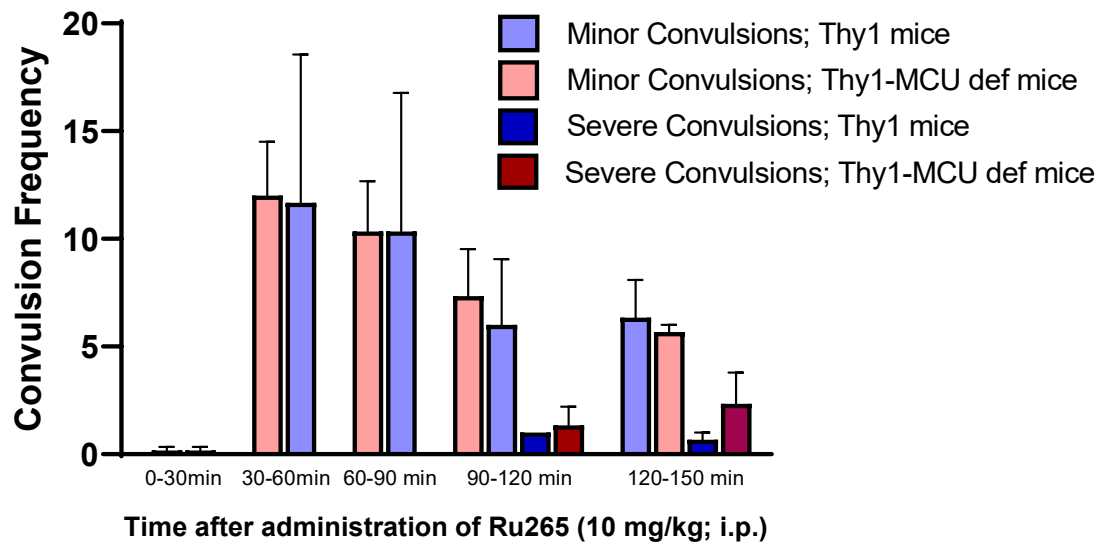
Figure 5.3. Ru265 promotes convulsions by a non-MCU mechanism

Thy1 and Thy1-MCU deficient (def) mice were injected with 10 mg/kg (i.p.) of Ru265 and the frequency of minor (lasting 2-3 min or less) and severe (lasting 10 min or more) convulsions was measured over a 150 min period by raters unaware of treatment conditions. Bars show the mean ± SD; n = 3 mice/group.

5.3 Discussion

5.3.1 Ru265 Reduced HI-induced Brain Injury

Intraperitoneal (i.p.) injections of 1 and 10 mg/kg of Ru265 in adult male C57Bl/6 mice produced a dose-dependent elevation of plasma and forebrain Ru concentrations 1 hr after injection. Although Ru265 reached detectable concentrations in the brain at a dose injection of 1 mg/kg (i.p.), the forebrain concentrations, even at a dose of 10 mg/kg, were still less than 10% of the EC_{50} for protecting cortical neurons from OGD-induced cell death. One explanation for this discrepancy is that Ru265 becomes concentrated in neurons and astrocytes. In support of this hypothesis, Ru265 is a substrate for organic cation transporter 3 (OCT3) (Woods et al., 2020) that is enriched in forebrain neurons and astrocytes (Gasser et al., 2017; Gasser et al., 2009). Forebrain Ru measurements may therefore have underestimated the uptake of Ru265 by neurons and astrocytes.

5.3.2 Ru265 Produced Dose-dependent Convulsions in Mice through a Non-MCU_{cx} Mechanism

A clear adverse effect of Ru265 is the induction of convulsions in mice at doses of 10 and 30 mg/kg (i.p.). To overcome this complication, a low dose of Ru265 (3 mg/kg, i.p.) that did not produce convulsions was used to assess efficacy in the HI brain model. At a dose of 10 mg/kg, convulsions started in mice about 45 min after injection, and the severity of convulsions increased over time, resulting in the animals having to be euthanized after a few hours. It has been previously

reported that RuRed induces convulsions, but at lower doses (4.4 mg/kg, i.p.) than Ru265. RuRed was also shown to reduce the viability of rat cortical neuron cultures by 50% after 24 hr of exposure (Velasco et al., 1995; Velasco & Tapia, 1997, 2000), which was not the case for Ru265 in mouse cortical neurons. This suggests that mechanisms other than MCU_{cx} inhibition account for the neurotoxic actions of RuRed. To examine whether the Ru265-induced convulsions were dependent on the MCU_{cx}, we employed Thy1-MCU deficient mice. It should be noted that Thy1-MCU deficient mice appear healthy and do not display spontaneous convulsions. However, compared to WT mice subjected to HI brain injury, convulsions are more likely to occur in global MCU nulls subjected to HI brain injury (unpublished observations). Thy1 and Thy1-MCU deficient mice displayed the same number of minor (lasting 2-3 min or less) and severe (lasting 10 min or more) convulsions. These results suggests that the pro-convulsant effects of Ru265 at not mediated by the MCU_{cx} and reflect off target activity.

Chapter 6: Novel Os-based MCU$_{cx}$ Inhibitors Preserve Cell Viability and Mitochondrial Function in Cortical Neuron Cultures Subjected to OGD but Induce Seizure-like Behaviours

6.1 Introduction

Data presented in Chapter 3 showed that Ru265 protects primary cultures of mouse cortical neurons from ischemic/reperfusion injury by blocking mitochondrial Ca^{2+} overloading. However, the results from animal studies described in Chapter 5 indicate that Ru265 suffers from low brain permeability and undesirable off target activity which induces convulsions. The goal of this chapter is to determine whether these limitations can be overcome by modifications to the chemical structure of Ru265. The first strategy was to examine the effects of changing the metal center of Ru265. In this case, two structural analogues of Ru265 were synthesized. For the first, the two Ru atoms were replaced with Os atoms to create a nitrido-bridged diosmium compound, termed Os245 (Figure 6.1A). For the second, the axial chlorido ligands were replaced with coordinated water molecules to generate its aqua-capped analogue termed Os245' (Figure 6.1B). A consequence of substituting Os for Ru in these compounds is that the resultant compounds have improved stability and slower substitution kinetics of the axial ligands (Bruijnincx & Sadler, 2009). In comparison to the Ru-based inhibitor Ru265 (k_{obs} = 4.92 x 10^{-3} sec^{-1}), the axial ligand exchange kinetics of Os245 are two orders of magnitude slower (k_{obs} = 1.63 x 10^{-5} sec^{-1}) at 37°C. The MCU$_{cx}$-inhibitory properties of Os245 and Os245'

were also different (Os245 IC_{50} for MCU_{cx} inhibition = 103 nM; Os2450 IC_{50} for MCU_{cx} inhibition = 2.3 nM), indicating that the axial ligands of these compounds play an important role in regulating interactions with this channel. Os245 and Os245' therefore permit the examination of how changes in the axial ligands impact cellular uptake and interactions with the MCU_{cx}. In addition, analogues of Ru265 and Os245' were generated by the addition of adamantane molecules and termed RuOAd and OsOAd, respectively (Figure 6.1C-D). These chemical modifications were made because adamantane has neuroprotective properties in models of ischemic stroke by blocking the excessive activation of ionotropic glutamate receptors (Kadernani et al., 2014). The goals of this chapter were to compare the cellular uptake and neuroprotective properties of these Ru265 analogues in primary cultures of mouse cortical neurons, as well as their pro-convulsant effects in mice.
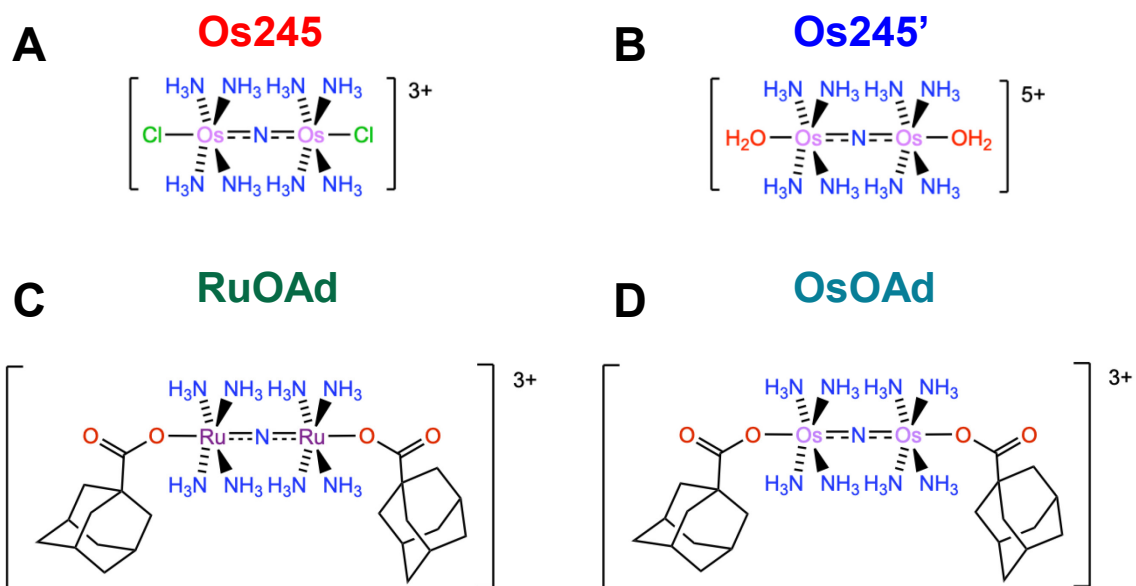
Figure 6.1. Chemical Structures of Os245 (A), Os245' (B), RuOAd (C), and OsOAd (D)

6.2 Results

6.2.1 Os245 and Os245' Enter the Cytosol of Cultured Cortical Neurons

Primary cortical neuron cultures were treated with Os245 or Os245' at concentrations of 10, 30, or 50 µM for 30 min, 3 hr, or 24 hr. Cellular uptake of either Os245 or Os245' was estimated by measuring concentrations of Os yielded by cell lysis. Since these compounds each contain two Os atoms, concentrations were considered half of the Os values determined by ICP-MS. Treatment of cortical neuron cultures with either Os245 or Os245' produced concentration- and time-dependent increases in intracellular Os levels (Figure 6.2A-C). The intracellular Os levels produced by Os245' were consistently greater than those generated by Os245 at the equivalent concentrations and time points. These findings indicate that compared to Os245, Os245' displays more rapid and greater cellular uptake by cortical neurons (Figure 6.2A-C).
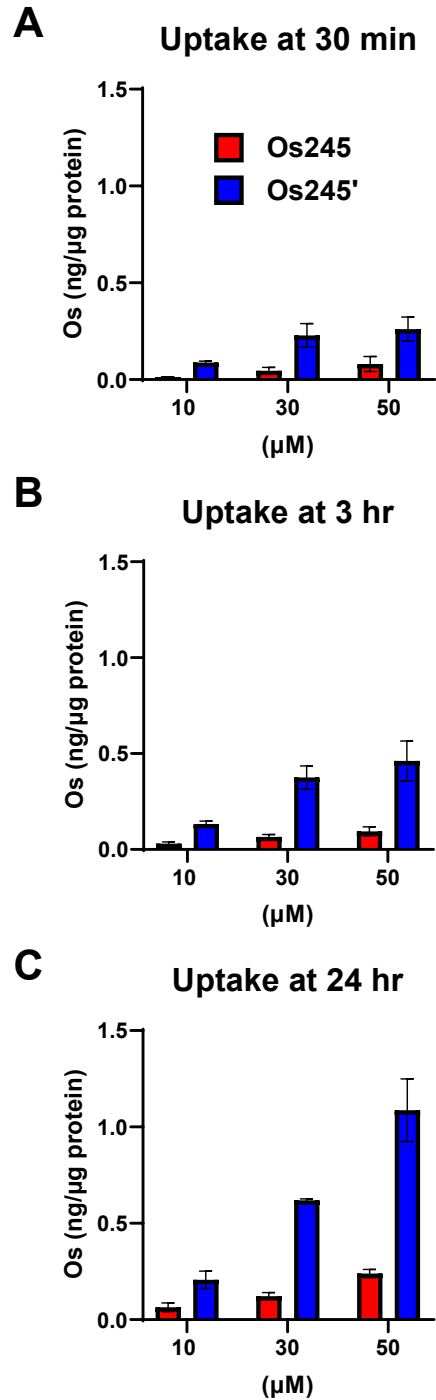
Figure 6.2. Cellular uptake of Os245 and Os245' in primary cortical neuron cultures

Os concentrations in cell lysates of primary cortical neuron cultures 30 min (A), 3 hr (B), and 24 hr (C) after treatment with Os245 (10, 30, or 50 μM) or Os245' (10, 30, or 50 μM). Concentrations are expressed as ng of Os per μg of protein. Bars show the mean ± SD of 3 wells/concentration.

6.2.2 Os245 and Os245' Produced Comparable Concentration-dependent Protection of Cortical Neurons Subjected to OGD

The ability of Os245 and Os245' to protect cortical neurons against OGD was investigated by treating cultures with increasing concentrations (1, 2.5, 5, 10, 30, or 50 µM) of Os245 or Os245' for 3 hr before exposure to 90 min of OGD. Viability was then measured 24 hr later using the MTT assay, and percent viability was calculated relative to No OGD control cultures. Both compounds elicited very similar concentration-dependent increases in cell viability, with 30 µM and 50 µM of Os245 elevating viability from 39.5 ± 7.0% to 75 ± 21.9% and 90 ± 18.1% (mean ± SD), respectively (Figure 6.3A), and 30 µM and 50 µM of Os245' elevating viability from 41.8 ± 6.4% to 75 ± 17.9% and 94 ± 19.7% (mean ± SD), respectively (Figure 6.3B). This shows that these new MCU_{cx} inhibitors have similar potency and efficacy at protecting cortical neurons from OGD-induced cell viability loss. Compared to Ru265 (EC_{50}=4.1 µM) they are equally efficacious but about 5-6-fold less potent (EC_{50}~20-25 µM) at preserving cell viability after OGD.
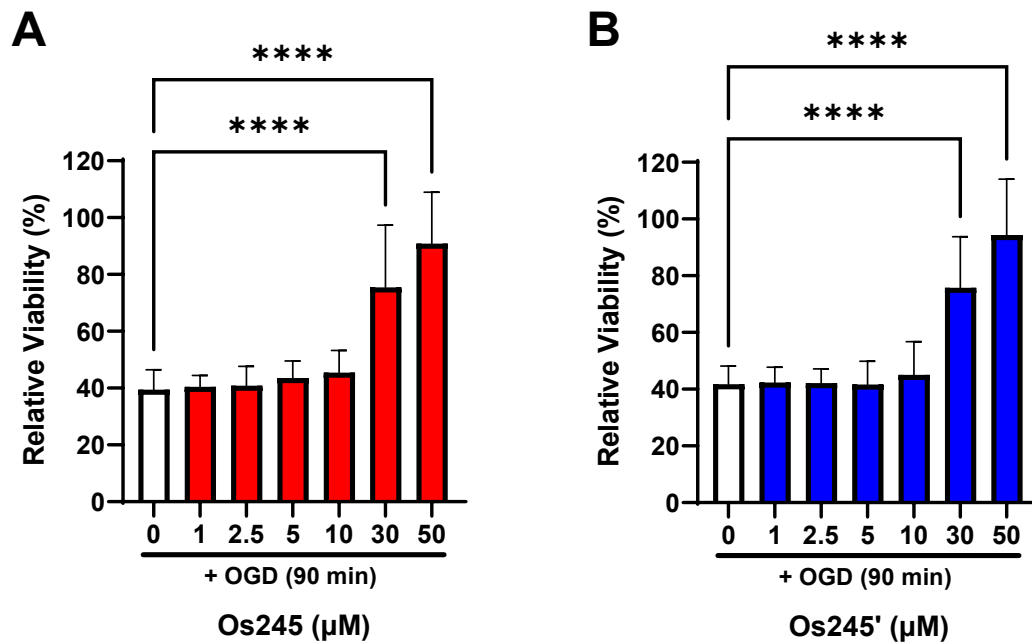
Figure 6.3. Os245 and Os245' protect cortical neuron cultures against OGD-induced cell death

Percent cell viability in primary cortical neuron cultures treated with vehicle (Type 1 H_2O) or increasing concentrations (1, 2.5, 5, 10, 30, or 50 μM) of Os245 (A) or Os245' (B) for 3 hr before OGD (90 min). Cell viability was measured 24 hr after OGD using the MTT assay. Values represent percent viability relative to control (No OGD) cultures (100% cell viability). Bars show the mean ± SD of data from 4 experiments, 6 wells/experiment. ****$p < 0.0001$; ordinary one-way ANOVA followed by Tukey's multiple comparisons test.

6.2.3 Os245 and Os245' Preserve OCR and ECAR in Cortical Neurons

Exposed to OGD

The effects of Os245 and Os245' on mitochondrial function in cortical neurons

subjected to OGD were assessed using the Seahorse XFe24 extracellular flux

assay analyser. Like earlier experiments with Ru265, pilot studies demonstrated

that higher concentrations (75 µM) of Os245 and Os245' were required to

suppress OGD-induced cell viability loss in the XF24 plates. Under normal

culture conditions (No OGD), treatment with Os245 or Os245' (75 µM) for 3 hr

did not alter the basal OCR, FCCP-induced maximal OCR, or residual OCR after

the addition of rotenone and antimycin relative to vehicle (Figure 6.4A).

Compared to vehicle, the ECAR was also unchanged by Os245 or Os245' (75

µM) (Figure 6.4B). Consistent with previous studies (section 3.3.5), OCR and

ECAR were significantly reduced 2 hr after exposure to 30 min of OGD (Figure

6.4C-F). In contrast, treatment with 75 µM of Os245 or Os245' for 3 hr prior to

OGD effectively preserved mitochondrial respiration and glycolysis (Figure 6.4C-

F). Relative to vehicle-treated cultures, these compounds prevented the

reduction in basal respiration and the loss of FCCP-induced maximal respiratory

capacity, as well as the drop in ECAR levels, after OGD.
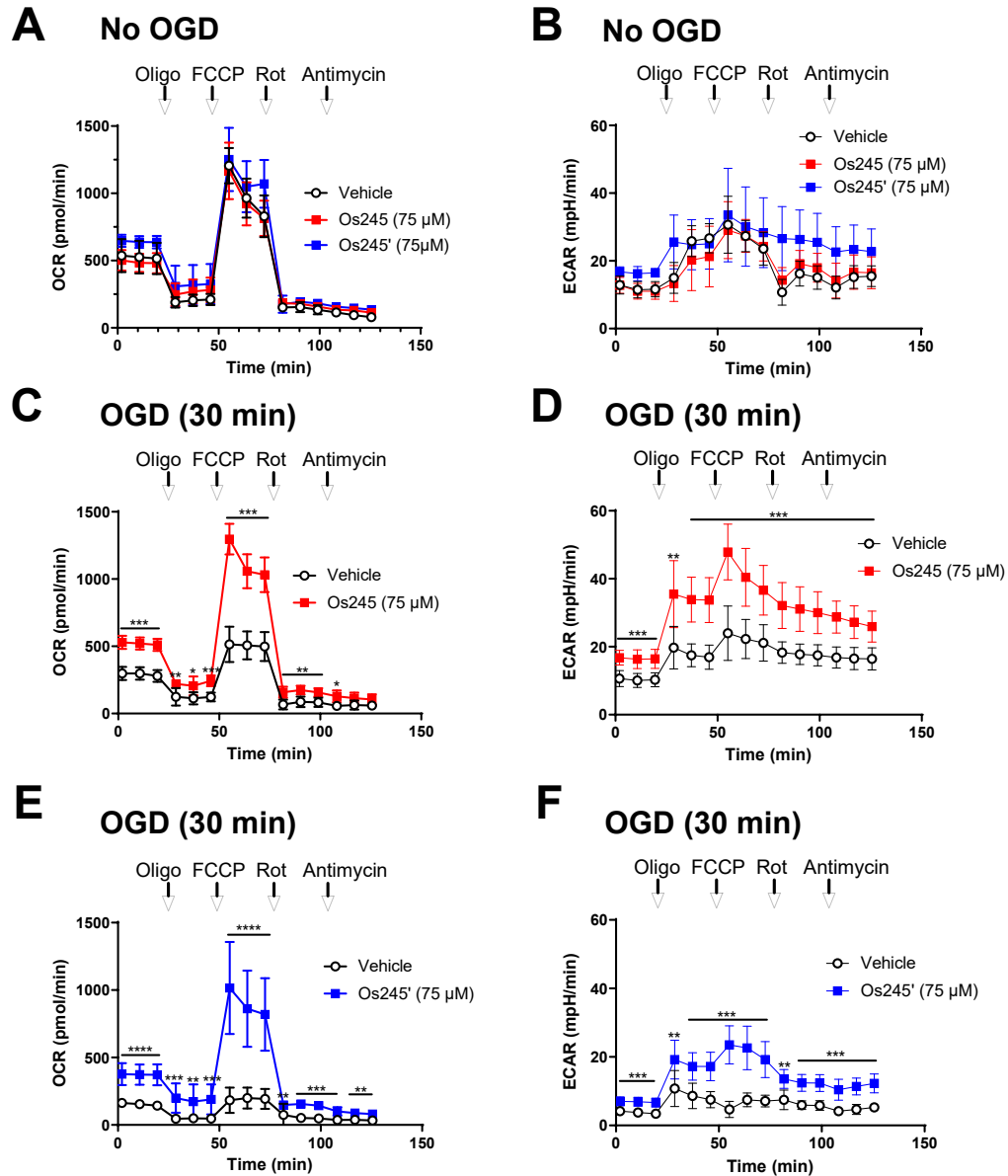
Figure 6.4. Os245 and Os245' preserve mitochondrial function in primary cortical neuron cultures subjected to OGD

Primary cortical neuron cultures were treated with vehicle (Type 1 H_2O), Os245 (75 μM), or Os245' (75 μM) for 3 hr and left as control (A and B) or subjected to 30 min of OGD (C-F). OCR and ECAR were measured after the sequential addition of Oligo (1 μM), FCCP (2 μM), Rot (300 nM) and Antimycin (5 μM). Traces of OCR (A) and ECAR (B) under control (No OGD) conditions for cultures treated with vehicle, Os245, or Os245'. OCR and ECAR levels 2 hr after OGD in vehicle or Os245 treated cultures (C and D) and vehicle or Os245' treated cultures (E and F). Bars show the mean ± SD of data representative of 3 experiments, 5 wells/experiment. *$p<0.05$, **$p<0.01$, ***$p <0.001$, ****$p<0.0001$; two-way ANOVA followed by Bonferroni's post hoc test.

118

6.2.4 Relative to Ru265, Mice Injected with Os245 or Os245' Showed Delayed but Equally Severe Convulsions

Since Os245 and Os245' displayed reduced cellular uptake and required higher concentrations to preserve cortical neuron viability after OGD compared to Ru265, their abilities to cause convulsions may also be different. To test this hypothesis, male C57Bl/6 mice were injected with 10 mg/kg (i.p.) of either Ru265, Os245, or Os245', and then monitored for motor convulsions. As seen in the earlier studies (section 5.2.2), mice injected with 10 mg/kg of Ru265 (i.p.) displayed convulsions approximately 45 min later (Figure 6.5). For mice injected with 10 mg/kg (i.p.) of either Os245 or Os245', the onset of convulsions was delayed compared to Ru265 (Figure 6.5). For example, convulsions lasting over 6 min were observed 75 min post-injection of Ru265, whereas it took about 30 min longer for mice treated with either Os245 or Os245' to display convulsions of the same duration (Figure 6.4). Furthermore, convulsions severity increased over time to the point that all animals had to be euthanized approximately 3 hr after the injection of either Ru265, or Os245, or Os245'.
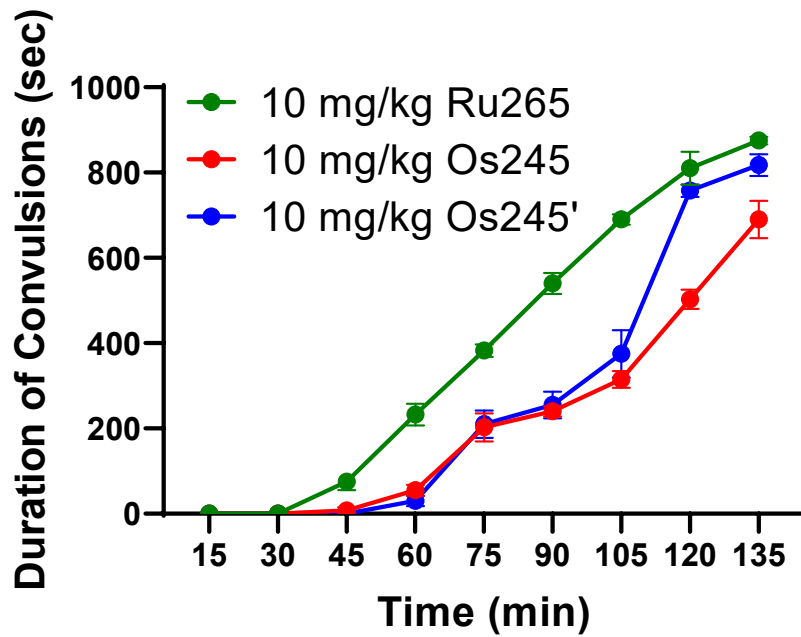
Figure 6.5. Os245 and Os245' also produced convulsions in mice

Adult male C57Bl/6 mice were injected with 10 mg/kg (i.p.) of Ru265, Os245, or Os245' and observed over a 135 min period. The duration of convulsions detected over the test period was recorded by raters unaware of treatment conditions. Data represent the mean ± SD; n = 4 mice/group.

6.2.5 Adamantane Derivatives of Ru265 (RuOAd) and Os245' (OsOAd)

Potently Protect Cortical Neurons Against OGD-induced Cell Viability Loss

In a further effort to develop MCU_{cx} complex inhibitors with superior

neuroprotective potency against OGD, analogues of Ru265 and Os245'

containing adamantane ligands were generated and called RuOAd and OsOAd,

respectively (Figure 6.1C and D). Like the previous experiments with Ru265 and

Os245', primary cortical neuron cultures were treated with increasing

concentrations (1, 3, 5, or 10 µM) of RuOAd or OsOAd for 3 hr before being

subjected to 90 min of OGD, and cell viability was assessed 24 hr after OGD

using the MTT assay (Figure 6.6A-B). Percent viability was calculated relative to

No OGD control cultures. Both compounds significantly increased cell viability

from 32.5 ± 11% to 68 ± 19.5% (mean ± SD) at concentrations as low as 1 µM

for RuOAd, and from 36.8 ± 13.6% to 81 ± 11.8% (mean ± SD) for 3 µM of

OsOAd (Figure 6.6A-B). At a concentration of 3 µM for RuOAd and 5 µM for

OsOAd, these compounds produce a near complete preservation of percent cell

viability at 95% or above (Figure 6.5A-B). Based on earlier experiments with

Ru265 and Os245' (Figures 3.4A and 6.2B, respectively), RuOAd (EC_{50} ~ 0.8

µM) is about 5x more potent than Ru265 and OsOAd (EC_{50} ~ 2 µM) is

approximately 20x more potent than Os245'.
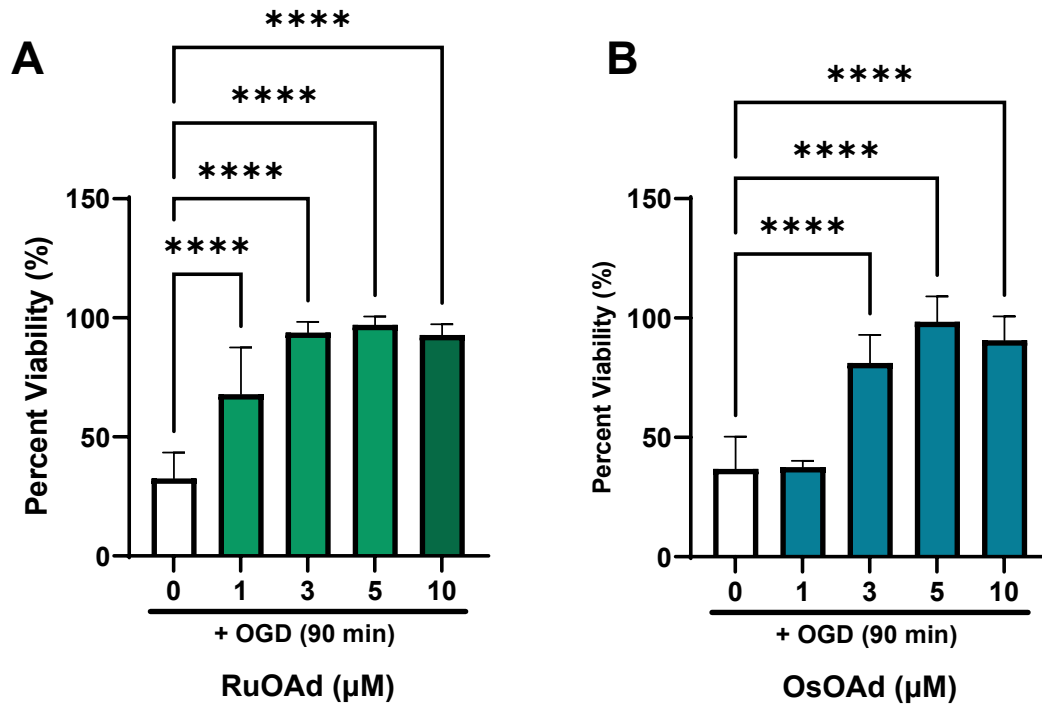
Figure 6.6. RuOAd and OsOAd potently protect cortical neurons against OGD

Percent cell viability in primary cortical neuron cultures treated with vehicle (Type 1 H_2O) or increasing concentrations (1, 3, 5, or 10 µM) of RuOAd (A) or OsOAd (B) for 3 hr before OGD (90 min). Cell viability was measured 24 hr after OGD using the MTT assay. Values represent viability relative to control (No OGD) cultures (100% cell viability). Bars show the mean ± SD of data from 3 experiments, 6 wells/experiment. ****$p < 0.0001$; ordinary one-way ANOVA followed by Tukey's multiple comparisons test.

6.3 Discussion

6.3.1 The Dinuclear Nitrido-bridged Os Complexes Os245 and Os245' show Cell Permeability in Primary Cortical Neuron Cultures

Os245 and Os245' produced concentration and time dependent increases in intracellular Os levels, confirming that both compounds penetrate the plasma membrane of cortical neurons. Consistent with observations in HeLa cells, Os245' accumulates in neurons to a greater extent than Os245. This is suggestive of differences in the uptake systems utilized by the chlorido-capped and aqua-capped compounds to cross the cell membrane. Indeed, other studies have reported different cellular uptake pathways for structurally similar metal complexes with distinct terminal ligands (Liu et al., 2011; Novohradsky et al., 2014; Romero-Canelon et al., 2012; Romero-Canelón et al., 2013). The higher cellular uptake of Os245' than Os245 may reflect the permissive effects of increased positive charge on drug uptake by cationic transporters. For instance, studies using HeLa cells have shown that inhibition of the OCT3 had no effect on the cellular accumulation of Os245, but significantly reduced the cellular accumulation of Os245'. This suggests that transport by OCT3 may enable Os245' to reach higher intracellular concentrations than Os245. Given that the presence of hydrogen-bond acceptors is an important factor in substrate binding to organic cation and anion transporters (Ahlin et al., 2008; Ahn et al., 2009), it is possible that the terminal aqua ligands of Os245′ make this complex a better substrate for OCT3 than its chlorido-capped analogue, Os245. Further studies with HeLa cells that were incubated with Os245 or Os245' in conditions that

diminish energy-dependent cellular uptake showed that there was a slight

decrease in cellular accumulation of Os245 but not Os245'. This suggests that

the chloride-cap of Os245 may allow this compound to cross the cell membrane

in an energy-dependent manner, whereas the aqua-cap of Os245' may not. The

differing cellular uptake of Os245 and Os245' indicate the importance of the axial

ligands in influencing the biological activity of this class of MCU_{cx} inhibitors.

These findings provide insights into structural properties that may be utilized to

develop MCU_{cx} inhibitors with improved biological properties.

6.3.2 Os245 and Os245' Prevent Cell Death and Preserve Mitochondrial

Function in Primary Cortical Neurons Subjected to a Lethal Period of OGD

After examination of the cell permeability of Os245 and Os245' in neurons, their

ability to protect against OGD-induced cell death was assessed. Both

compounds produced a concentration-dependent increase in cell viability,

indicating that these new inhibitors can protect neurons from the toxic

mitochondrial Ca^{2+} overload responsible for viability loss after a lethal period of

OGD. Despite differences in cellular uptake between Os245 and Os245', both

compounds generated comparable protection at similar concentrations. Also,

compared to Ru265, these Os compounds are approximately 5-6-fold less potent

at preserving cell viability in the OGD model. This was unexpected because

Os245' and R265 are equally potent MCU_{cx} inhibitors in permeablized HeLa

cells. The reasons for differences in the cytoprotective potencies of Ru265 and

Os245' are unclear but may reflect the lower cellular uptake in cortical neurons, different intracellular binding, and slower reaction kinetics of Os245'.

In the Seahorse assay analysis that was used to measure mitochondrial function, treatment of cortical neuron cultures with Os245 or Os245' under normal culture conditions did not alter OCR or ECAR levels, indicating that neither of these compounds negatively affected mitochondrial bioenergetics. In addition, both compounds were able to completely preserve mitochondrial respiration and glycolysis when added to cortical neuron cultures before exposure to OGD. This is consistent with their abilities to inhibit mitochondrial Ca^{2+} uptake in intact cells and in line with the earlier findings with Ru265. That is, preventing MCU_{cx}-mediated mitochondrial Ca^{2+} overload blocks the subsequent collapse of mitochondrial function in cell-based models of ischemic/reperfusion injury (Kwong et al., 2015; Nichols et al., 2018).

6.3.3 Relative to Ru265, Convulsion Onset was Delayed but Convulsions Were Equally Severe in Mice Treated with Os245 or Os245'

Since Os245 and Os245' were shown to be less potent neuroprotectants and to have slower reaction kinetics compared to Ru265, it was speculated that these compounds may be less likely to cause convulsions in mice. However, both Os245 and Os245' induced convulsions in adult male mice, although the onset of this activity was delayed when compared to Ru265. This delay may likely be a consequence of their slower and lower cellular uptake compared Ru265 (Figures

6.2 and 3.2). Importantly, the slower onset of convulsions with Os245 and Os245'

has potentially important implications for the therapeutic development of MCU_{cx}

inhibitors by showing that structural modifications influence the onset of

convulsions.

6.3.4 The Addition of Adamantane Ligands to Ru265 and Os245' Resulted in Improved Neuroprotective Potency

The last analogues assessed were adamantane derivatives of Ru265 (RuOAd)

and Os245' (OsOAd). These analogues have an adamantane carboxylic acid

ligand added to each side of the parent compound. This chemical strategy was

designed to further assess the effects of changes in the axial ligands on cellular

uptake and neuroprotective potency. The addition of adamantane was selected

to improve cellular uptake based on unpublished observations in intact HeLa

cells (Wilson Lab). In cortical neuron cultures, treatment with RuOAd or OsOAd

resulted in improved potency against OGD-induced cell death when compared to

Ru265 or Os245' respectively. This improved potency was especially

pronounced with OsOAd compared to Os245'.

It is possible that this improved potency might be due to the presence of the

adamantane itself, which has been shown to block excitotoxic cell death

implicated in ischemic stroke (Kadernani et al., 2014). Furthermore, adamantane

derivatives have been reported to be neuroprotective in a variety of cell based

and animal models of neurodegenerative disorders (Danysz et al., 2021;

Kadernani et al., 2014). In particular, the adamantane derivatives amantadine and memantine are approved drugs for the treatment of Parkinson's disease and Alzheimer's disease (Danysz et al., 2021; Ossola et al., 2011; Quarato et al., 2014; Robinson & Keating, 2006). Amantadine and memantine are weak antagonists of the N-methyl-D-aspartate (NMDA) receptor (Kadernani et al., 2014; Ossola et al., 2011; Robinson & Keating, 2006). Although NMDA receptor antagonism is thought to contribute to the neuroprotective effects of these drugs, other mechanisms may be involved (Kadernani et al., 2014; Ossola et al., 2011; Robinson & Keating, 2006). For example, amantadine and memantine may exert neuroprotective effects by increasing the expression of brain-derived neurotrophic factor in the brain (Marvanová et al., 2001; Zhong et al., 2020). These drugs are also anti-inflammatory. Amantadine and memantine block the induction of pro-inflammatory cytokines by LPS (Ossola et al., 2011; Rosi et al., 2009). As discussed in more detail below, amantadine and memantine have been shown to target mitochondria and reduce injurious oxidative stress (McAllister et al., 2008; Quarato et al., 2014). It is therefore likely that the therapeutic effects of RuOAd and OsOAd stem from a combination of actions (Danysz et al., 2021).

In addition to Parkinson's disease and Alzheimer's disease, there is amounting evidence from animal and human studies suggesting that amantadine and adamantane derivatives might be neuroprotective in other neurodegenerative conditions including stroke, Huntington's disease, and infectious diseases

(Danysz et al., 2021; Kadernani et al., 2014; Krivonos et al., 2010). There are a few animal studies indicating that amantadine protects the brain from damage by an ischemic and hemorrhagic stroke (Krivonos et al., 2010; Mirzoyan et al., 2014). There is also evidence supporting the protective effects of amantadine against mitochondrial dysfunction caused by hepatitis C infection (Quarato et al., 2014). Hepatitis C viral proteins are known to induce mitochondrial dysfunction consisting of an increase in mitochondrial Ca^{2+} uptake and ROS production, and reduced oxygen consumption and depolarization of the $\Delta\Psi_m$ (Quarato et al., 2014). Amantadine was able to effectively preserve cellular bioenergetics and redox homeostasis, and prevent hepatitis C viral protein-induced mitochondrial dysfunction, possibly through inhibition of intracellular Ca^{2+} flux-regulating channels or other cation channels (Quarato et al., 2014). This suggests that adamantane may be providing additional protective benefits against OGD in cortical neuron cultures through further inhibition of Ca^{2+} overloading, anti-oxidative actions, and/or preservation of mitochondrial function. It is thought that the adamantane ligands dissociate from the parent compound after entering the cell, resulting in both adamantane and Ru265 or Os245' being present in the cells. As a result, the presence of both compounds might protect against OGD-induced cell death by distinct mechanisms. With respect to opposing mitochondrial Ca^{2+} overloading, unpublished findings from the Wilson laboratory indicate that adamantane (50 µM) does not block mitochondrial Ca^{2+} uptake in HeLa cells. Hence, adamantane does not appear to reduce mitochondrial Ca^{2+}overloading by blocking the MCU_{cx}. Further experiments in the Wilson

128

laboratory have shown that RuOAd and OsOAd have higher IC_{50s} for MCU_{cx} inhibition (RuOAd IC_{50} = 50.5 nM; OsOAd IC_{50} = 309 nM) compared to Ru265 (IC_{50} = 8.6 nM) and Os245' (IC_{50} = 5.7 nM) in permeabilized HEK293T cells. Despite their higher IC_{50s} for MCU_{cx} inhibition compared to Ru265, both RuOAd and OsOAd had EC_{50s} lower than Ru265 for preserving cell viability after OGD in primary cortical neuron cultures. This suggests that following dissociation from RuOAd and OsOAd, adamantane interacts with neuroprotective targets other than the MCU_{cx} to promote additional protective benefits.

The increased potency of RuOAd or OsOAd relative to Ru265 demonstrates how modifications can be made to this class of inhibitors to alter their pharmacological properties. This opens the door to examining other iterations of these compounds with the goal of developing compounds with a lower probability of inducing convulsions. The enhanced potency against OGD-induced cell viability loss produced by the addition of adamantane to Ru265 or Os245' is also encouraging in this regard. Whether this chemical strategy also improves the safety of these compounds awaits the results of future studies.

Chapter 7: NCLX Activation Enhanced the Preservation of Cell Viability and Mitochondrial Function in Cortical Neuron Cultures Subjected to OGD by MCU$_{cx}$ Inhibition

7.1 Introduction

Despite the promising neuroprotective properties displayed by Ru265, the therapeutic use of this MCU$_{cx}$ inhibitor is limited by the induction of convulsions at higher doses. One strategy to overcome this problem is to identify a complimentary approach that enables the use of a lower dose of Ru265 to achieve neuroprotection with a reduced risk of adverse side effects. In this regard, an attractive approach to mitigate the risk of toxic mitochondrial Ca^{2+} overloading is to combine activation of mitochondrial Ca^{2+} efflux with MCU$_{cx}$ inhibition. The NCLX is the main exchanger protein involved in mitochondrial Ca^{2+} efflux, and unlike other Na^+/Ca^{2+} exchanger proteins, it is uniquely able to mediate mitochondrial Na^+ or Li^+ influx and Ca^{2+} efflux (Palty et al., 2010; Roy et al., 2017). The regulatory domain of this exchanger contains a cluster of positively charged residues that are thought to act like a channel voltage sensor (Kostic et al., 2018). Studies monitoring NCLX activity under variations in the $\Delta\Psi_m$ suggest that this site senses the $\Delta\Psi_m$ and tunes NCLX activity accordingly (Kostic et al., 2018). The NCLX imports 3 Na^+ ions in exchange for the export of 1 Ca^{2+} ion from the mitochondrial matrix. The net positive charge in the matrix is offset by the strong negative charge generated by the $\Delta\Psi_m$ (-180 mV). NCLX activity is therefore electrogenic and depends on the $\Delta\Psi_m$ to provide the driving

force. This suggests that depolarization of the $\Delta\Psi_m$ during cerebral ischemia increases the probability of mitochondrial Ca^{2+} overloading by suppressing NCLX activity (Giorgio et al., 2018; Kostic et al., 2018). In support of this hypothesis, selective NCLX deletion in cardiac myocytes at adulthood causes sudden death with less than 13% of affected mice surviving after 14 days (Luongo et al., 2017). Lethality was attributed to mitochondrial Ca^{2+} overloading resulting in necrotic cardiac cell death (Luongo et al., 2017). Conversely, overexpression of the NCLX in cardiac myocytes protects the heart against ischemic/reperfusion injury (Luongo et al., 2017). Increasing NCLX activity is therefore an alternative approach to reduce the risk of mitochondrial Ca^{2+} overloading.

The NCLX regulatory domain, a loop that joins the α1 and α2 transmembrane domains located within the mitochondrial matrix, contains several phosphorylation sites, notably for PKA and Ca^{2+}/calmodulin-dependent kinase 2 (Katoshevski et al., 2021). Phosphorylation of these sites increases NCLX activity (Katoshevski et al., 2022; Kostic et al., 2018; Kostic et al., 2015). Mitochondrial PKA activation markedly increases NCLX activity by phosphorylating a serine residue (S258) in the regulatory domain of this exchanger (Kostic et al., 2018; Kostic et al., 2015). PKA is allosterically activated by a rise in cAMP levels (Acin-Perez et al., 2009). PDE inhibitors that block the degradation of cAMP therefore stimulate PKA activity (Conti & Beavo, 2007). PDE2A contains a mitochondrial translocation signal that targets this PDE subtype to the mitochondrial matrix (Acin-Perez et al., 2011). PDE2A inhibitors

have been shown to increase NCLX activity by enhancing the PKA-mediated phosphorylation of serine S258 (Kostic et al., 2018; Kostic et al., 2015). The resultant increase in NCLX activity protects neurons from excitotoxicity by opposing mitochondrial Ca^{2+} overloading (Rozenfeld et al., 2022). Impaired PTEN-induced putative kinase 1 (PINK1) function, implicated in Parkinson disease, suppresses NCLX activity resulting in mitochondrial Ca^{2+} overloading (Kostic et al., 2015). The PKA agonist forskolin preserves PINK1-deficient dopaminergic neurons by increasing NCLX activity (Kostic et al., 2015).

Based on these findings, it was reasoned that combining low concentrations Ru265 and a PDE2A inhibitor would generate synergistic neuroprotection, thus reducing the risk of adverse side effects with Ru265. To test this hypothesis, cortical neuron cultures were treated with various concentrations of Ru265 and the potent PDE2A inhibitor PF-05180999 (Figure 7.1A; IC_{50}=2 nM) (Helal et al., 2018) either alone or in combination, and then subjected to OGD. Cell viability, cytotoxicity, and mitochondrial function were then measured to determine the potential benefits of combining Ru265 and PF-05180999.

7.2 Results

7.2.1 NCLX Activation with the PDE2A Inhibitor PF-05180999 did not Alter OGD-induced Cell Viability Loss or Cytotoxicity

To examine the protective effects of NCLX activation by the inhibition of PDE2A, primary cortical neuron cultures were treated with increasing concentrations of

PF-05180999 (10, 30, 50, 100, 300, or 500 nM) for 24 hr before being subjected

to 90 min of OGD. Cell viability or cytotoxicity was measured 24 hr after OGD.

Percent cell viability, measured using the MTT assay, was calculated relative to

control (No OGD) cultures (Figure 7.1B). Percent cytotoxicity, measured using

the LDH assay, was calculated relative to maximal LDH release in control

cultures subjected to complete cell lysis. (Figure 7.1C). None of the PF-

05180999 concentrations altered cortical neuron viability loss or cell cytotoxicity

24 hr after OGD (Figure 7.1B-C).

PF-05180999
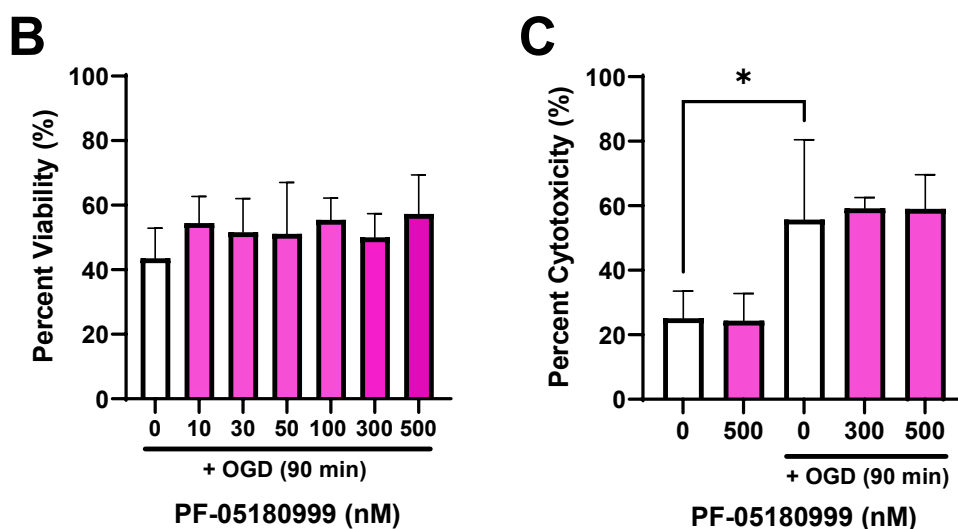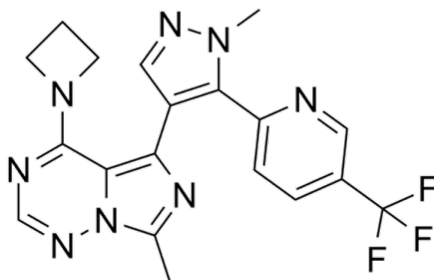
Figure 7.1. PF-05180999 was not able to preserve cell viability or prevent cell cytotoxicity after OGD

Chemical structure of PF-05180999 (A). Primary cortical neuron cultures were treated with vehicle (DMSO) or increasing concentrations of PF-05180999 for 24 hr before being subjected to OGD (90 min). Cell viability was assessed using the MTT assay (B) and cell cytotoxicity was assessed using the LDH assay (C) 24 hr after OGD. Values represent the percent cell viability relative to control (No OGD) cultures (100% cell viability) (B) and percent cytotoxicity relative to maximal LDH release in cultures subjected to complete cell lysis (100% cell cytotoxicity) (C). Bars show the mean ± SD of data from 3 experiments, 6 wells/experiment. *$p < 0.05$; ordinary one-way ANOVA followed by Tukey's multiple comparisons test.

7.2.2 Combining Ineffective Concentrations of Ru265 and PF-05180999 Markedly Protected Cortical Neuron Cultures Against OGD-induced Cell Death

To test whether combining MCU_{cx} inhibition with NCLX activation would result in greater neuroprotection, primary cortical neurons cultures were treated with both Ru265 and PF-05180999 for 24 hr before being subjected to OGD. Based on previous experiments (Figure 3.4A), a concentration of 3 µM of Ru265 was selected for testing in combination with varying concentrations of PF-05180999. Cortical neuron cultures were treated with either Ru265 (3 µM) only, PF-05180999 (500 nM) only, or Ru265 (3 µM) plus increasing concentrations of PF-05180999 (10, 30, 50, 100, 300, or 500 nM) for 24 hr before being subjected to 90 min of OGD. Percent cell viability, measured using the MTT assay, was calculated relative to control (No OGD) cultures (Figure 7.2A). Percent cytotoxicity, measured using the LDH assay, was calculated relative to maximal LDH release in control cultures subjected to complete cell lysis (Figure 7.2B). Co-treatment with 3 µM of Ru265 and increasing concentrations of PF-05180999 (50, 100, 300, or 500 nM) resulted in higher percent cell viability than either Ru265 (3 µM) or PF-05180999 (500 nM) 24 hr after 90 min of OGD (Figure 7.2A). Ru265 (3 µM) plus PF-05180999 (300 nM) and Ru265 (3 µM) plus PF-05180999 (500 nM) increased percent viabilities in OGD-treated cells from 43.5 ± 9.4% to 81 ± 10.2% and 84 ± 10.6% (mean ± SD), respectively (Figure 7.2A). Ru265 (3 µM) plus PF-05180999 (300 nM) and Ru265 (3 µM) plus PF-05180999 (500 nM) also reduced percent cytotoxicity from 55 ± 24.8% to 28 ± 9.7% and 19

± 3.5% (mean ± SD), respectively (Figure 7.2B). These results show that combining ineffective concentrations of Ru265 and PF-05180999 markedly protects cortical neurons from OGD-induced cell death.
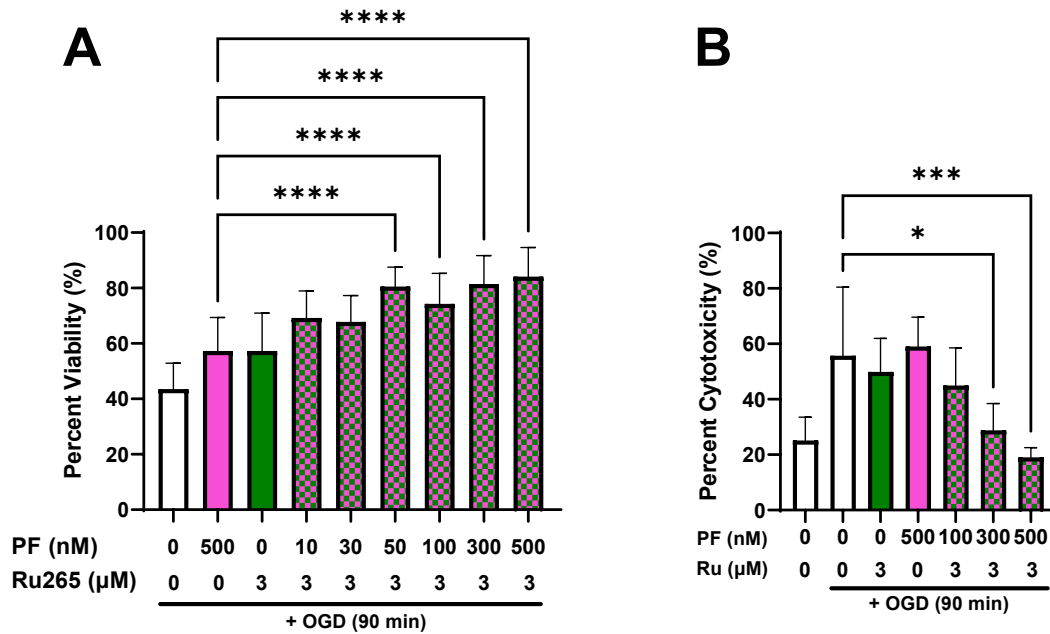
Figure 7.2. Co-treatment with ineffective concentrations of Ru265 and PF-05180999 significantly improves protection against OGD

Primary cortical neuron cultures were co-treated with Ru265 (3 µM) and increasing concentrations of PF-05180999 (10-500 nM) for 24 hr before OGD (90 min). Cell viability was assessed using the MTT assay (A) and cell cytotoxicity was assessed using the LDH assay (B) 24 hr after OGD. Percent viability values represent viability relative to control (No OGD) cultures (100% cell viability) (A), and percent cytotoxicity values represent cytotoxicity relative to maximal LDH release in cultures subjected to complete cell lysis (100% cell cytotoxicity) (B). Bars show the mean ± SD of data from 3 experiments, 6 wells/experiment. *p<0.05, ***p<0.001, ****p<0.0001; ordinary one-way ANOVA followed by Tukey's multiple comparisons test.

7.2.3 Combining Ru265 with PF-05180999 Synergistically Increases Cell Viability

To examine if combining Ru265 and PF-05180999 produces synergistic neuroprotection, cortical neuron cultures were treated with increasing concentrations of Ru265 (1, 2, 3, 5, or 10 µM) and PF-05180999 (10, 30, 50, 100, 300, or 500 nM) for 24 hr, subjected to OGD (90 min), and assessed for cell viability 24 hr later using the MTT assay. Percent viability was calculated relative to control (No OGD) cultures and the resultant values were used to calculate synergy scores using the SynergyFinder software and the Bliss independence drug interactions model (Ianevski et al., 2022). The 3D matrix map shows which combinations of Ru265 and PF-05180999 are potentially synergistic (Figure 7.3). Based on this 3D map, the most synergistic region was predicted to correspond to the combination of 3-5 µM of Ru265 and 100-500 nM of PF-05180999 (Figure 7.3). Co-treatment of 3 µM of Ru265 and either 50 or 300 or 500 nM of PF-05180999 resulted in synergy scores greater than 10, indicating that combining these concentrations of Ru265 and PF-05180999 yielded a synergistic increase in cell viability for cortical neuron cultures subjected to OGD (Table 3).
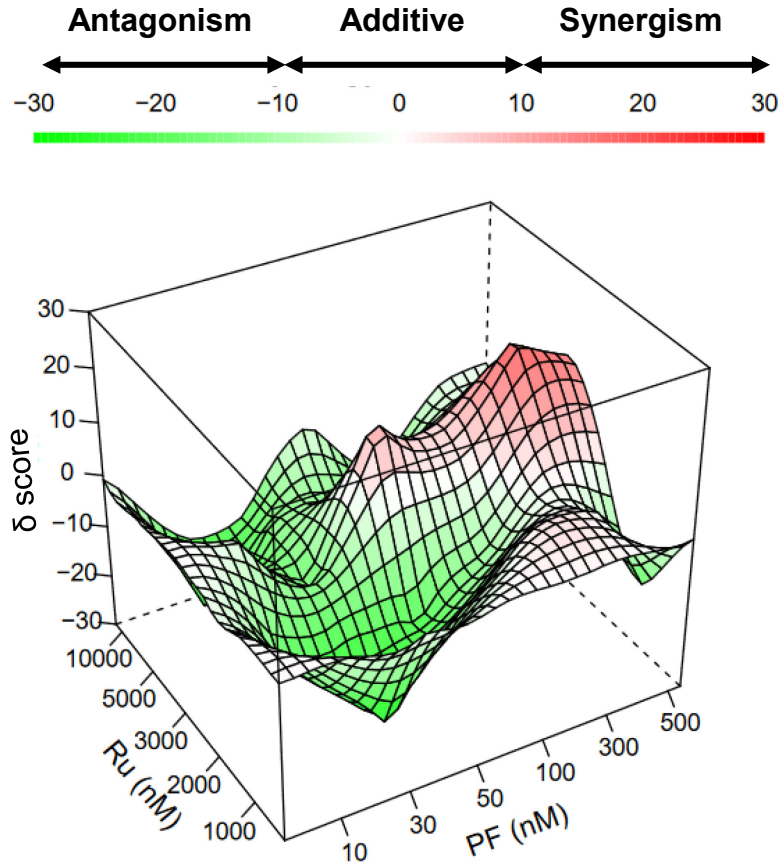
Figure 7.3. Combining Ru265 with PF-05180999 synergistically increases cell viability

Primary cortical neuron cultures were treated with increasing concentrations of Ru265 (1, 2, 3, 5, or 10 µM) and PF-05180999 (10, 30, 50, 100, 300, or 500 nM) for 24 hr before OGD (90 min), and cell viability relative to control (No OGD) cultures was assessed 24 hr later using the MTT assay. Percent cell viability calculations were then inputted into the SynergyFinder software to generate a 3D synergy map using the Bliss independence drug interactions model to assess the potential, antagonistic, additive, or synergistic effects of combining Ru265 with PF-05180999. Scores <-10 (green areas) indicate potential antagonism, scores between -10 and 10 (white areas) indicate potential additivity, and scores >10 (red areas) indicate potential synergy.

Table 3. Concentrations of Ru265 and PF-05180999 that produced the greatest synergy scores

[Ru265] (µM)	[PF-05180999] (nM)	Synergy Score
3	300	18.72
3	50	12.4
3	500	11.83
3	100	3.63
2	300	2.79

Note: Scores >10 = likely synergistic; scores between -10 and 10 = likely additive.

7.2.4 Combining Ineffective Concentrations of Ru265 and PF-05180999 Markedly Preserves OCR after OGD

Finally, mitochondrial respiration parameters such as basal respiration, maximal respiratory capacity, and SRC were assessed in primary cortical neuron cultures co-treated with Ru265 and PF-05180999 using the Seahorse XFe96 extracellular flux assay analyser (Figure 7.4A-C). These experiments were performed using the newer and more sensitive Seahorse XFe96 analyzer. Pilot experiments showed that unlike earlier experiments using the Seahorse XFe24 analyser where 50 µM of Ru265 was required for neuroprotection, a lower concentration of Ru265 (10 µM) was sufficient to reduce OGD-induced cell death in the Seahorse XFe96 plates. Titration experiments determined that 1 µM was the optimal concentration of FCCP for inducing maximal respiration with this analyser and cell type, and that 90 min of OGD was necessary to consistently produce about a 50% loss of neuronal cell viability in the XFe96 plates. In keeping with earlier experiments, vehicle-treated neuron cultures that were subjected to OGD exhibited a marked suppression of OCR relative to vehicle-treated No OGD cultures (Figure 7.4A-C). Treatment with 10 µM of Ru265 for 24 hr before OGD effectively preserved mitochondrial respiration 2 hr after OGD while 3 µM of Ru265 was ineffective (Figure 7.4A). At concentrations of 300 and 500 nM, PF-05180999 also failed to prevent the decline in OCR produced by OGD (Figure 7.4B). In dramatic contrast, combining ineffective concentrations of Ru265 and PF-05180999 either partially [Ru265 (3 µM) plus PF-05180999 (300 nM)] or

completely [Ru265 (3 µM) plus PF-05180999 (500 nM)] preserved mitochondrial

respiration 2 hr after OGD (Figure 7.4C).
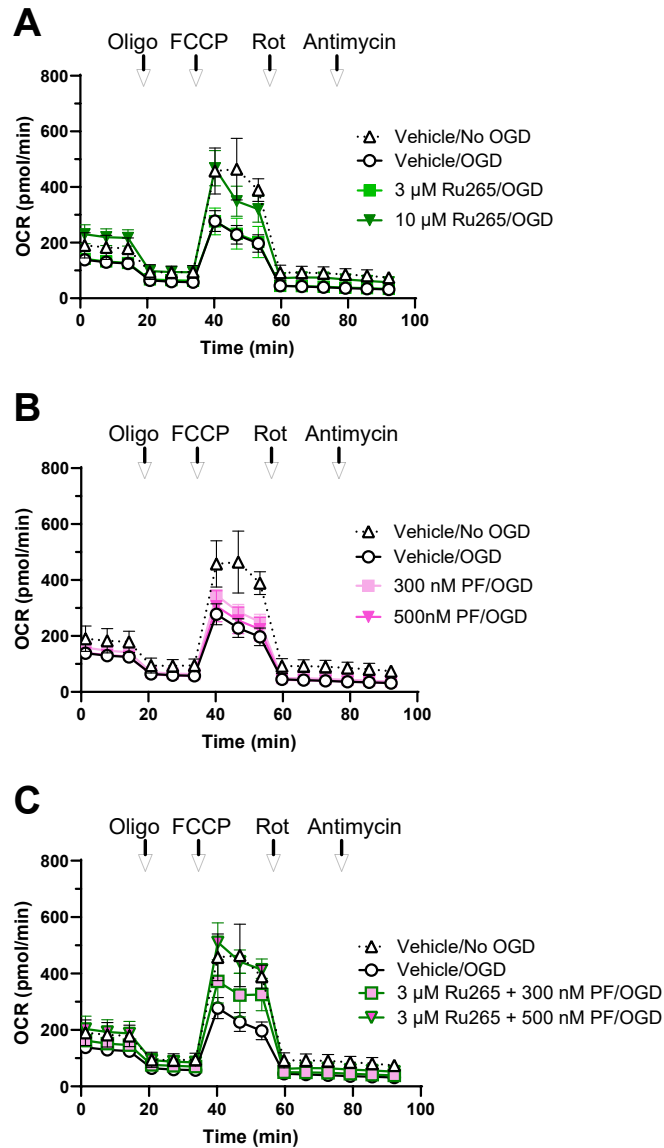
Figure 7.4. Co-treatment with Ru265 and PF-05180999 produced a supra-additive preservation of mitochondrial respiration in cortical neuron cultures subjected to OGD

The Seahorse XFe96 extracellular flux analyser was used to measure mitochondrial respiration in primary cortical neuron cultures. OCR are shown for cortical neuron cultures after the sequential addition of Oligo (1 μM), FCCP (1 μM), Rot (300 nM) and Antimycin (5 μM). OCR was measured 2 hr after OGD (90 min) in cortical neuron cultures treated with either vehicle (DMSO), 3 or 10 μM of Ru265 (A), 300 or 500 nM of PF-05180999 (B) or a combination of 3 μM Ru265 and 300 or 500 nM PF-05180999 (C) for 24 hr before OGD. Traces with white triangles represent vehicle-treated control (No OGD) cultures, and traces with white circles represent vehicle-treated OGD cultures. Bars show the mean ± SD of data representative of 2 experiments, 8 wells/experiment.

7.2.5 Combining Ineffective Concentrations of Ru265 and PF-05180999

Markedly Preserves Various Aspects of Mitochondrial Function

Lastly, the effects of either Ru265, PF-05180999, or Ru265 plus PF-05180999 on various aspects of mitochondrial respiration were analyzed. Treatment with 3 µM of Ru265 failed to reduce the loss of basal respiration, maximal respiratory capacity, and SRC 2 hr after OGD (Figure 7.5A, C, E). By contrast, treatment with 10 µM of Ru265 completely preserved basal respiration, maximal respiratory capacity, and SRC 2 hr after OGD (Figure 7.5A, C, E). Treatment with 300 or 500 nM of PF-05180999 failed to reduce the loss of basal respiration, maximal respiratory capacity, and SRC 2 hr after OGD (Figure 7.5B, D, F). Combining the ineffective concentration of Ru265 (3 µM) with the lower ineffective concentration of PF-05180999 (300 nM) partially prevented the loss of basal respiration after OGD (Figure 7.6A). By contrast, combining the ineffective concentration of Ru265 (3 µM) with the higher ineffective concentration of PF-05180999 (500 nM) completely prevented the loss of basal respiration after OGD (Figure 7.6B). Furthermore, co-treatment with the ineffective concentration of Ru265 (3 µM) and the lower ineffective concentration of PF-05180999 (300 nM) completely preserved maximal respiration and SRC (Figure 7.6C, E). Similarly, combining the ineffective concentration of Ru265 (3 µM) with the higher ineffective concentration of PF-05180999 (500 nM) completely preserved maximal respiration and SRC (Figure 7.6D, and F). These findings suggest that synergistic neuroprotection produced by combining Ru265 and PF-05180999 is mediated by the preservation of multiple aspects of mitochondrial function.
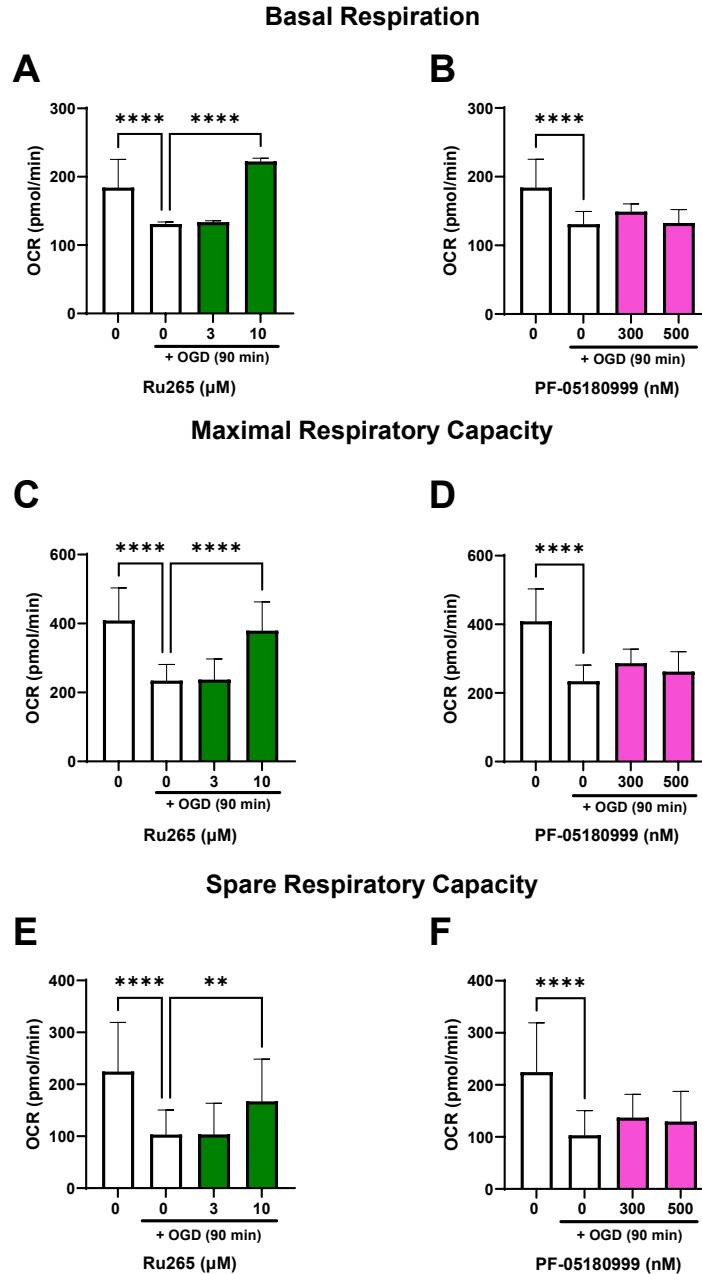
Figure 7.5. Mitochondrial respiration parameters of primary cortical neurons treated with Ru265 or PF-05180999 and then subjected to OGD

Basal respiration (A-B), maximal respiratory capacity (C-D), and spare respiratory capacity (E-F) of primary cortical neuron cultures treated vehicle (DMSO), 3 or 10 µM of Ru265 (A, C, E), or 300 or 500 nM of PF-05180999 (B, D, F) for 24 hr before OGD (90 min). OCR was measured under control (No OGD) conditions and 2 hr after OGD. Bars show the mean ± SD of data representative of 2 experiments, 8 wells/experiment. **p<0.01, ****p<0.0001; ordinary one-way ANOVA followed by Tukey's multiple comparisons test.

145
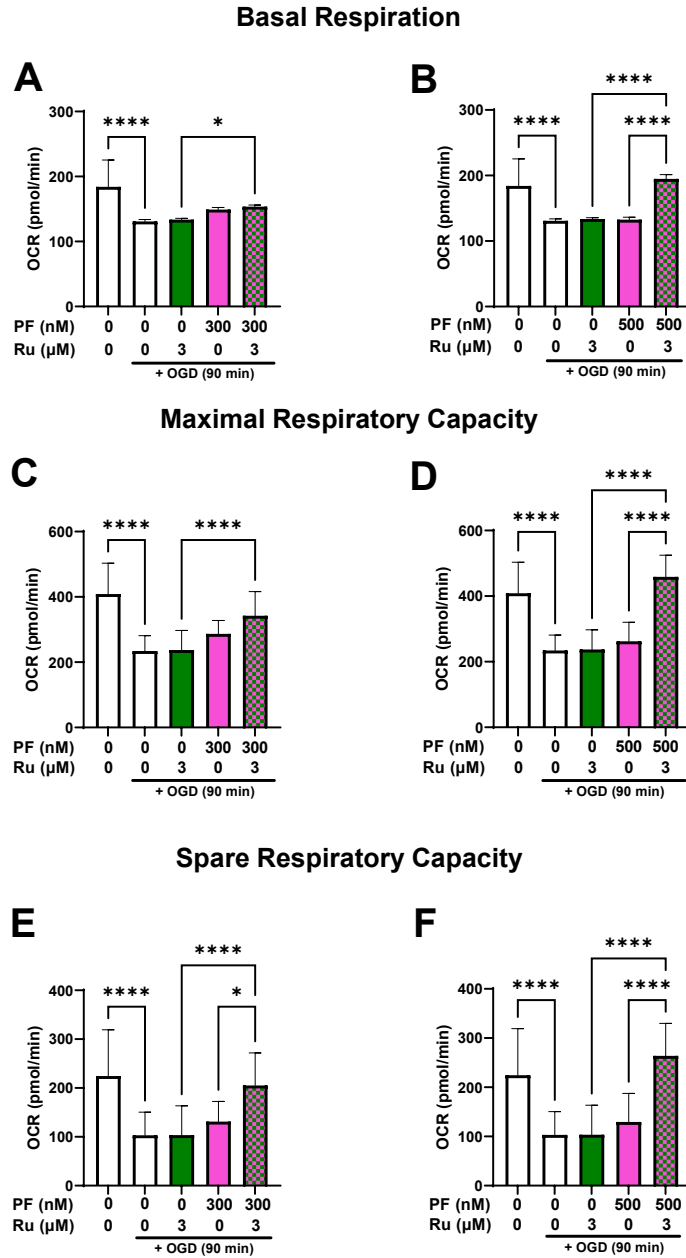
Figure 7.6. Mitochondrial respiration parameters of primary cortical neurons treated with 3 µM Ru265 and PF-05180999 and then subjected to OGD

Basal respiration (A-B), maximal respiratory capacity (C-D), and spare respiratory capacity (E-F) of primary cortical neuron cultures treated with vehicle (DMSO), 3 µM Ru265 and 300 nM PF-05180999 (A, C, E), or 3 µM Ru265 and 500 nM PF-05180999 (B, D, F) for 24 hr before OGD (90 min). OCR was measured under control (No OGD) conditions and 2 hr after OGD. Bars show the mean ± SD of data representative of 2 experiments, 8 wells/experiment. *p<0.05, ****p<0.0001; ordinary one-way ANOVA followed by Tukey's multiple comparisons test.

7.3 Discussion

7.3.1 Combining Ineffective Concentrations of Ru265 with PF-05180999 Synergistically Protected Cortical Neuron Cultures Against OGD-induced Cell Death

First, the protective effects of NCLX activation with the PDE2A inhibitor PF-05180999 were assessed in the OGD model. No concentrations of PF-05180999 tested (10-500 nM) were able to prevent cortical neuron cell death 24 hr after injury. It is possible that higher concentrations might have elicited an increase in viability, however, PF-05180999 partially blocks other PDEs at micromolar (μM) concentrations (Helal et al., 2018). Higher (μM) concentrations of PF-05180999 were therefore avoided to maintain selectivity for PDE2A inhibition. Since the rate of Ca^{2+} efflux by NCLX is much slower than MCU_{cx}-mediated mitochondrial Ca^{2+} influx (Palty et al., 2010), NCLX activation alone might not be sufficient to mitigate the rapid overloading of mitochondria with Ca^{2+} that is responsible for OGD-induced cell death. However, when combined with concentrations of Ru265 (3 μM) that were ineffective at protecting neurons from OGD-induced cell death, PF-05180999 (50-500 nM) was able to markedly increase cell viability. This suggests that PF-05180999 did enhance some degree of mitochondrial Ca^{2+} efflux, however, mitochondrial Ca^{2+} levels will have to be measured to see if this is the case. When taken together, these finding indicate that targeting both mitochondrial Ca^{2+} influx and efflux to reduce mitochondrial Ca^{2+} overloading confers profound protection in this model. It should therefore be possible to use lower doses of each compound to safely achieve protection in animal models of

ischemic stroke. This predicted outcome would encourage the clinical testing of

Ru265 and PF-05180999 for safety and efficacy in ischemic stroke.

The SynergyFinder 3.0 software system was employed to determine which

concentration combinations of Ru265 and PF-05180999 potentially produced a

synergistic preservation of cortical neuron viability after OGD treatment. Potential

synergy was assessed using the Bliss independence model, which assumes

independent sites of action for Ru265 and PF-05180999 (Ianevski et al., 2022).

The resultant synergy score for combining Ru265 with PF-05180999 indicated

that the observed protection was greater than for what would be expected for

either compound alone. This demonstrates that combining MCU_{cx} inhibition with

NCLX activation is a viable strategy to reduce the concentration of Ru265

required to protect cortical neurons from OGD-induced cell viability loss.

7.3.2 Combining Ineffective Concentrations of Ru265 and PF-05180999 Markedly Preserves Various Aspects of Mitochondrial Function

Based on the concentration combinations that were predicted to be the most

synergistic, low concentrations of Ru265 and PF-05180999 were chosen to

assess the benefits of combining MCU_{cx} inhibition with NCLX activation at

preserving mitochondrial function after OGD. The XF96 extracellular Flux

Analyzer was used to measure various aspects of mitochondrial function and to

evaluate overall mitochondrial health and bioenergetics. The addition of

oligomycin inhibits ATP synthase, which allows for a measure of ATP production

at basal respiration (Brand & Nicholls, 2011). The response of the neuron cultures to the uncoupling of ATP production from ETC activity after the addition of the uncoupler FCCP represents the maximal respiratory capacity of the cultures (Brand & Nicholls, 2011). This uncoupling demonstrates the maximum activity of electron transport and substrate oxidation that is achievable by these cells, and a decrease in this measurement is a strong indicator of potential mitochondrial dysfunction (Brand & Nicholls, 2011). The difference in maximal respiratory capacity and basal respiration is the SRC, which is an important measurement of mitochondrial bioenergetics in cells such as neurons that can experience variation in ATP demand (Brand & Nicholls, 2011). As with maximal respiratory capacity, a low SRC indicates potential mitochondrial dysfunction, and suggests that the neurons are operating close to their bioenergetic limit and have a reduced ability to respond rapidly and effectively to changes in metabolic demands (Brand & Nicholls, 2011). Taken together, these parameters provide a framework to assess mitochondrial function under different conditions or stressors.

As seen in earlier experiments, OGD treatment suppressed basal respiration and FCCP-induced maximal respiratory capacity and resulted in a loss of SRC in vehicle treated cortical neuron cultures. Treatment with Ru265 (10 µM), but not PF-05180999 (300 or 500 nM), prevented reductions in all mitochondrial respiratory parameters after OGD. This finding is in line with the earlier cell viability and toxicity experiments showing the neuroprotective effects of Ru265

(10 µM). In comparison, combining an ineffective concentration of Ru265 (3 µM) with PF-05180999 (300 or 500 nM) produced a similarly complete preservation of basal respiration, maximal respiratory capacity, and SRC after OGD. Co-treatment with ineffective concentrations of Ru265 and PF-05180999 therefore prevented the dysregulation of mitochondrial bioenergetics from occurring after OGD. SRC was also maintained, indicating that the cultures were able to respond normally to increased metabolic demands.

The ability of combining ineffective concentrations of Ru265 and PF-05180999 to preserve mitochondrial function to the same degree as 10 µM of Ru265 indicates that partial MCU_{cx} inhibition combined with NCLX activation markedly opposed OGD-induced mitochondrial Ca^{2+} overloading. These results reflect the importance of preserving mitochondrial Ca^{2+} handling dynamics during and after periods of ischemic injury and suggest that the synergistic neuroprotection produced by combining Ru265 and PF-05180999 is mediated by the preservation of multiple aspects of mitochondrial function. Since 10 µM of Ru265 produced the near complete protection against OGD, these results showing comparable protection with Ru265 and PF-05180999 co-treatment highlights the potential to improve the safety and efficacy of these compounds through combined treatment. In addition, these results support the potential of combining a low dose of Ru265 with other neuroprotective strategies, like NCLX activation, to effectively reduce ischemic brain injury by preventing mitochondrial Ca^{2+} overloading. Future studies will be required to determine if combining MCU_{cx}

inhibition with NCLX activation safely and effectively protects mice subjected to

an experimental stroke against sensorimotor deficits and neuronal cell loss.

Chapter 8: Discussion

Stroke is a leading cause of death and disability worldwide (Grefkes & Fink, 2020). Moreover, as the population continues to age, the need for drugs that protect the brain from damage by a stroke will become increasingly urgent (Feigin et al., 2022). Despite large scale efforts by many major pharmaceutical companies, a viable protective strategy has yet to emerge (Chamorro et al., 2021). One strategy to overcome this problem is to identify and target a pivotal upstream event responsible for initiating the vast array of injury mechanisms implicated in ischemic brain damage. In this regard, models of ischemic stroke have shown that mitochondrial dysfunction is an early pathological event which triggers a complex death cascade (Green et al., 2014; He et al., 2020). Mitochondria are widely regarded as the 'powerhouse of the cell' that generate ATP which fuels the chemical reactions essential for life (Lehninger, 1979). Mitochondrial Ca^{2+} uptake provides crucial metabolic support by stimulating ATP synthesis and buffering cytosolic Ca^{2+} (Duchen, 2000). The brain is therefore highly reliant on high-capacity mitochondrial Ca^{2+} uptake to meet the dynamic metabolic demands imposed by neurotransmission (Kann & Kovacs, 2007). However, excessive mitochondrial Ca^{2+} uptake rapidly damages these delicate organelles, resulting in metabolic collapse and the release of numerous pro-death factors (Duchen, 2012). During cerebral ischemia, neurons are subjected to massive elevations in cytosolic Ca^{2+} levels that increase the risk of toxic mitochondrial Ca^{2+} overloading (Vakifahmetoglu-Norberg et al., 2017; Yang et al., 2018). The MCU_{cx} mediates high-capacity mitochondrial Ca^{2+} uptake

152

responsible for ischemic neuronal cell death (Nichols et al., 2017; Nichols et al., 2018). This suggest that the MCU_{cx} is a promising drug target for ischemic stroke. This thesis therefore examined the ability of MCU_{cx} inhibitors to protect neurons from ischemic cell death by preserving mitochondrial function.

A second explanation for the repeated clinical failure of putative protectants for ischemic stroke has been the focus on neuronal cell death. In addition to neurons, vascular cells and glia are damaged by an ischemic stroke (Iadecola, 2017). Vascular cells, glia, and neurons form an intricate structure known as the NVU (Iadecola, 2017). These cells interact to restrict the movement of potentially toxic metabolites and proteins into the brain, and rapidly adjust CBF in crucial support of increased brain activity (Iadecola, 2017). It is now clear that the NVU is exquisitely sensitive to damage by cerebral ischemia (Schaeffer & Iadecola, 2021). This suggests that to effectively treat ischemic stroke, it is necessary to not only protect neurons but also other components of the NVU. Hence, this thesis also investigated the ability of MCU_{cx} inhibitors to protect astrocytes subjected to a lethal period of OGD from viability loss and mitochondrial dysfunction.

A third explanation for the lack of clinical efficacy of putative protectants for ischemic stroke is their inability to suppress inflammation. The generation of pro-inflammatory mediators after the initial wave of damage is thought to exacerbate brain injury. Mitochondrial damage results in the production of DAMPs and

activation of the NLRP3 inflammasome, which potently induce pro-inflammatory signalling (Gong et al., 2018). Excessive mitochondrial Ca^{2+} uptake may also promote inflammation by inducing the overproduction of ROS that activates pro-inflammatory cytokine expression by the redox-sensitive transcriptional regulating factor NF-κB (Piette et al., 1997). Hence, this thesis examined the ability of MCU$_{cx}$ inhibitors to suppress the elevation of pro-inflammatory cytokine mRNA levels in astrocytes and endothelial cells treated with an inflammatory mediator.

8.1 MCU$_{cx}$ Inhibition as an Effective Strategy of Neuroprotection against Ischemic Injury

Mitochondrial Ca^{2+} overloading is an early pathological event in ischemic brain injury that initiates diverse cell death pathways (Duchen, 2012; Halestrap, 2006). Since the MCU$_{cx}$ mediates high-capacity mitochondrial Ca^{2+} uptake, it is an attractive drug target for ischemic stroke. Ru265 was therefore employed to assess the neuroprotective potential of a potent MCU$_{cx}$ inhibitor in cell-based and animal models of ischemic brain injury. In Chapter 3, Ru265 was first shown to suppress mitochondrial Ca^{2+} uptake in cortical neurons cultures treated with the MCU$_{cx}$ activator kaempferol. In keeping with the ability of Ru265 to inhibit toxic mitochondrial Ca^{2+} overloading, Ru265 preserved cell viability, plasma membrane integrity, mitochondrial bioenergetics, and MCU$_{cx}$ subunit expression in primary cultures of mouse cortical neurons subjected to a lethal period of OGD. In Chapter 4, Ru265 was shown to also preserve cell viability in primary cultures of mouse cortical astrocytes subjected to a lethal period of OGD. Ru265

treatment also mitigated LPS-induced increases in pro-inflammatory cytokine expression in astrocytes and endothelial cells. Interestingly, Ru265 also increased anti-inflammatory cytokine expression in astrocytes, suggesting that MCU_{cx} inhibition may reduce ischemic brain injury by promoting the resolution of inflammation and creating a pro-repair environment. In support of these findings, data presented in Chapter 5 demonstrated that an injection of Ru265 (3 mg/kg, i.p.) given 30 min before HI brain injury reduced sensorimotor deficits and infarct volumes in mice 24 hr later. Taken together, these results suggest that by blocking the MCU_{cx}, Ru265 prevented mitochondrial Ca^{2+} overloading responsible for mitochondrial dysfunction and ischemic brain injury. Although Ru265 has excellent neuroprotective potential for the treatment of ischemic brain injury, as described in Chapter 5, Ru265 produced clear seizure activity and convulsions in mice. In Chapter 6, chemical modifications of Ru265 were therefore performed in an attempt to develop novel MCU_{cx} inhibitors with improved safety.

8.2 Importance of Structure to the Biological Activity of MCU_{cx} Inhibitors

This thesis also explored the protective effects of structural analogues of Ru265 to gain a better understanding of how the structure of these compounds impacts their pharmacological activities. Ru265 is a structural analogue of the prototypical MCU_{cx} inhibitor Ru360 (Woods et al., 2019). Data presented in Chapter 3 of this thesis has demonstrated that relative to Ru360, Ru265 has improved cellular

uptake and neuroprotective potency. These findings indicate that it is possible to influence the pharmacological activities of these MCU_{cx} inhibitors by modifying their chemical structure. One property that has been shown to change with structural modifications to these Ru-based MCU_{cx} inhibitors is their redox stability (Woods et al., 2020). Ru360 undergoes reduction when incubated with biologically relevant reducing agents under physiological conditions (pH=7.4) (Woods et al., 2020). In contrast, the nitride-bridge of Ru265 produces redox stability under such physiological conditions (Woods et al., 2020). Similarly, the nitride-bridge in the Os-based MCU_{cx} inhibitors, Os245 and Os245', also confers redox stability. Furthermore, unlike Ru265, Ru360 loses its ability to inhibit the MCU_{cx} in permeabilized HeLa cells when incubated with biologically relevant reducing agents under physiological pH (Woods et al., 2020). Hence, redox stability is critical for effective MCU_{cx} inhibition. This property may also, in part, contribute to differences in the cellular uptake between Ru360 and Ru265. Ru265 is taken up into HeLa cells in an energy-independent manner (Woods et al., 2020). HEK293 cells overexpressing the energy-independent transporter OCT3 demonstrated significantly greater uptake of Ru265, which was attenuated by treatment with the OCT3 inhibitor corticosterone (Woods et al., 2020). By contrast, Ru360 uptake was not enhanced by OCT3 overexpression, nor reduced by corticosterone (Woods et al., 2020). These findings show that Ru265 and Ru360 enter cells by different mechanisms. Given that OCT3 is expressed by multiple cell types such as neurons and glia throughout the brain (Amphoux et al., 2006; Gasser et al., 2009), this transporter may account for the superior

cellular uptake and neuroprotective potency of Ru265 compared to Ru360 in cortical neuron cultures.

A second structural feature that affects the pharmacological properties of these Ru-based MCU_{cx} inhibitors is the axial ligands of these compounds (Woods et al., 2020). These ligands influence both cellular uptake and MCU_{cx} inhibitory properties. Due to the rapid aquation rate of Ru265 (2 min), it is not possible to use Ru265 to study how terminal chloride and aqua ligands influence the pharmacological actions of this MCU_{cx} inhibitor (Woods et al., 2020). However, Os compounds display slower substitution kinetics. This property enabled a comparison of the pharmacological impact of chloride and aqua axial ligands using Os245 and Os245', respectively. Experiments described in Chapter 6 with Os245 and Os245' demonstrated that the axial ligands alter the cellular uptake pathways utilized by these compounds, as well as their MCU_{cx} inhibitory potency. The aqua-capped Os245' demonstrated superior cellular uptake relative to Os245 which may reflect increased transport by OCT3. The addition of adamantane ligands to Ru265 and Os245' greatly increased their potency at protecting cortical neuron cultures from OGD-induced cell death. This improved potency is thought to be a consequence of enhanced cellular uptake due to changes in the axial ligands, as well as additional neuroprotective actions of adamantane independent of MCU_{cx} inhibition. The differences in the uptake and potency of these analogues demonstrate the importance of the axial ligands in regulating their biological activities. However, as shown in Chapter 6, Os245 and

Os245' also produced convulsions. The failure of MCU deletion in Thy1-expressing neurons to reduce the pro-convulsant effects of Ru265 in mice suggests that this adverse side effect is mediated by off-target activity.

8.3 Inhibition of P/Q Type Ca^{2+} Channels Potentially Contributes to the Induction of Convulsions by Ru265

In the quest to develop safer MCU_{cx} inhibitors, it is necessary to understand the underlying mechanisms that may be responsible for the seizure activity observed with Ru265. Identification of this mechanism would also allow for the use of a counter screen to dial out this pro-convulsant activity. Ru265 is thought to inhibit mitochondrial Ca^{2+} uptake by blocking the mouth of the Ca^{2+} channel created by the pore forming subunits of the MCU_{cx} (Woods et al., 2019; Woods et al., 2021). This suggests that binding to a Ca^{2+} channel may, at least in part, confer the off-target activity responsible for Ru265-induced convulsions. The P/Q-type Ca^{2+} channel, also referred to as Cav2.1, is a potential target for Ru265 in the brain. This voltage gated calcium channel, located on the surface of axon terminals, is highly expressed in Purkinje and granule cells in the cerebellum and is implicated in seizure disorders (Rajakulendran et al., 2012). The P/Q-type Ca^{2+} channel plays an important role in coupling Ca^{2+} influx to neurotransmitter release from synaptic terminals (Rajakulendran et al., 2012). As discussed below, mutations of the P/Q-type Ca^{2+} channel have been linked to epilepsy.

In a series of experiments performed by our collaborator, Dr. Terrance Snutch, at the University of British Colombia, the ability of Ru265 to inhibit P/Q-type Ca^{2+} channels was assessed. To confirm that Ru265 inhibits the P/Q-type Ca^{2+} channel, voltage-gated calcium current (ICa) was measured in patch-clamp recordings of HEK cells expressing the human Cav2.1 subunit and the accessory subunits necessary for channel activity. Bath applications of increasing concentrations of Ru265 slowly inhibited ICa with incomplete inhibition observed after 5 min of exposure. This inhibition was partially reversed by washout of Ru265. Analysis of the dose-response curve for ICa inhibition by Ru265 at 5 min post exposure generated an IC_{50} of approximately 2.5 µM for inhibition of the P/Q-type Ca^{2+} channel. These experiments demonstrated that Ru265 blocks P/Q-type Ca^{2+} channels that mediate neurotransmitter release in the brain. This finding suggests that Ru265 may produce convulsions by blocking the release of neurotransmitters that oppose brain seizure activity.

Evidence to support this hypothesis comes from the seizure phenotype produced by loss-of-function mutations of the P/Q-type Ca^{2+} channel. It has been well described that several spontaneously occurring mutations of the P/Q-type Ca^{2+} channel observed in the tottering, rocker, and leaner mouse cause seizures (Catterall, 2000; Imbrici et al., 2004). Specifically, mutations in the CACNA1A α subunit gene, which encodes the main pore forming subunit of P/Q-type Ca^{2+} channels, results in reduced current level and channel dysfunction, and are responsible for episodic ataxia type 2, a genetic disorder characterized by

seizures (Alehabib et al., 2021; Guida et al., 2001; Imbrici et al., 2004; Rajakulendran et al., 2010). In mice with adult-onset ablation of the P/Q-type Ca^{2+} channel alpha subunit, ataxia, dystonia, and absence epilepsy identical to inborn-loss of function phenotypes are observed (Miao et al., 2020). This indicates that mutations in P/Q-type Ca^{2+} channels do not rely upon deficits occurring during development to produce an epileptic phenotype (Miao et al., 2020). In addition, multiple human studies have also shown a link between mutations that result in a reduction or loss of function of the P/Q-type Ca^{2+} channel and the presentation of episodic ataxia, epilepsy and generalized seizures (Alehabib et al., 2021; Imbrici et al., 2004; Rajakulendran et al., 2010; Rajakulendran et al., 2012). These findings suggest that P/Q-type Ca^{2+} channel inhibition may mediate the pro-convulsant effects of Ru265.

This hypothesis is further supported by the lower Ru265 IC_{50} (2.5 μM) for inhibition of the P/Q type Ca^{2+} channel than the Ru265 EC_{50} (4.1 μM) for preservation of cortical neuron viability in the OGD model. However, the IC_{50} of Ru265 for inhibiting the MCU_{cx} in permeabilized cells is extremely low at 2.5 nM (Woods et al., 2019). The fact that Ru265 is 1000 times more potent at blocking the MCU_{cx} than the P/Q-type Ca^{2+} channel means that it will be difficult to develop inhibitors that better discriminate between these two targets. Nevertheless, by making chemical modifications that increase the cellular uptake and decrease potency at the P/Q-type Ca^{2+} channel, it may be possible to increase the therapeutic window of this MCU_{cx} inhibitor.

8.4 Combining MCU$_{cx}$ Inhibition with NCLX Activation to Achieve Synergistic Neuroprotection

An alternative approach to overcoming the pro-convulsant effects of Ru265 is to identify an additional mechanism for opposing mitochondrial Ca^{2+} overloading, thereby allowing the use of lower amounts of Ru265 that are safer. NCLX activation protects neurons from excitotoxicity by increasing mitochondrial Ca^{2+} efflux (Hagenston et al., 2022). Inhibition of PDE2A, localized in mitochondria, increases NCLX activity by stimulating PKA-mediated phosphorylation of the catalytic domain of this Ca^{2+} exchanger (Kostic et al., 2015). Studies conducted in Chapter 7 of this thesis have shown that co-treatment with Ru265 and the PDE2A inhibitor PF-05180999 synergistically protected cortical neuron cultures from OGD-induced viability loss by preserving mitochondrial function. These findings suggest that it may be possible to improve the therapeutic window for Ru265 by combining this MCU$_{cx}$ inhibitor with an NCLX activator. However, future experimentation using animal models of ischemic stroke will be required to validate this hypothesis.

8.5 Local Delivery of Ru265 to the Ischemic Penumbra to Protect the Brain with a Reduced Risk of Convulsions

Another approach to improve the safety of Ru265 in the treatment of stroke would be to preferentially deliver Ru265 to the ischemic penumbra. The penumbra is a region of reduced blood flow surrounding the necrotic core. Neurons in the penumbra are viable but electrically silent (Hakim, 1987). This

suggests that P/Q-type Ca^{2+} channel inhibition in the penumbra by Ru265 will be unable to promote seizure activity. This situation opens the possibility of overcoming the risk of convulsions by injecting Ru265 locally in the penumbra. For example, Ru265 could be delivered via the stent removal cannula immediately after removal of a blood clot. This would allow for the local and rapid delivery of Ru265 to rescuable brain tissues, thus reducing the risk of exposing healthy tissues to concentrations that promote brain seizure activity. Preliminary studies conducted in the laboratory of our collaborator, Dr. Sean Christie in the Division of Neurosurgery at Dalhousie University, have demonstrated that the local epidural application of Ru265 protects the spinal cord from contusive injury at concentrations that do not produce seizure activity (Brittain, 2022). This exciting finding not only suggests that the targeted delivery of Ru265 to ischemic tissues should be safe and effective, but also extends the neuroprotective potential of Ru265 to traumatic spinal cord injury. The ability of Ru265 to suppress pro-inflammatory and increase anti-inflammatory cytokine expression in astrocytes also suggests that this novel MCU_{cx} inhibitor should also promote functional recovery after an ischemic stroke.

A final approach to improve the safety and efficacy of Ru265 would be to encapsulate this compound in lipid nanoparticles designed to preferentially target ischemic tissues. Nanoparticles can be formulated with different polymers that enable them to have tunable drug release properties, high drug-loading capacities, and excellent safety profiles (Hrkach et al., 2012; Kamaly et al.,

2016). It is also possible to incorporate linkers into the polymer backbone that enable selective drug release in ischemic tissues subjected to high oxidative stress. This have been achieved using ROS-sensitive linkers that degrade under low pH conditions (Deng & Liu, 2021; Lv et al., 2018; Zhao et al., 2016). A further advantage of this approach is the preferential delivery of Ru265 to dysfunctional mitochondria that produce excessive amounts of ROS (Deng & Liu, 2021; Lv et al., 2018). Decorating nanoparticles with a stroke homing peptide that binds preferentially to metabolically compromised neural cells in the penumbra is another useful strategy to preferentially target rescuable brain tissues (Zhao et al., 2016). It should be noted that despite the tremendous promise of nanoparticle-based drug delivery, a clinically effective formulation for the treatment of stroke has yet to emerge. Nevertheless, the remarkable success of nanoparticle-based vaccines for COVID-19 will likely fuel further innovations in this promising field.

8.6 Limitations and Future Directions

Ischemic strokes can be highly variable in severity and affect people in diverse ways, making it a complex condition to accurately model. This thesis utilized primary cortical neuron cultures subjected to a lethal period of OGD as an *in vitro* model of ischemic stroke. These neuronal cultures were derived from the cortices of embryos at days 14-16 in utero and used at DIV10-13. These embryonic neuronal cultures are therefore developmentally immature, and thus exhibit properties that differ from adult neurons. Similarly, the primary cortical astrocyte

cultures were derived from postnatal day 0 pups and used at DIV16-20 and were therefore also developmentally immature. Considering stroke is a condition that predominately occurs in older individuals, modeling ischemic injury in immature cell cultures does not accurately recapitulate all the signalling pathways and cellular processes that occur in mature cells during injury. For instance, caspase-3 mediates ischemic cell death in the immature brain but does not in the mature brain because this apoptotic protease is massively downregulated at adulthood (Han et al., 2002). Nevertheless, Ru265 still protected adult mice from HI brain injury, indicating that the cell-based findings translated to mature animals.

Furthermore, although different cell types were evaluated in this thesis, these cell types were not co-cultured. As a result, single cell type cultures do not represent the diverse cellular population of the brain and the vast communication network between components of the NVU that occurs in the adult brain. The effects of MCU_{cx} inhibition may therefore differ in more complex cultures. Future studies should also examine the effects of MCU_{cx} inhibitors on additional cell types that comprise the NVU such as microglia, pericytes, and oligodendrocytes. This would provide a more complete picture of how Ru265 and MCU_{cx} inhibition impacts the inflammatory process and the therapeutic potential of this approach to preserve the function and integrity of the NVU. In this regard, it would also be valuable to co-culture different vascular, glial, and neuronal cell types to better model the NVU.

PF-05180999 was used to inhibit PDE2A as an indirect method of NCLX activation. Although multiple studies indicate that inhibiting PDE2A increases NCLX activity by elevating cAMP levels, stimulating PKA activity, and enhancing NCLX phosphorylation, no direct measurements of cAMP levels, PKA activity, NCLX phosphorylation, or NCLX activity were assessed in this thesis. Future studies will need to be performed to measure cAMP levels, PKA activity, NCLX phosphorylation, and mitochondrial Ca^{2+} efflux rates in cortical neuron cultures treated with PF-05180999 to confirm these mechanisms. Also, conducting experiments utilizing a different PDE2A inhibitor, such as Bay 60-7550 (Soares et al., 2017), would strengthen the results of these co-treatment studies. Showing that a different PDE2A inhibitor also improves cell viability after OGD when co-treated with an MCU_{cx} inhibitor would reinforce the validity of combining MCU_{cx} inhibition with NCLX activation as an effective neuroprotective strategy for ischemic stroke. Furthermore, future studies testing this co-treatment strategy in mouse models of stroke are necessary to determine if this is a safe and viable strategy to reduce mitochondrial damage and neural cell loss, and improve functional outcomes after an ischemic stroke.

The mouse model of stroke used in this thesis was the HI model of stroke. This model is limited by a high mortality rate that increases with time. As such, animals were allowed to recover for only 24 hr to limit animal loss. The findings from these studies are therefore only relevant to the relatively early events responsible for HI brain injury and do not represent the more long-term

pathophysiology that may also contribute to stroke damage. In addition, healthy and young male mice aged 8-12 weeks were used to limit mortality. The young age of these mice is therefore not representative of the older population who are more likely to experience a stroke. In this model, mice were placed in a closed chamber to induce HI, which prevents the measurement of CBF and results in systemic hypoxia, which can impact tissues beyond the desired brain region. Furthermore, only male mice were assessed in the HI model and used for the Ru265-induced seizure activity studies. Hence, potential sex differences were not assessed in this thesis. Therefore, employing an additional model of stroke injury and performing experiments with female and aged mice are required to better assess the neuroprotective potential of Ru265 and the other MCU_{cx} inhibitors *in vivo*. It should be noted, however, that one female mouse was injected with 10 mg/kg of Ru265 and exhibited identical seizure-like behaviour to male mice. Further studies assessing the seizure-like behaviours and convulsions in female mice were not preformed to limit the number of animals that experienced this adverse activity.

Finally, given the profound neuroprotective effects of Ru265, future studies examining the feasibility of strategies to improve the safety of Ru265 are of particular importance. For instance, encapsulating Ru265 in nanoparticle formulations designed to selectively target and release Ru265 in ischemic brain tissues may improve delivery and safety. Using P/Q-type Ca^{2+} channel inhibition

as a screening strategy to identify MCU_{cx} inhibitors less likely to promote seizure activity may also be a fruitful approach.

8.7 Conclusions

The results generated from the studies in this thesis have demonstrated that MCU_{cx} inhibition during ischemic injury is an effective strategy for preserving cell viability. The use of compounds that are cell permeable and effectively inhibit the MCU_{cx} illustrate that preventing mitochondrial Ca^{2+} overloading and preserving mitochondrial function during cerebral ischemic injury are important for preventing subsequent ischemic cell death. Thus, MCU_{cx} inhibitors are attractive options for the treatment of ischemic stroke. These compounds, however, also produce undesirable off target seizure activity, highlighting the need for future studies that investigate how modifications of the structure and/or delivery of these MCU_{cx} inhibitors can be utilized to realize their therapeutic potential for the treatment of ischemic stroke.

References

Acin-Perez, R., Russwurm, M., Gunnewig, K., Gertz, M., Zoidl, G., Ramos, L., Buck, J., Levin, L. R., Rassow, J., Manfredi, G., & Steegborn, C. (2011). A phosphodiesterase 2A isoform localized to mitochondria regulates respiration. *J Biol Chem, 286*(35), 30423-30432. https://doi.org/10.1074/jbc.M111.266379

Acin-Perez, R., Salazar, E., Kamenetsky, M., Buck, J., Levin, L. R., & Manfredi, G. (2009). Cyclic AMP produced inside mitochondria regulates oxidative phosphorylation. *Cell Metab, 9*(3), 265-276. https://doi.org/10.1016/j.cmet.2009.01.012

Adhami, F., Liao, G., Morozov, Y. M., Schloemer, A., Schmithorst, V. J., Lorenz, J. N., Dunn, R. S., Vorhees, C. V., Wills-Karp, M., Degen, J. L., Davis, R. J., Mizushima, N., Rakic, P., Dardzinski, B. J., Holland, S. K., Sharp, F. R., & Kuan, C. Y. (2006). Cerebral ischemia-hypoxia induces intravascular coagulation and autophagy. *Am J Pathol, 169*(2), 566-583. https://doi.org/10.2353/ajpath.2006.051066

Ahlin, G., Karlsson, J., Pedersen, J. M., Gustavsson, L., Larsson, R., Matsson, P. R., Norinder, U., Bergström, C. A., & Artursson, P. (2008). Structural requirements for drug inhibition of the liver specific human organic cation transport protein 1. *Journal of Medicinal Chemistry, 51*(19), 5932-5942.

Ahn, S.-Y., Eraly, S. A., Tsigelny, I., & Nigam, S. K. (2009). Interaction of organic cations with organic anion transporters. *Journal of Biological Chemistry, 284*(45), 31422-31430.

Al-Mufti, F., Amuluru, K., Roth, W., Nuoman, R., El-Ghanem, M., & Meyers, P. M. (2018). Cerebral Ischemic Reperfusion Injury Following Recanalization of Large Vessel Occlusions. *Neurosurgery, 82*(6), 781-789. https://doi.org/10.1093/neuros/nyx341

Alehabib, E., Esmaeilizadeh, Z., Ranji-Burachaloo, S., Tafakhori, A., Darvish, H., & Movafagh, A. (2021). Clinical and molecular spectrum of P/Q type calcium channel Cav2. 1 in epileptic patients. *Orphanet Journal of Rare Diseases, 16*, 1-10.

Amphoux, A., Vialou, V., Drescher, E., Bruss, M., Mannoury La Cour, C., Rochat, C., Millan, M. J., Giros, B., Bonisch, H., & Gautron, S. (2006). Differential pharmacological in vitro properties of organic cation transporters and regional distribution in rat brain. *Neuropharmacology, 50*(8), 941-952. https://doi.org/10.1016/j.neuropharm.2006.01.005

An, H., Zhou, B., & Ji, X. (2021). Mitochondrial quality control in acute ischemic stroke. *J Cereb Blood Flow Metab*, *41*(12), 3157-3170. https://doi.org/10.1177/0271678x211046992

Anderson, C. S., Carter, K. N., Brownlee, W. J., Hackett, M. L., Broad, J. B., & Bonita, R. (2004). Very long-term outcome after stroke in Auckland, New Zealand. *Stroke*, *35*(8), 1920-1924. https://doi.org/10.1161/01.STR.0000133130.20322.9f

Anrather, J., & Iadecola, C. (2016). Inflammation and stroke: an overview. *Neurotherapeutics*, *13*, 661-670.

Ashrafi, G., de Juan-Sanz, J., Farrell, R. J., & Ryan, T. A. (2020). Molecular Tuning of the Axonal Mitochondrial Ca(2+) Uniporter Ensures Metabolic Flexibility of Neurotransmission. *Neuron*, *105*(4), 678-687 e675. https://doi.org/10.1016/j.neuron.2019.11.020

Baldassarro, V. A., Marchesini, A., Facchinetti, F., Villetti, G., Calzà, L., & Giardino, L. (2018). Cell death in pure-neuronal and neuron-astrocyte mixed primary culture subjected to oxygen-glucose deprivation: The contribution of poly (ADP-ribose) polymerases and caspases. *Microchemical Journal*, *136*, 215-222.

Bantle, C. M., Hirst, W. D., Weihofen, A., & Shlevkov, E. (2021). Mitochondrial dysfunction in astrocytes: a role in Parkinson's disease? *Frontiers in Cell and Developmental Biology*, *8*, 608026.

Baradaran, R., Wang, C., Siliciano, A. F., & Long, S. B. (2018). Cryo-EM structures of fungal and metazoan mitochondrial calcium uniporters. *Nature*, *559*(7715), 580-584. https://doi.org/10.1038/s41586-018-0331-8

Barsoum, M. J., Yuan, H., Gerencser, A. A., Liot, G., Kushnareva, Y., Gräber, S., Kovacs, I., Lee, W. D., Waggoner, J., Cui, J., White, A. D., Bossy, B., Martinou, J. C., Youle, R. J., Lipton, S. A., Ellisman, M. H., Perkins, G. A., & Bossy-Wetzel, E. (2006). Nitric oxide-induced mitochondrial fission is regulated by dynamin-related GTPases in neurons. *EMBO J*, *25*(16), 3900-3911. https://doi.org/10.1038/sj.emboj.7601253

Baughman, J. M., Perocchi, F., Girgis, H. S., Plovanich, M., Belcher-Timme, C. A., Sancak, Y., Bao, X. R., Strittmatter, L., Goldberger, O., Bogorad, R. L., Koteliansky, V., & Mootha, V. K. (2011). Integrative genomics identifies MCU as an essential component of the mitochondrial calcium uniporter. *Nature*, *476*(7360), 341-345. https://doi.org/10.1038/nature10234

Blaser, H., Dostert, C., Mak, T. W., & Brenner, D. (2016). TNF and ROS Crosstalk in Inflammation. *Trends Cell Biol*, *26*(4), 249-261. https://doi.org/10.1016/j.tcb.2015.12.002

Brand, M. D., & Nicholls, D. G. (2011). Assessing mitochondrial dysfunction in cells. *Biochem J*, *435*(2), 297-312. https://doi.org/10.1042/BJ20110162

Brittain, K. (2022). *Neuroprotection after traumatic spinal cord injury through mitochondrial calcium uniporter inhibition* [MSc Thesis Dalhousie University].

Broekemeier, K. M., Krebsbach, R. J., & Pfeiffer, D. R. (1994). Inhibition of the mitochondrial Ca2+ uniporter by pure and impure ruthenium red. *Mol Cell Biochem*, *139*(1), 33-40. https://doi.org/10.1007/BF00944201

Bruijnincx, P. C., & Sadler, P. J. (2009). Controlling platinum, ruthenium, and osmium reactivity for anticancer drug design. *Advances in inorganic chemistry*, *61*, 1-62.

Cai, W., Zhang, K., Li, P., Zhu, L., Xu, J., Yang, B., Hu, X., Lu, Z., & Chen, J. (2017). Dysfunction of the neurovascular unit in ischemic stroke and neurodegenerative diseases: An aging effect. *Ageing Research Reviews*, *34*, 77-87. https://doi.org/10.1016/j.arr.2016.09.006

Cao, C., Wang, S., Cui, T., Su, X. C., & Chou, J. J. (2017). Ion and inhibitor binding of the double-ring ion selectivity filter of the mitochondrial calcium uniporter. *Proc Natl Acad Sci U S A*, *114*(14), E2846-E2851. https://doi.org/10.1073/pnas.1620316114

Casaubon, L. K., Boulanger, J.-M., Glasser, E., Blacquiere, D., Boucher, S., Brown, K., Goddard, T., Gordon, J., Horton, M., & Lalonde, J. (2016). Canadian stroke best practice recommendations: acute inpatient stroke care guidelines, update 2015. *International Journal of Stroke*, *11*(2), 239-252.

Catterall, W. A. (2000). Structure and regulation of voltage-gated Ca2+ channels. *Annual review of cell and developmental biology*, *16*(1), 521-555.

Chamorro, A., Lo, E. H., Renu, A., van Leyen, K., & Lyden, P. D. (2021). The future of neuroprotection in stroke. *J Neurol Neurosurg Psychiatry*, *92*(2), 129-135. https://doi.org/10.1136/jnnp-2020-324283

Chang, K. T., Niescier, R. F., & Min, K. T. (2011). Mitochondrial matrix Ca2+ as an intrinsic signal regulating mitochondrial motility in axons. *Proc.Natl.Acad.Sci.U.S.A*, *108*(37), 15456-15461. https://doi.org/10.1073/pnas.1106862108

Charuk, J. H., Pirraglia, C. A., & Reithmeier, R. A. (1990). Interaction of ruthenium red with Ca2(+)-binding proteins. *Anal Biochem*, *188*(1), 123-131. https://doi.org/10.1016/0003-2697(90)90539-l

Chen, Y., Qin, C., Huang, J., Tang, X., Liu, C., Huang, K., Xu, J., Guo, G., Tong, A., & Zhou, L. (2020). The role of astrocytes in oxidative stress of central nervous system: A mixed blessing. *Cell Proliferation*, *53*(3). https://doi.org/10.1111/cpr.12781

Choi, S. S., Lee, H. J., Lim, I., Satoh, J.-i., & Kim, S. U. (2014). Human astrocytes: secretome profiles of cytokines and chemokines. *PLoS One*, *9*(4), e92325.

Cibulsky, S. M., & Sather, W. A. (1999). Block by ruthenium red of cloned neuronal voltage-gated calcium channels. *J Pharmacol Exp Ther*, *289*(3), 1447-1453. https://www.ncbi.nlm.nih.gov/pubmed/10336538

Conti, M., & Beavo, J. (2007). Biochemistry and Physiology of Cyclic Nucleotide Phosphodiesterases: Essential Components in Cyclic Nucleotide Signaling. *Annual Review of Biochemistry*, *76*(1), 481-511. https://doi.org/10.1146/annurev.biochem.76.060305.150444

Crack, P. J., & Wong, C. H. (2008). Modulation of neuro-inflammation and vascular response by oxidative stress following cerebral ischemia-reperfusion injury. *Current Medicinal Chemistry*, *15*(1), 1-14.

Csordas, G., Golenar, T., Seifert, E. L., Kamer, K. J., Sancak, Y., Perocchi, F., Moffat, C., Weaver, D., de la Fuente, P. S., Bogorad, R., Koteliansky, V., Adijanto, J., Mootha, V. K., & Hajnoczky, G. (2013). MICU1 controls both the threshold and cooperative activation of the mitochondrial Ca(2)(+) uniporter. *Cell Metab*, *17*(6), 976-987. https://doi.org/10.1016/j.cmet.2013.04.020

Danysz, W., Dekundy, A., Scheschonka, A., & Riederer, P. (2021). Amantadine: reappraisal of the timeless diamond—target updates and novel therapeutic potentials. *Journal of Neural Transmission*, *128*, 127-169.

Davoli, M. A., Fourtounis, J., Tam, J., Xanthoudakis, S., Nicholson, D., Robertson, G. S., Ng, G. Y., & Xu, D. (2002). Immunohistochemical and biochemical assessment of caspase-3 activation and DNA fragmentation following transient focal ischemia in the rat [S0306452202003767 pii]. *Neuroscience*, *115*(1), 125-136. https://doi.org/10.1016/s0306-4522(02)00376-7

Deng, Z., & Liu, S. (2021). Inflammation-responsive delivery systems for the treatment of chronic inflammatory diseases [10.1007/s13346-021-00977-8 pii]. *Drug Deliv Transl Res*, *11*(4), 1475-1497. https://doi.org/10.1007/s13346-021-00977-8

Denton, R. M. (2009). Regulation of mitochondrial dehydrogenases by calcium ions [S0005-2728(09)00012-7 pii]. *Biochim Biophys Acta*, *1787*(11), 1309-1316. https://doi.org/10.1016/j.bbabio.2009.01.005

Desler, C., Hansen, T. L., Frederiksen, J. B., Marcker, M. L., Singh, K. K., & Juel, R. L. (2012). Is There a Link between Mitochondrial Reserve Respiratory Capacity and Aging? [10.1155/2012/192503 doi]. *J.Aging Res.*, *2012*, 192503. PM:22720157

Divakaruni, A. S., & Brand, M. D. (2011). The regulation and physiology of mitochondrial proton leak [26/3/192 pii]. *Physiology (Bethesda)*, *26*(3), 192-205. https://doi.org/10.1152/physiol.00046.2010

Dobolyi, A., Vincze, C., Pál, G., & Lovas, G. (2012). The Neuroprotective Functions of Transforming Growth Factor Beta Proteins. *International Journal of Molecular Sciences*, *13*(7), 8219-8258. https://doi.org/10.3390/ijms13078219

Dray, A., Forbes, C. A., & Burgess, G. M. (1990). Ruthenium red blocks the capsaicin-induced increase in intracellular calcium and activation of membrane currents in sensory neurones as well as the activation of peripheral nociceptors in vitro [0304-3940(90)90786-9 pii]. *Neuroscience Letters*, *110*(1-2), 52-59. PM:1691472

Duchen, M. R. (2000). Mitochondria and calcium: from cell signalling to cell death [PHY_1346 pii]. *J Physiol*, *529 Pt 1*(Pt 1), 57-68. https://doi.org/10.1111/j.1469-7793.2000.00057.x

Duchen, M. R. (2012). Mitochondria, calcium-dependent neuronal death and neurodegenerative disease. *Pflugers Arch*, *464*(1), 111-121. https://doi.org/10.1007/s00424-012-1112-0

Emerson, J., Clarke, M. J., Ying, W. L., & Sanadi, D. R. (2002). The component of "ruthenium red" responsible for inhibition of mitochondrial calcium ion transport. Spectra, electrochemistry, and aquation kinetics. Crystal structure of .mu.-O-[(HCO2)(NH3)4Ru]2Cl3. *Journal of the American Chemical Society*, *115*(25), 11799-11805. https://doi.org/10.1021/ja00078a019

Fan, C., Fan, M., Orlando, B. J., Fastman, N. M., Zhang, J., Xu, Y., Chambers, M. G., Xu, X., Perry, K., Liao, M., & Feng, L. (2018). X-ray and cryo-EM structures of the mitochondrial calcium uniporter [10.1038/s41586-018-0330-9 pii]. *Nature, 559*(7715), 575-579. https://doi.org/10.1038/s41586-018-0330-9

Fan, M., Zhang, J., Tsai, C.-W., Orlando, B. J., Rodriguez, M., Xu, Y., Liao, M., Tsai, M.-F., & Feng, L. (2020). Structure and mechanism of the mitochondrial Ca2+ uniporter holocomplex. *Nature, 582*(7810), 129-133. https://doi.org/10.1038/s41586-020-2309-6

Feigin, V. L., Brainin, M., Norrving, B., Martins, S., Sacco, R. L., Hacke, W., Fisher, M., Pandian, J., & Lindsay, P. (2022). World Stroke Organization (WSO): Global Stroke Fact Sheet 2022. *Int J Stroke, 17*(1), 18-29. https://doi.org/10.1177/17474930211065917

Feigin, V. L., Forouzanfar, M. H., Krishnamurthi, R., Mensah, G. A., Connor, M., Bennett, D. A., Moran, A. E., Sacco, R. L., Anderson, L., Truelsen, T., O'Donnell, M., Venketasubramanian, N., Barker-Collo, S., Lawes, C. M., Wang, W., Shinohara, Y., Witt, E., Ezzati, M., Naghavi, M., Murray, C. (2014). Global and regional burden of stroke during 1990-2010: findings from the Global Burden of Disease Study 2010 [S0140-6736(13)61953-4 pii]. *Lancet, 383*(9913), 245-254. https://doi.org/10.1016/s0140-6736(13)61953-4

Feno, S., Munari, F., Reane, D. V., Gissi, R., Hoang, D. H., Castegna, A., Chazaud, B., Viola, A., Rizzuto, R., & Raffaello, A. (2021). The dominant-negative mitochondrial calcium uniporter subunit MCUb drives macrophage polarization during skeletal muscle regeneration. *Sci Signal, 14*(707), eabf3838. https://doi.org/10.1126/scisignal.abf3838

Frenkel, D., Huang, Z., Maron, R., Koldzic, D. N., Moskowitz, M. A., & Weiner, H. L. (2005). Neuroprotection by IL-10-producing MOG CD4+ T cells following ischemic stroke. *Journal of the Neurological Sciences, 233*(1-2), 125-132.

Garbincius, J. F., & Elrod, J. W. (2022). Mitochondrial calcium exchange in physiology and disease [10.1152/physrev.00041.2020 doi]. *Physiol Rev, 102*(2), 893-992. https://doi.org/10.1152/physrev.00041.2020

Garcia-Rivas, G., Carvajal, K., Correa, F., & Zazueta, C. (2006). Ru360, a specific mitochondrial calcium uptake inhibitor, improves cardiac post-ischaemic functional recovery in rats in vivo [0706932 pii]. *Br J Pharmacol, 149*(7), 829-837. https://doi.org/10.1038/sj.bjp.0706932

Garcia-Ugalde, G., & Tapia, R. (1991). Convulsions and wet-dog shakes produced by systemic or intrahippocampal administration of ruthenium red in the rat. *Exp Brain Res*, *86*(3), 633-640. https://doi.org/10.1007/BF00230537

Garg, V., Suzuki, J., Paranjpe, I., Unsulangi, T., Boyman, L., Milescu, L. S., Lederer, W. J., & Kirichok, Y. (2021). The mechanism of MICU-dependent gating of the mitochondrial Ca(2+)uniporter. *Elife*, *10*. https://doi.org/10.7554/eLife.69312

Gasser, P. J., Hurley, M. M., Chan, J., & Pickel, V. M. (2017). Organic cation transporter 3 (OCT3) is localized to intracellular and surface membranes in select glial and neuronal cells within the basolateral amygdaloid complex of both rats and mice [10.1007/s00429-016-1315-9 doi ;10.1007/s00429-016-1315-9 pii]. *Brain Struct.Funct.*, *222*(4), 1913-1928. PM:27659446

Gasser, P. J., Orchinik, M., Raju, I., & Lowry, C. A. (2009). Distribution of organic cation transporter 3, a corticosterone-sensitive monoamine transporter, in the rat brain [10.1002/cne.21921 doi]. *J Comp Neurol*, *512*(4), 529-555. https://doi.org/10.1002/cne.21921

Gilgun-Sherki, Y. (2002). Antioxidant Therapy in Acute Central Nervous System Injury: Current State. *Pharmacological Reviews*, *54*(2), 271-284. https://doi.org/10.1124/pr.54.2.271

Giorgio, V., Guo, L., Bassot, C., Petronilli, V., & Bernardi, P. (2018). Calcium and regulation of the mitochondrial permeability transition [S0143-4160(17)30084-2 pii]. *Cell Calcium*, *70*, 56-63. https://doi.org/10.1016/j.ceca.2017.05.004

Gladstone, D. J., Black, S. E., Hakim, A. M., Heart, & Stroke Foundation of Ontario Centre of Excellence in Stroke, R. (2002). Toward wisdom from failure: lessons from neuroprotective stroke trials and new therapeutic directions. *Stroke*, *33*(8), 2123-2136. https://doi.org/10.1161/01.str.0000025518.34157.51

Goldman, S. A., & Chen, Z. (2011). Perivascular instruction of cell genesis and fate in the adult brain. *Nat Neurosci*, *14*(11), 1382-1389. https://doi.org/10.1038/nn.2963

Gong, T., Yang, Y., Jin, T., Jiang, W., & Zhou, R. (2018). Orchestration of NLRP3 Inflammasome Activation by Ion Fluxes [S1471-4906(18)30020-6 pii]. *Trends Immunol*, *39*(5), 393-406. https://doi.org/10.1016/j.it.2018.01.009

González-Reyes, R. E., Nava-Mesa, M. O., Vargas-Sánchez, K., Ariza-Salamanca, D., & Mora-Muñoz, L. (2017). Involvement of astrocytes in Alzheimer's disease from a neuroinflammatory and oxidative stress perspective. *Frontiers in molecular neuroscience*, *10*, 427.

Gordon, G. R. J., Mulligan, S. J., & MacVicar, B. A. (2007). Astrocyte control of the cerebrovasculature. *Glia*, *55*(12), 1214-1221. https://doi.org/10.1002/glia.20543

Gottschalk, B., Klec, C., Leitinger, G., Bernhart, E., Rost, R., Bischof, H., Madreiter-Sokolowski, C. T., Radulovic, S., Eroglu, E., Sattler, W., Waldeck-Weiermair, M., Malli, R., & Graier, W. F. (2019). MICU1 controls cristae junction and spatially anchors mitochondrial Ca(2+) uniporter complex [10.1038/s41467-019-11692-x pii]. *Nat Commun*, *10*(1), 3732. https://doi.org/10.1038/s41467-019-11692-x

Gottschalk, B., Koshenov, Z., Waldeck-Weiermair, M., Radulović, S., Oflaz, F. E., Hirtl, M., Bachkoenig, O. A., Leitinger, G., Malli, R., & Graier, W. F. (2022). MICU1 controls spatial membrane potential gradients and guides Ca(2+) fluxes within mitochondrial substructures. *Commun Biol*, *5*(1), 649. https://doi.org/10.1038/s42003-022-03606-3

Green, D. R., Galluzzi, L., & Kroemer, G. (2014). Cell biology. Metabolic control of cell death [345/6203/1250256 pii]. *Science*, *345*(6203), 1250256. https://doi.org/10.1126/science.1250256

Grefkes, C., & Fink, G. R. (2020). Recovery from stroke: current concepts and future perspectives. *Neurological research and practice*, *2*(1), 1-10.

Grubb, S., Lauritzen, M., & Aalkjær, C. (2021). Brain capillary pericytes and neurovascular coupling. *Comp Biochem Physiol A Mol Integr Physiol*, *254*, 110893. https://doi.org/10.1016/j.cbpa.2020.110893

Guida, S., Trettel, F., Pagnutti, S., Mantuano, E., Tottene, A., Veneziano, L., Fellin, T., Spadaro, M., Stauderman, K. A., & Williams, M. E. (2001). Complete loss of P/Q calcium channel activity caused by a CACNA1A missense mutation carried by patients with episodic ataxia type 2. *The American Journal of Human Genetics*, *68*(3), 759-764.

Guo, H., Liu, Z. Q., Zhou, H., Wang, Z. L., Tao, Y. H., & Tong, Y. (2018). P2Y1 receptor antagonists mitigate oxygen and glucose deprivation-induced astrocyte injury. *Molecular Medicine Reports*, *17*(1), 1819-1824.

Guo, J., Duckles, S. P., Weiss, J. H., Li, X., & Krause, D. N. (2012). 17β-Estradiol prevents cell death and mitochondrial dysfunction by an estrogen receptor-dependent mechanism in astrocytes after oxygen–glucose deprivation/reperfusion. *Free Radical Biology and Medicine*, *52*(11-12), 2151-2160.

Hagenston, A. M., Yan, J., Bas-Orth, C., Tan, Y., Sekler, I., & Bading, H. (2022). Disrupted expression of mitochondrial NCLX sensitizes neuroglial networks to excitotoxic stimuli and renders synaptic activity toxic [S0021-9258(21)01318-1 pii]. *J Biol Chem*, *298*(2), 101508. https://doi.org/10.1016/j.jbc.2021.101508

Hakim, A. M. (1987). The cerebral ischemic penumbra. *Can J Neurol Sci*, *14*(4), 557-559. https://www.ncbi.nlm.nih.gov/pubmed/2446732

Halestrap, A. P. (2006). Calcium, mitochondria and reperfusion injury: a pore way to die [BST20060232 pii]. *Biochem Soc Trans*, *34*(Pt 2), 232-237. https://doi.org/10.1042/BST20060232

Han, B. H., Xu, D., Choi, J., Han, Y., Xanthoudakis, S., Roy, S., Tam, J., Vaillancourt, J., Colucci, J., Siman, R., Giroux, A., Robertson, G. S., Zamboni, R., Nicholson, D. W., & Holtzman, D. M. (2002). Selective, reversible caspase-3 inhibitor is neuroprotective and reveals distinct pathways of cell death after neonatal hypoxic-ischemic brain injury [10.1074/jbc.M202931200 doi ;M202931200 pii]. *Journal of Biological Chemistry*, *277*(33), 30128-30136. PM:12058036

Hansson, E., Werner, T., Björklund, U., & Skiöldebrand, E. (2016). Therapeutic innovation: inflammatory-reactive astrocytes as targets of inflammation. *IBRO reports*, *1*, 1-9.

Harris, J. J., Jolivet, R., & Attwell, D. (2012). Synaptic energy use and supply [S0896-6273(12)00756-8 pii]. *Neuron, 75*(5), 762-777. https://doi.org/10.1016/j.neuron.2012.08.019

He, Z., Ning, N., Zhou, Q., Khoshnam, S. E., & Farzaneh, M. (2020). Mitochondria as a therapeutic target for ischemic stroke. *Free Radic Biol Med*, *146*, 45-58. https://doi.org/10.1016/j.freeradbiomed.2019.11.005

Helal, C. J., Arnold, E., Boyden, T., Chang, C., Chappie, T. A., Fisher, E., Hajos, M., Harms, J. F., Hoffman, W. E., & Humphrey, J. M. (2018). Identification of a potent, highly selective, and brain penetrant phosphodiesterase 2A inhibitor clinical candidate. *Journal of Medicinal Chemistry*, *61*(3), 1001-1018.

Howard, G., & Goff, D. C. (2012). Population shifts and the future of stroke: forecasts of the future burden of stroke. *Annals of the New York Academy of Sciences*, *1268*(1), 14-20.

Hrkach, J., Von Hoff, D., Mukkaram Ali, M., Andrianova, E., Auer, J., Campbell, T., De Witt, D., Figa, M., Figueiredo, M., Horhota, A., Low, S., McDonnell, K., Peeke, E., Retnarajan, B., Sabnis, A., Schnipper, E., Song, J. J., Song, Y. H., Summa, J., Tompsett, D., Troiano, G., Van Geen Hoven, T., Wright, J., LoRusso, P., Kantoff, P.W., Bander, N.H., Sweeney, C. Farokhzad, O.C., Langer, R., Zale, S. (2012). Preclinical development and clinical translation of a PSMA-targeted docetaxel nanoparticle with a differentiated pharmacological profile. *Sci Transl Med*, *4*(128), 128ra139. https://doi.org/10.1126/scitranslmed.3003651

Huang, Q., Zhang, R., Zou, L. Y., Cao, X., & Chu, X. (2013). Cell death pathways in astrocytes with a modified model of oxygen-glucose deprivation. *PLoS One*, *8*(4), e61345.

Huet, O., Petit, J. M., Ratinaud, M. H., & Julien, R. (1992). NADH-dependent dehydrogenase activity estimation by flow cytometric analysis of 3-(4, 5-dimethylthiazolyl-2-yl)-2, 5-diphenyltetrazolium bromide (MTT) reduction. *Cytometry: The Journal of the International Society for Analytical Cytology*, *13*(5), 532-539.

Iadecola, C. (2004). Neurovascular regulation in the normal brain and in Alzheimer's disease. *Nat Rev Neurosci*, *5*(5), 347-360. https://doi.org/10.1038/nrn1387

Iadecola, C. (2017). The Neurovascular Unit Coming of Age: A Journey through Neurovascular Coupling in Health and Disease. *Neuron*, *96*(1), 17-42. https://doi.org/10.1016/j.neuron.2017.07.030

Iadecola, C., Buckwalter, M. S., & Anrather, J. (2020). Immune responses to stroke: mechanisms, modulation, and therapeutic potential. *Journal of Clinical Investigation*, *130*(6), 2777-2788. https://doi.org/10.1172/jci135530

Ianevski, A., Giri, K. A., & Aittokallio, T. (2022). SynergyFinder 3.0: an interactive analysis and consensus interpretation of multi-drug synergies across multiple samples. *Nucleic Acids Research*, *gkac382*. https://doi.org/ https://doi.org/10.1093/nar/gkac382

Imbrici, P., Jaffe, S. L., Eunson, L. H., Davies, N. P., Herd, C., Robertson, R., Kullmann, D. M., & Hanna, M. G. (2004). Dysfunction of the brain calcium channel CaV2. 1 in absence epilepsy and episodic ataxia. *Brain*, *127*(12), 2682-2692.

Islam, M. M., Takeuchi, A., & Matsuoka, S. (2020). Membrane current evoked by mitochondrial Na(+)-Ca(2+) exchange in mouse heart. *J Physiol Sci*, *70*(1), 24. https://doi.org/10.1186/s12576-020-00752-3

Jayaraj, R. L., Azimullah, S., Beiram, R., Jalal, F. Y., & Rosenberg, G. A. (2019). Neuroinflammation: friend and foe for ischemic stroke. *Journal of Neuroinflammation*, *16*(1), 1-24.

Joshi, A. U., Minhas, P. S., Liddelow, S. A., Haileselassie, B., Andreasson, K. I., Dorn, G. W., & Mochly-Rosen, D. (2019). Fragmented mitochondria released from microglia trigger A1 astrocytic response and propagate inflammatory neurodegeneration. *Nature Neuroscience*, *22*(10), 1635-1648.

Jurcau, A., & Simion, A. (2022). Neuroinflammation in cerebral ischemia and ischemia/reperfusion injuries: from pathophysiology to therapeutic strategies. *International Journal of Molecular Sciences*, *23*(1), 14.

Kadernani, Y. E., Zindo, F. T., Kapp, E., Malan, S. F., & Joubert, J. (2014). Adamantane amine derivatives as dual acting NMDA receptor and voltage-gated calcium channel inhibitors for neuroprotection. *MedChemComm*, *5*(11), 1678-1684.

Kamaly, N., Yameen, B., Wu, J., & Farokhzad, O. C. (2016). Degradable Controlled-Release Polymers and Polymeric Nanoparticles: Mechanisms of Controlling Drug Release. *Chem Rev*, *116*(4), 2602-2663. https://doi.org/10.1021/acs.chemrev.5b00346

Kamer, K. J., Grabarek, Z., & Mootha, V. K. (2017). High-affinity cooperative Ca(2+) binding by MICU1-MICU2 serves as an on-off switch for the uniporter. *EMBO Rep.*, *18*(8), 1397-1411. https://doi.org/10.15252/embr.201643748

Kann, O., & Kovacs, R. (2007). Mitochondria and neuronal activity [00222.2006 pii]. *Am J Physiol Cell Physiol*, *292*(2), C641-657. https://doi.org/10.1152/ajpcell.00222.2006

Katoshevski, T., Bar, L., Tikochinsky, E., Harel, S., Ben-Kasus Nissim, T., Bogeski, I., Hershfinkel, M., Attali, B., & Sekler, I. (2022). CKII Control of Axonal Plasticity Is Mediated by Mitochondrial Ca2+ via Mitochondrial NCLX. *Cells*, *11*(24), 3990. https://doi.org/10.3390/cells11243990

Katoshevski, T., Ben-Kasus Nissim, T., & Sekler, I. (2021). Recent studies on NCLX in health and diseases [S0143-4160(20)30187-1 pii]. *Cell Calcium*, *94*, 102345. https://doi.org/10.1016/j.ceca.2020.102345

Khananshvili, D. (2017). Structure-Dynamic Coupling Through Ca(2+)-Binding Regulatory Domains of Mammalian NCX Isoform/Splice Variants. *Adv Exp Med Biol*, *981*, 41-58. https://doi.org/10.1007/978-3-319-55858-5_3

Kintner, D. B., Luo, J., Gerdts, J., Ballard, A. J., Shull, G. E., & Sun, D. (2007). Role of Na+-K+-Cl− cotransport and Na+/Ca2+ exchange in mitochondrial dysfunction in astrocytes following in vitro ischemia. *American Journal of Physiology-Cell Physiology*, *292*(3), C1113-C1122.

Konig, T., Troder, S. E., Bakka, K., Korwitz, A., Richter-Dennerlein, R., Lampe, P. A., Patron, M., Muhlmeister, M., Guerrero-Castillo, S., Brandt, U., Decker, T., Lauria, I., Paggio, A., Rizzuto, R., Rugarli, E. I., De Stefani, D., & Langer, T. (2016). The m-AAA Protease Associated with Neurodegeneration Limits MCU Activity in Mitochondria [S1097-2765(16)30462-2 pii]. *Mol Cell*, *64*(1), 148-162. https://doi.org/10.1016/j.molcel.2016.08.020

Kostic, M., Katoshevski, T., & Sekler, I. (2018). Allosteric Regulation of NCLX by Mitochondrial Membrane Potential Links the Metabolic State and Ca(2+) Signaling in Mitochondria [S2211-1247(18)31875-8 pii]. *Cell Rep*, *25*(12), 3465-3475 e3464. https://doi.org/10.1016/j.celrep.2018.11.084

Kostic, M., Ludtmann, M. H., Bading, H., Hershfinkel, M., Steer, E., Chu, C. T., Abramov, A. Y., & Sekler, I. (2015). PKA phosphorylation of NCLX reverses mitochondrial calcium overload and depolarization, promoting survival of PINK1-deficient dopaminergic neurons. *Cell Reports*, *13*(2), 376-386. https://doi.org/10.1016/j.celrep.2015.08.079

Kovacs-Bogdan, E., Sancak, Y., Kamer, K. J., Plovanich, M., Jambhekar, A., Huber, R. J., Myre, M. A., Blower, M. D., & Mootha, V. K. (2014). Reconstitution of the mitochondrial calcium uniporter in yeast [1400514111 pii]. *Proc Natl Acad Sci U S A*, *111*(24), 8985-8990. https://doi.org/10.1073/pnas.1400514111

Kristián, T., & Siesjö, B. K. (1998). Calcium in ischemic cell death. *Stroke*, *29*(3), 705-718.

Krivonos, O., Amosova, N., & Smolentseva, I. (2010). Use of the glutamate NMDA receptor antagonist PK-Merz in acute stroke. *Neuroscience and behavioral physiology*, *40*, 529-532.

Kugler, E. C., Greenwood, J., & MacDonald, R. B. (2021). The "Neuro-Glial-Vascular" Unit: The Role of Glia in Neurovascular Unit Formation and Dysfunction [Review]. *Frontiers in Cell and Developmental Biology*, *9*. https://doi.org/10.3389/fcell.2021.732820

Kwilasz, A., Grace, P., Serbedzija, P., Maier, S., & Watkins, L. (2015). The therapeutic potential of interleukin-10 in neuroimmune diseases. *Neuropharmacology*, *96*, 55-69.

Kwong, J. Q., Lu, X., Correll, R. N., Schwanekamp, J. A., Vagnozzi, R. J., Sargent, M. A., York, A. J., Zhang, J., Bers, D. M., & Molkentin, J. D. (2015). The Mitochondrial Calcium Uniporter Selectively Matches Metabolic Output to Acute Contractile Stress in the Heart [S2211-1247(15)00585-9 pii]. *Cell Rep*, *12*(1), 15-22. https://doi.org/10.1016/j.celrep.2015.06.002

Lambert, J. P., Luongo, T. S., Tomar, D., Jadiya, P., Gao, E., Zhang, X., Lucchese, A. M., Kolmetzky, D. W., Shah, N. S., & Elrod, J. W. (2019). MCUB Regulates the Molecular Composition of the Mitochondrial Calcium Uniporter Channel to Limit Mitochondrial Calcium Overload During Stress. *Circulation*, *140*(21), 1720-1733. https://doi.org/10.1161/CIRCULATIONAHA.118.037968

Lehninger, A. L. (1979). Some aspects of energy coupling by mitochondria. *Advances in Experimental Medicine and Biology*, *111*, 1-16. PM:34317 (NOT IN FILE)

Li, K., Li, J., Zheng, J., & Qin, S. (2019). Reactive astrocytes in neurodegenerative diseases. *Aging and disease*, *10*(3), 664.

Lin, M. T., & Beal, M. F. (2006). Mitochondrial dysfunction and oxidative stress in neurodegenerative diseases [nature05292 pii]. *Nature*, *443*(7113), 787-795. https://doi.org/10.1038/nature05292

Liu, C., Gao, Y., Barrett, J., & Hu, B. (2010). Autophagy and protein aggregation after brain ischemia [JNC6905 pii]. *J Neurochem*, *115*(1), 68-78. https://doi.org/10.1111/j.1471-4159.2010.06905.x

Liu, Z., Salassa, L., Habtemariam, A., Pizarro, A. M., Clarkson, G. J., & Sadler, P. J. (2011). Contrasting reactivity and cancer cell cytotoxicity of isoelectronic organometallic iridium (III) complexes. *Inorganic chemistry*, *50*(12), 5777-5783.

Llorente-Folch, I., Rueda, C. B., Pardo, B., Szabadkai, G., Duchen, M. R., & Satrustegui, J. (2015). The regulation of neuronal mitochondrial metabolism by calcium. *J Physiol*, *593*(16), 3447-3462. https://doi.org/10.1113/JP270254

Lo, E. H., Dalkara, T., & Moskowitz, M. A. (2003). Mechanisms, challenges and opportunities in stroke [nrn1106 pii]. *Nat Rev Neurosci*, *4*(5), 399-415. https://doi.org/10.1038/nrn1106

Lobo-Silva, D., Carriche, G. M., Castro, A. G., Roque, S., & Saraiva, M. (2016). Balancing the immune response in the brain: IL-10 and its regulation. *Journal of Neuroinflammation*, *13*(1), 1-10.

Logan, C. V., Szabadkai, G., Sharpe, J. A., Parry, D. A., Torelli, S., Childs, A. M., Kriek, M., Phadke, R., Johnson, C. A., Roberts, N. Y., Bonthron, D. T., Pysden, K. A., Whyte, T., Munteanu, I., Foley, A. R., Wheway, G., Szymanska, K., Natarajan, S., Abdelhamed, Z. A., Morgan, J.E., Roper, H., Santen, G.W., Niks, E.H., van der Pol, W.L., Lindhout, D., Raffaello, A., De Stefani, D., den Dunnen, J.T., Sun, Y., Ginjaar, I., Sewry, C.A., Hurles, M., Rizzuto, R., Duchen, M.R., Munton, F., Sheridan, E. (2014). Loss-of-function mutations in MICU1 cause a brain and muscle disorder linked to primary alterations in mitochondrial calcium signaling [ng.2851 pii]. *Nat Genet*, *46*(2), 188-193. https://doi.org/10.1038/ng.2851

Longden, T. A., Hill-Eubanks, D. C., & Nelson, M. T. (2016). Ion channel networks in the control of cerebral blood flow. *J Cereb Blood Flow Metab*, *36*(3), 492-512. https://doi.org/10.1177/0271678x15616138

Loscher, W., & Potschka, H. (2005). Role of drug efflux transporters in the brain for drug disposition and treatment of brain diseases [S0301-0082(05)00044-4 pii]. *Prog Neurobiol*, *76*(1), 22-76. https://doi.org/10.1016/j.pneurobio.2005.04.006

Luongo, T. S., Lambert, J. P., Gross, P., Nwokedi, M., Lombardi, A. A., Shanmughapriya, S., Carpenter, A. C., Kolmetzky, D., Gao, E., Van Berlo, J. H., Tsai, E. J., Molkentin, J. D., Chen, X., Madesh, M., Houser, S. R., & Elrod, J. W. (2017). The mitochondrial Na+/Ca2+ exchanger is essential for Ca2+ homeostasis and viability. *Nature*, *545*(7652), 93-97. https://doi.org/10.1038/nature22082

Luongo, T. S., Lambert, J. P., Yuan, A., Zhang, X., Gross, P., Song, J., Shanmughapriya, S., Gao, E., Jain, M., Houser, S. R., Koch, W. J., Cheung, J. Y., Madesh, M., & Elrod, J. W. (2015). The Mitochondrial Calcium Uniporter Matches Energetic Supply with Cardiac Workload during Stress and Modulates Permeability Transition [S2211-1247(15)00615-4 pii]. *Cell Rep*, *12*(1), 23-34. https://doi.org/10.1016/j.celrep.2015.06.017

Lv, W., Xu, J., Wang, X., Li, X., Xu, Q., & Xin, H. (2018). Bioengineered Boronic Ester Modified Dextran Polymer Nanoparticles as Reactive Oxygen Species Responsive Nanocarrier for Ischemic Stroke Treatment. *ACS Nano.*, *12*(6), 5417-5426. https://doi.org/10.1021/acsnano.8b00477

Lytton, J. (2007). Na+/Ca2+ exchangers: three mammalian gene families control Ca2+ transport [BJ20070619 pii]. *Biochem J*, *406*(3), 365-382. https://doi.org/10.1042/BJ20070619

Mallilankaraman, K., Cardenas, C., Doonan, P. J., Chandramoorthy, H. C., Irrinki, K. M., Golenar, T., Csordas, G., Madireddi, P., Yang, J., Muller, M., Miller, R., Kolesar, J. E., Molgo, J., Kaufman, B., Hajnoczky, G., Foskett, J. K., & Madesh, M. (2012). MCUR1 is an essential component of mitochondrial Ca2+ uptake that regulates cellular metabolism. *Nature Cell Biology*, *14*(12), 1336-1343. https://doi.org/10.1038/ncb2622

Markus, N. M., Hasel, P., Qiu, J., Bell, K. F., Heron, S., Kind, P. C., Dando, O., Simpson, T. I., & Hardingham, G. E. (2016). Expression of mRNA Encoding Mcu and Other Mitochondrial Calcium Regulatory Genes Depends on Cell Type, Neuronal Subtype, and Ca2+ Signaling [PONE-D-15-42475 pii]. *PLoS One*, *11*(2), e0148164. https://doi.org/10.1371/journal.pone.0148164

Marvanová, M., Lakso, M., Pirhonen, J., Nawa, H., Wong, G., & Castrén, E. (2001). The neuroprotective agent memantine induces brain-derived neurotrophic factor and trkB receptor expression in rat brain. *Mol Cell Neurosci*, *18*(3), 247-258. https://doi.org/10.1006/mcne.2001.1027

Mathiisen, T. M., Lehre, K. P., Danbolt, N. C., & Ottersen, O. P. (2010). The perivascular astroglial sheath provides a complete covering of the brain microvessels: an electron microscopic 3D reconstruction. *Glia*, *58*(9), 1094-1103. https://doi.org/10.1002/glia.20990

Mayo, L., Cunha, A. P. D., Madi, A., Beynon, V., Yang, Z., Alvarez, J. I., Prat, A., Sobel, R. A., Kobzik, L., & Lassmann, H. (2016). IL-10-dependent Tr1 cells attenuate astrocyte activation and ameliorate chronic central nervous system inflammation. *Brain*, *139*(7), 1939-1957.

McAllister, J., Ghosh, S., Berry, D., Park, M., Sadeghi, S., Wang, K. X., Parker, W. D., & Swerdlow, R. H. (2008). Effects of memantine on mitochondrial function. *Biochemical Pharmacology*, *75*(4), 956-964. https://doi.org/10.1016/j.bcp.2007.10.019

Miao, Q.-L., Herlitze, S., Mark, M. D., & Noebels, J. L. (2020). Adult loss of Cacna1a in mice recapitulates childhood absence epilepsy by distinct thalamic bursting mechanisms. *Brain*, *143*(1), 161-174.

Mirzoyan, R. S., Gan'shina, T. S., Maslennikov, D. V., Kovalev, G. I., Zimin, I. A., Pyatin, B. M., Avdyunina, N. I., Kukhtarova, A. M., Khostikyan, N. G., & Meliksetyan, V. S. (2014). Cerebrovascular and neuroprotective effects of adamantane derivative. *BioMed Research International*, *2014*.

Montero, M., Lobaton, C. D., Hernandez-Sanmiguel, E., Santodomingo, J., Vay, L., Moreno, A., & Alvarez, J. (2004). Direct activation of the mitochondrial calcium uniporter by natural plant flavonoids [BJ20040990 pii]. *Biochem J*, *384*(Pt 1), 19-24. https://doi.org/10.1042/BJ20040990

Moore, C. L. (1971). Specific inhibition of mitochondrial Ca++ transport by ruthenium red. *Biochemical and Biophysical Research Communications*, *42*(2), 298-305.

Mukda, S., Tsai, C.-Y., Leu, S., Yang, J.-L., & Chan, S. H. (2019). Pinin protects astrocytes from cell death after acute ischemic stroke via maintenance of mitochondrial anti-apoptotic and bioenergetics functions. *Journal of Biomedical Science*, *26*(1), 1-14.

Muoio, V., Persson, P. B., & Sendeski, M. M. (2014). The neurovascular unit - concept review. *Acta Physiol (Oxf)*, *210*(4), 790-798. https://doi.org/10.1111/apha.12250

Nathan, S. R., Pino, N. W., Arduino, D. M., Perocchi, F., MacMillan, S. N., & Wilson, J. J. (2017). Synthetic Methods for the Preparation of a Functional Analogue of Ru360, a Potent Inhibitor of Mitochondrial Calcium Uptake [10.1021/acs.inorgchem.6b03108 pii]. *Inorg Chem*, *56*(6), 3123-3126. https://doi.org/10.1021/acs.inorgchem.6b03108

Nathan, S. R., & Wilson, J. J. (2017). Synthesis and Evaluation of a Ruthenium-based Mitochondrial Calcium Uptake Inhibitor. *J Vis Exp*(128). https://doi.org/10.3791/56527

Nguyen, N. X., Armache, J. P., Lee, C., Yang, Y., Zeng, W., Mootha, V. K., Cheng, Y., Bai, X. C., & Jiang, Y. (2018). Cryo-EM structure of a fungal mitochondrial calcium uniporter. *Nature*, *559*(7715), 570-574. https://doi.org/10.1038/s41586-018-0333-6

Nichols, M., Elustondo, P. A., Warford, J., Thirumaran, A., Pavlov, E. V., & Robertson, G. S. (2017). Global ablation of the mitochondrial calcium uniporter increases glycolysis in cortical neurons subjected to energetic stressors [0271678X16682250 pii]. *J Cereb Blood Flow Metab*, *37*(8), 3027-3041. https://doi.org/10.1177/0271678X16682250

Nichols, M., Pavlov, E. V., & Robertson, G. S. (2018). Tamoxifen-induced knockdown of the mitochondrial calcium uniporter in Thy1-expressing neurons protects mice from hypoxic/ischemic brain injury [10.1038/s41419-018-0607-9 pii]. *Cell Death Dis*, *9*(6), 606. https://doi.org/10.1038/s41419-018-0607-9

Niescier, R. F., Chang, K. T., & Min, K. T. (2013). Miro, MCU, and calcium: bridging our understanding of mitochondrial movement in axons [10.3389/fncel.2013.00148 doi]. *Front Cell Neurosci.*, *7*, 148. PM:24058334

Norden, D. M., Fenn, A. M., Dugan, A., & Godbout, J. P. (2014). TGFβ produced by IL-10 redirected astrocytes attenuates microglial activation. *Glia*, *62*(6), 881-895.

Novohradsky, V., Liu, Z., Vojtiskova, M., Sadler, P. J., Brabec, V., & Kasparkova, J. (2014). Mechanism of cellular accumulation of an iridium (III) pentamethylcyclopentadienyl anticancer complex containing a C, N-chelating ligand. *Metallomics*, *6*(3), 682-690.

Nunnari, J., & Suomalainen, A. (2012). Mitochondria: in sickness and in health. *Cell*, *148*(6), 1145-1159.

Ossola, B., Schendzielorz, N., Chen, S.-H., Bird, G. S., Tuominen, R. K., Männistö, P. T., & Hong, J.-S. (2011). Amantadine protects dopamine neurons by a dual action: reducing activation of microglia and inducing expression of GNDF in astroglia. *Neuropharmacology*, *61*(4), 574-582.

Oxenoid, K., Dong, Y., Cao, C., Cui, T., Sancak, Y., Markhard, A. L., Grabarek, Z., Kong, L., Liu, Z., Ouyang, B., Cong, Y., Mootha, V. K., & Chou, J. J. (2016). Architecture of the mitochondrial calcium uniporter [nature17656 pii]. *Nature*, *533*(7602), 269-273. https://doi.org/10.1038/nature17656

Palty, R., Silverman, W. F., Hershfinkel, M., Caporale, T., Sensi, S. L., Parnis, J., Nolte, C., Fishman, D., Shoshan-Barmatz, V., Herrmann, S., Khananshvili, D., & Sekler, I. (2010). NCLX is an essential component of mitochondrial Na+/Ca2+ exchange. *Proc.Natl.Acad.Sci.U.S.A*, *107*(1), 436-441. https://doi.org/10.1073/pnas.0908099107 doi

Panattoni, G., Amoriello, R., Memo, C., Thalhammer, A., Ballerini, C., & Ballerini, L. (2021). Diverse inflammatory threats modulate astrocytes Ca 2+ signaling via connexin43 hemichannels in organotypic spinal slices. *Molecular Brain*, *14*, 1-15.

Park, J. Y., Lee, K.-H., Park, H. S., & Choi, S. J. (2017). LPS sensing mechanism of human astrocytes: evidence of functional TLR4 expression and requirement of soluble CD14. *Journal of Bacteriology and Virology*, *47*(4), 189-198.

Parker, S., & Ali, Y. (2015). Changing contraindications for t-PA in acute stroke: review of 20 years since NINDS. *Current cardiology reports*, *17*, 1-6.

Patel, A., Pietromicca, J. G., Venkatesan, M., Maity, S., Bard, J. E., Madesh, M., & Alevriadou, B. R. (2023). Modulation of the mitochondrial Ca2+ uniporter complex subunit expression by different shear stress patterns in vascular endothelial cells. *Physiol Rep*, *11*(3), e15588. https://doi.org/10.14814/phy2.15588

Patron, M., Checchetto, V., Raffaello, A., Teardo, E., Vecellio Reane, D., Mantoan, M., Granatiero, V., Szabo, I., De Stefani, D., & Rizzuto, R. (2014). MICU1 and MICU2 finely tune the mitochondrial Ca2+ uniporter by exerting opposite effects on MCU activity [S1097-2765(14)00074-4 pii]. *Mol Cell*, *53*(5), 726-737. https://doi.org/10.1016/j.molcel.2014.01.013

Patron, M., Granatiero, V., Espino, J., Rizzuto, R., & De, S. D. (2019). MICU3 is a tissue-specific enhancer of mitochondrial calcium uptake. *Cell Death.Differ.*, *26*(1), 179-195. https://doi.org/10.1038/s41418-018-0113-8

Peng, T.-I., & Jou, M.-J. (2010). Oxidative stress caused by mitochondrial calcium overload. *Annals of the New York Academy of Sciences*, *1201*(1), 183-188. https://doi.org/10.1111/j.1749-6632.2010.05634.x

Petzold, G. C., & Murthy, V. N. (2011). Role of Astrocytes in Neurovascular Coupling. *Neuron*, *71*(5), 782-797. https://doi.org/10.1016/j.neuron.2011.08.009

Piette, J., Piret, B., Bonizzi, G., Schoonbroodt, S., Merville, M. P., Legrand-Poels, S., & Bours, V. (1997). Multiple redox regulation in NF-kappaB transcription factor activation. *Biological Chemistry*, *378*(11), 1237-1245. http://europepmc.org/abstract/MED/9426183

Puckett, C. A., Ernst, R. J., & Barton, J. K. (2010). Exploring the cellular accumulation of metal complexes. *Dalton Trans*, *39*(5), 1159-1170. https://doi.org/10.1039/b922209j

Quarato, G., Scrima, R., Ripoli, M., Agriesti, F., Moradpour, D., Capitanio, N., & Piccoli, C. (2014). Protective role of amantadine in mitochondrial dysfunction and oxidative stress mediated by hepatitis C virus protein expression. *Biochemical Pharmacology*, *89*(4), 545-556.

Raffaello, A., De, S. D., Sabbadin, D., Teardo, E., Merli, G., Picard, A., Checchetto, V., Moro, S., Szabo, I., & Rizzuto, R. (2013). The mitochondrial calcium uniporter is a multimer that can include a dominant-negative pore-forming subunit. *EMBO Journal*, *32*(17), 2362-2376. https://doi.org/10.1038/emboj.2013.157

Rahman, M. H., & Suk, K. (2020). Mitochondrial dynamics and bioenergetic alteration during inflammatory activation of astrocytes. *Frontiers in Aging Neuroscience*, *12*, 614410.

Rajakulendran, S., Graves, T. D., Labrum, R. W., Kotzadimitriou, D., Eunson, L., Davis, M. B., Davies, R., Wood, N. W., Kullmann, D. M., & Hanna, M. G. (2010). Genetic and functional characterisation of the P/Q calcium channel in episodic ataxia with epilepsy. *The Journal of physiology*, *588*(11), 1905-1913.

Rajakulendran, S., Kaski, D., & Hanna, M. G. (2012). Neuronal P/Q-type calcium channel dysfunction in inherited disorders of the CNS. *Nature Reviews Neurology*, *8*(2), 86-96.

Reichard, A., & Asosingh, K. (2019). The role of mitochondria in angiogenesis. *Molecular Biology Reports*, *46*(1), 1393-1400. https://doi.org/10.1007/s11033-018-4488-x

Rizzuto, R., De, S. D., Raffaello, A., & Mammucari, C. (2012). Mitochondria as sensors and regulators of calcium signalling [nrm3412 pii ;10.1038/nrm3412 doi]. *Nature Reviews: Molecular Cell Biology*, *13*(9), 566-578. PM:22850819

Robinson, D. M., & Keating, G. M. (2006). Memantine. *Drugs*, *66*(11), 1515-1534. https://doi.org/10.2165/00003495-200666110-00015

Romero-Canelon, I., Pizarro, A. M., Habtemariam, A., & Sadler, P. J. (2012). Contrasting cellular uptake pathways for chlorido and iodido iminopyridine ruthenium arene anticancer complexes. *Metallomics*, *4*(12), 1271-1279.

Romero-Canelón, I., Salassa, L., & Sadler, P. J. (2013). The contrasting activity of iodido versus chlorido ruthenium and osmium arene azo-and imino-pyridine anticancer complexes: control of cell selectivity, cross-resistance, p53 dependence, and apoptosis pathway. *Journal of Medicinal Chemistry*, *56*(3), 1291-1300.

Rosi, S., Ramirez-Amaya, V., Vazdarjanova, A., Esparza, E. E., Larkin, P. B., Fike, J. R., Wenk, G. L., & Barnes, C. A. (2009). Accuracy of hippocampal network activity is disrupted by neuroinflammation: rescue by memantine. *Brain*, *132*(9), 2464-2477. https://doi.org/10.1093/brain/awp148

Rossi, D. J., Brady, J. D., & Mohr, C. (2007). Astrocyte metabolism and signaling during brain ischemia. *Nature Neuroscience*, *10*(11), 1377-1386.

Roy, S., Dey, K., Hershfinkel, M., Ohana, E., & Sekler, I. (2017). Identification of residues that control Li(+) versus Na(+) dependent Ca(2+) exchange at the transport site of the mitochondrial NCLX. *Biochim Biophys Acta Mol Cell Res*, *1864*(6), 997-1008. https://doi.org/10.1016/j.bbamcr.2017.01.011

Rozenfeld, M., Azoulay, I. S., Ben Kasus Nissim, T., Stavsky, A., Melamed, M., Stutzmann, G., Hershfinkel, M., Kofman, O., & Sekler, I. (2022). Essential role of the mitochondrial Na(+)/Ca(2+) exchanger NCLX in mediating PDE2-dependent neuronal survival and learning. *Cell Rep, 41*(10), 111772. https://doi.org/10.1016/j.celrep.2022.111772

Sancak, Y., Markhard, A. L., Kitami, T., Kovacs-Bogdan, E., Kamer, K. J., Udeshi, N. D., Carr, S. A., Chaudhuri, D., Clapham, D. E., Li, A. A., Calvo, S. E., Goldberger, O., & Mootha, V. K. (2013). EMRE is an essential component of the mitochondrial calcium uniporter complex. *Science, 342*(6164), 1379-1382. https://doi.org/10.1126/science.1242993

Sanjabi, S., Zenewicz, L. A., Kamanaka, M., & Flavell, R. A. (2009). Anti-inflammatory and pro-inflammatory roles of TGF-β, IL-10, and IL-22 in immunity and autoimmunity. *Current opinion in pharmacology, 9*(4), 447-453.

Schaeffer, S., & Iadecola, C. (2021). Revisiting the neurovascular unit. *Nature Neuroscience, 24*(9), 1198-1209. https://doi.org/10.1038/s41593-021-00904-7

Shamseldin, H. E., Alasmari, A., Salih, M. A., Samman, M. M., Mian, S. A., Alshidi, T., Ibrahim, N., Hashem, M., Faqeih, E., Al-Mohanna, F., & Alkuraya, F. S. (2017). A null mutation in MICU2 causes abnormal mitochondrial calcium homeostasis and a severe neurodevelopmental disorder [4222759 pii]. *Brain, 140*(11), 2806-2813. https://doi.org/10.1093/brain/awx237

Shen, Q., Goderie, S. K., Jin, L., Karanth, N., Sun, Y., Abramova, N., Vincent, P., Pumiglia, K., & Temple, S. (2004). Endothelial cells stimulate self-renewal and expand neurogenesis of neural stem cells. *Science, 304*(5675), 1338-1340. https://doi.org/10.1126/science.1095505

Shen, S. C., Chen, Y. C., Hsu, F. L., & Lee, W. R. (2003). Differential apoptosis-inducing effect of quercetin and its glycosides in human promyeloleukemic HL-60 cells by alternative activation of the caspase 3 cascade [10.1002/jcb.10559 doi]. *J Cell Biochem, 89*(5), 1044-1055. https://doi.org/10.1002/jcb.10559

Shi, K., Tian, D. C., Li, Z. G., Ducruet, A. F., Lawton, M. T., & Shi, F. D. (2019). Global brain inflammation in stroke. *Lancet Neurol, 18*(11), 1058-1066. https://doi.org/10.1016/s1474-4422(19)30078-x

Shin, S., Lee, Y., Chang, W. H., Sohn, M. K., Lee, J., Kim, D. Y., Shin, Y.-I., Oh, G.-J., Lee, Y.-S., Joo, M. C., Lee, S. Y., Song, M.-K., Han, J., Ahn, J., & Kim, Y.-H. (2022). Multifaceted Assessment of Functional Outcomes in Survivors of First-time Stroke. *JAMA Network Open, 5*(9), e2233094. https://doi.org/10.1001/jamanetworkopen.2022.33094

Singh, R., Bartok, A., Paillard, M., Tyburski, A., Elliott, M., & Hajnoczky, G. (2022). Uncontrolled mitochondrial calcium uptake underlies the pathogenesis of neurodegeneration in MICU1-deficient mice and patients. *Sci Adv*, *8*(11), eabj4716. https://doi.org/10.1126/sciadv.abj4716

Skrzypczak-Wiercioch, A., & Sałat, K. (2022). Lipopolysaccharide-induced model of neuroinflammation: Mechanisms of action, research application and future directions for its use. *Molecules*, *27*(17), 5481.

Smyth, L. C., Rustenhoven, J., Park, T. I.-H., Schweder, P., Jansson, D., Heppner, P. A., O'Carroll, S. J., Mee, E. W., Faull, R. L., & Curtis, M. (2018). Unique and shared inflammatory profiles of human brain endothelia and pericytes. *Journal of Neuroinflammation*, *15*(1), 1-18.

Soares, L. M., Meyer, E., Milani, H., Steinbusch, H. W., Prickaerts, J., & de Oliveira, R. M. (2017). The phosphodiesterase type 2 inhibitor BAY 60-7550 reverses functional impairments induced by brain ischemia by decreasing hippocampal neurodegeneration and enhancing hippocampal neuronal plasticity. *Eur J Neurosci*, *45*(4), 510-520. https://doi.org/10.1111/ejn.13461

Sofroniew, M. V., & Vinters, H. V. (2010). Astrocytes: biology and pathology. *Acta neuropathologica*, *119*, 7-35.

Song, L., Pei, L., Yao, S., Wu, Y., & Shang, Y. (2017). NLRP3 inflammasome in neurological diseases, from functions to therapies. *Frontiers in Cellular Neuroscience*, *11*, 63.

Stamatovic, S. M., Keep, R. F., & Andjelkovic, A. V. (2008). Brain endothelial cell-cell junctions: how to "open" the blood brain barrier. *Curr Neuropharmacol*, *6*(3), 179-192. https://doi.org/10.2174/157015908785777210

Stefani, D. D., Raffaello, A., Teardo, E., Szabo, I., & Rizzuto, R. (2011). A forty-kilodalton protein of the inner membrane is the mitochondrial calcium uniporter. *Nature*, *476*(7360), 336-340. https://doi.org/10.1038/nature10230

Strokin, M., Sergeeva, M., & Reiser, G. (2011). Proinflammatory treatment of astrocytes with lipopolysaccharide results in augmented Ca2+ signaling through increased expression of via phospholipase A2 (iPLA2). *American Journal of Physiology-Cell Physiology*, *300*(3), C542-C549.

Tapia, R. (1982). Antagonism of the ruthenium red-induced paralysis in mice by 4-aminopyridine, guanidine and lanthanum [0304-3940(82)90015-5 pii]. *Neurosci Lett*, *30*(1), 73-77. https://doi.org/10.1016/0304-3940(82)90015-5

Tapia, R., Meza-Ruiz, G., Duran, L., & Drucker-Colin, R. R. (1976). Convulsions or flaccid paralysis induced by ruthenium red depending on route of administration [0006-8993(76)90251-1 pii]. *Brain Res*, *116*(1), 101-109. https://doi.org/10.1016/0006-8993(76)90251-1

Tapia, R., & Velasco, I. (1997). Ruthenium red as a tool to study calcium channels, neuronal death and the function of neural pathways [S0197018696000563 pii]. *Neurochemistry International*, *30*(2), 137-147. PM:9017661

Territo, P. R., Mootha, V. K., French, S. A., & Balaban, R. S. (2000). Ca(2+) activation of heart mitochondrial oxidative phosphorylation: role of the F(0)/F(1)-ATPase. *Am J Physiol Cell Physiol*, *278*(2), C423-435. https://doi.org/10.1152/ajpcell.2000.278.2.C423

Tomar, D., Dong, Z., Shanmughapriya, S., Koch, D. A., Thomas, T., Hoffman, N. E., Timbalia, S. A., Goldman, S. J., Breves, S. L., Corbally, D. P., Nemani, N., Fairweather, J. P., Cutri, A. R., Zhang, X., Song, J., Jana, F., Huang, J., Barrero, C., Rabinowitz, J. E., Luongo, T.S., Schumacher, S.M., Rockman, M.E., Dietrich, A., Merali, S., Caplan, J., Stathopulos, P., Ahima, R.S., Cheung, J.Y., Houser, S.R., Koch, W.J., Patel, V., Gohil, V.M., Elrod, J.W., Rajan, S., Madesh, M. (2016). MCUR1 Is a Scaffold Factor for the MCU Complex Function and Promotes Mitochondrial Bioenergetics. *Cell Rep.*, *15*(8), 1673-1685. https://doi.org/10.1016/j.celrep.2016.04.050

Tsai, M. F., Phillips, C. B., Ranaghan, M., Tsai, C. W., Wu, Y., Willliams, C., & Miller, C. (2016). Dual functions of a small regulatory subunit in the mitochondrial calcium uniporter complex. *Elife*, *5*. https://doi.org/10.7554/eLife.15545

Tukhovskaya, E. A., Turovsky, E. A., Turovskaya, M. V., Levin, S. G., Murashev, A. N., Zinchenko, V. P., & Godukhin, O. V. (2014). Anti-inflammatory cytokine interleukin-10 increases resistance to brain ischemia through modulation of ischemia-induced intracellular Ca2+ response. *Neuroscience Letters*, *571*, 55-60.

Vakifahmetoglu-Norberg, H., Ouchida, A. T., & Norberg, E. (2017). The role of mitochondria in metabolism and cell death. *Biochemical and Biophysical Research Communications*, *482*(3), 426-431.

Vallabhapurapu, S., & Karin, M. (2009). Regulation and function of NF-kappaB transcription factors in the immune system. *Annu Rev Immunol*, *27*, 693-733. https://doi.org/10.1146/annurev.immunol.021908.132641

Velasco, I., Moran, J., & Tapia, R. (1995). Selective neurotoxicity of ruthenium red in primary cultures. *Neurochem Res, 20*(5), 599-604. https://doi.org/10.1007/BF01694542

Velasco, I., & Tapia, R. (1997). Ruthenium red neurotoxicity and interaction with gangliosides in primary cortical cultures [10.1002/(SICI)1097-4547(19970701)49:1<72::AID-JNR8>3.0.CO;2-A pii]. *J Neurosci Res, 49*(1), 72-79. https://www.ncbi.nlm.nih.gov/pubmed/9211991

Velasco, I., & Tapia, R. (2000). Alterations of intracellular calcium homeostasis and mitochondrial function are involved in ruthenium red neurotoxicity in primary cortical cultures [10.1002/(SICI)1097-4547(20000515)60:4<543::AID-JNR13>3.0.CO;2-Z pii]. *J Neurosci Res, 60*(4), 543-551. https://doi.org/10.1002/(SICI)1097-4547(20000515)60:4

Verma, S., Nakaoke, R., Dohgu, S., & Banks, W. A. (2006). Release of cytokines by brain endothelial cells: a polarized response to lipopolysaccharide. *Brain, Behavior, and Immunity, 20*(5), 449-455.

Villacampa, N., Almolda, B., Vilella, A., Campbell, I. L., González, B., & Castellano, B. (2015). Astrocyte-targeted production of IL-10 induces changes in microglial reactivity and reduces motor neuron death after facial nerve axotomy. *Glia, 63*(7), 1166-1184.

Walters, G. C., & Usachev, Y. M. (2023). Mitochondrial calcium cycling in neuronal function and neurodegeneration. *Front Cell Dev Biol, 11:1094356*. https://doi.org/ 10.3389/fcell.2023.1094356

Wang, L., Yang, X., Li, S., Wang, Z., Liu, Y., Feng, J., Zhu, Y., & Shen, Y. (2014). Structural and mechanistic insights into MICU1 regulation of mitochondrial calcium uptake. *The EMBO Journal, 33*(6), 594-604. https://doi.org/10.1002/embj.201386523

Wang, X., Carlsson, Y., Basso, E., Zhu, C., Rousset, C. I., Rasola, A., Johansson, B. R., Blomgren, K., Mallard, C., Bernardi, P., Forte, M. A., & Hagberg, H. (2009). Developmental shift of cyclophilin D contribution to hypoxic-ischemic brain injury [29/8/2588 pii]. *J Neurosci, 29*(8), 2588-2596. https://doi.org/10.1523/JNEUROSCI.5832-08.2009

Watanabe, A., Maeda, K., Nara, A., Hashida, M., Ozono, M., Nakao, A., Yamada, A., Shinohara, Y., & Yamamoto, T. (2022). Quantitative analysis of mitochondrial calcium uniporter (MCU) and essential MCU regulator (EMRE) in mitochondria from mouse tissues and HeLa cells. *FEBS Open Bio, 12*(4), 811-826. https://doi.org/10.1002/2211-5463.13371

Woods, J. J., Lovett, J., Lai, B., Harris, H. H., & Wilson, J. J. (2020). Redox Stability Controls the Cellular Uptake and Activity of Ruthenium-Based Inhibitors of the Mitochondrial Calcium Uniporter (MCU). *Angew Chem Int Ed Engl*, *59*(16), 6482-6491. https://doi.org/10.1002/anie.202000247

Woods, J. J., Nemani, N., Shanmughapriya, S., Kumar, A., Zhang, M., Nathan, S. R., Thomas, M., Carvalho, E., Ramachandran, K., Srikantan, S., Stathopulos, P. B., Wilson, J. J., & Madesh, M. (2019). A Selective and Cell-Permeable Mitochondrial Calcium Uniporter (MCU) Inhibitor Preserves Mitochondrial Bioenergetics after Hypoxia/Reoxygenation Injury. *ACS Cent Sci*, *5*(1), 153-166. https://doi.org/10.1021/acscentsci.8b00773

Woods, J. J., Rodriguez, M. X., Tsai, C.-W., Tsai, M.-F., & Wilson, J. J. (2021). Cobalt amine complexes and Ru265 interact with the DIME region of the mitochondrial calcium uniporter. *Chemical Communications*, *57*(50), 6161-6164.

Writing Group, M., Mozaffarian, D., Benjamin, E. J., Go, A. S., Arnett, D. K., Blaha, M. J., Cushman, M., Das, S. R., de Ferranti, S., Despres, J. P., Fullerton, H. J., Howard, V. J., Huffman, M. D., Isasi, C. R., Jimenez, M. C., Judd, S. E., Kissela, B. M., Lichtman, J. H., Lisabeth, L. D., Liu, S., Mackey, R.H., Magid, D.J., McGuire, D.K., Mohler, E.R., Moy, C.S., Munter, P., Mussolino, M.E., Nasir, K., Neymar, R.W., Nichol, G., Palaniappan, L., Pandey, D.K., Reeves, M.J., Rodriguez, C.J., Rosamond, W., Sorlie, P.D., Stein, J., Towfighi, A., Turan, T.N., Virani, S.S., Woo, D., Yeh, R.W., Turner, M.B., Stroke Statistics, S. (2016). Executive Summary: Heart Disease and Stroke Statistics--2016 Update: A Report From the American Heart Association. *Circulation*, *133*(4), 447-454. https://doi.org/10.1161/CIR.0000000000000366

Wu, J., Prole, D. L., Shen, Y., Lin, Z., Gnanasekaran, A., Liu, Y., Chen, L., Zhou, H., Chen, S. R., Usachev, Y. M., Taylor, C. W., & Campbell, R. E. (2014). Red fluorescent genetically encoded Ca2+ indicators for use in mitochondria and endoplasmic reticulum [BJ20140931 pii]. *Biochem J*, *464*(1), 13-22. https://doi.org/10.1042/BJ20140931

Xu, X., Zhang, S., Zhang, L., Yan, W., & Zheng, X. (2005). The Neuroprotection of puerarin against cerebral ischemia is associated with the prevention of apoptosis in rats [10.1055/s-2005-871261 doi]. *Planta Med.*, *71*(7), 585-591. PM:16041641

Yang, J.-L., Mukda, S., & Chen, S.-D. (2018). Diverse roles of mitochondria in ischemic stroke. *Redox biology*, *16*, 263-275.

Yoo, J., Wu, M., Yin, Y., Herzik, M. A., Jr., Lander, G. C., & Lee, S. Y. (2018). Cryo-EM structure of a mitochondrial calcium uniporter [science.aar4056 pii]. *Science*, *361*(6401), 506-511. https://doi.org/10.1126/science.aar4056

Zeiger, S. L., Stankowski, J. N., & McLaughlin, B. (2011). Assessing neuronal bioenergetic status. *Methods Mol Biol*, *758*, 215-235. https://doi.org/10.1007/978-1-61779-170-3_15

Zhang, H.-Y., Wang, Y., He, Y., Wang, T., Huang, X.-H., Zhao, C.-M., Zhang, L., Li, S.-W., Wang, C., & Qu, Y.-N. (2020). A1 astrocytes contribute to murine depression-like behavior and cognitive dysfunction, which can be alleviated by IL-10 or fluorocitrate treatment. *Journal of Neuroinflammation*, *17*(1), 1-13.

Zhao, R. Z., Jiang, S., Zhang, L., & Yu, Z. B. (2019). Mitochondrial electron transport chain, ROS generation and uncoupling. *International journal of molecular medicine*, *44*(1), 3-15.

Zhao, Y., Jiang, Y., Lv, W., Wang, Z., Lv, L., Wang, B., Liu, X., Liu, Y., Hu, Q., Sun, W., Xu, Q., Xin, H., & Gu, Z. (2016). Dual targeted nanocarrier for brain ischemic stroke treatment [S0168-3659(16)30252-8 pii]. *J Control Release*, *233*, 64-71. https://doi.org/10.1016/j.jconrel.2016.04.038

Zhong, J., Li, J., Ni, C., & Zuo, Z. (2020). Amantadine Alleviates Postoperative Cognitive Dysfunction Possibly by Preserving Neurotrophic Factor Expression and Dendritic Arborization in the Hippocampus of Old Rodents. *Front Aging Neurosci*, *12*, 605330. https://doi.org/10.3389/fnagi.2020.605330

Zhou, X., Chen, H., Wang, L., Lenahan, C., Lian, L., Ou, Y., & He, Y. (2021). Mitochondrial dynamics: a potential therapeutic target for ischemic stroke. *Frontiers in Aging Neuroscience*, *13*, 721428.

Zhu, C., Wang, X., Xu, F., Bahr, B. A., Shibata, M., Uchiyama, Y., Hagberg, H., & Blomgren, K. (2005). The influence of age on apoptotic and other mechanisms of cell death after cerebral hypoxia-ischemia [4401545 pii]. *Cell Death Differ*, *12*(2), 162-176. https://doi.org/10.1038/sj.cdd.4401545

Appendix

RP-9371 Requesting permission to use portions of article in final PhD thesis

Craig Myles (Jira) <permissions@sagepub.com>
Mon 3/27/2023 6:38 PM

To:Robyn Novorolsky <robyn.novorolsky@dal.ca>

CAUTION: The Sender of this email is not from within Dalhousie.

———·——·——

Reply above this line.

Craig Myles commented:

Dear Robyn Novorolsky,

Thank you for your ticket. As you are an author of "The cell-permeable mitochondrial calcium uniporter inhibitor Ru265 preserves cortical neuron respiration after lethal oxygen glucose deprivation and reduces hypoxic/ischemic brain injury," I am pleased to report we can grant your request to reuse your article, in whole or in part, without a fee as part of your thesis.

Please accept this email as permission for your request as you've detailed below. Permission is granted for the life of the thesis on a non-exclusive basis, in the English language, throughout the world in all formats provided full citation is made to the original SAGE publication. Permission does not include any third-party material found within the work. Please contact us for any further usage of the material.

If you have any questions, or if we may be of further assistance, please let us know.

Kind regards,

Craig Myles

Senior Rights Coordinator

SAGE Publishing

2455 Teller Road

Thousand Oaks, CA 91320

USA

www.sagepublishing.com

View request · Turn off this request's notifications

This is shared with Robyn Novorolsky.

SAGE, powered by Jira Service Management, sent you this message.

Details   27-Mar-23 17:59 BST (+0100)

SAGE Material
Journal

Author
Robyn J Novorolsky, Matthew Nichols, Jong S Kim, Evgeny V Pavlov, Joshua J Woods,
Justin J Wilson, George S Robertson

Page numbers
1172-1181

Title of Journal
Journal of Cerebral Blood Flow and Metabolism

Title of Article
The cell-permeable mitochondrial calcium uniporter inhibitor Ru265 preserves cortical
neuron respiration after lethal oxygen glucose deprivation and reduces
hypoxic/ischemic brain injury

Volume/Issue
40 (6)

Year
2020

Portion
Full Article

Use type
Non-commercial

Organizational Institution
Dalhousie University

I am the author of the SAGE content being requested
Yes

Formats
Both Print and Electronic

Languages
English only

Please indicate the anticipated duration of your reuse.
Life of the Work

Product Rights required
Main Product

Reusing Royal Society of Chemistry material

Reuse permissions requests

Material published by the Royal Society of Chemistry (RSC) and other publishers is subject to all applicable copyright, database protection and other rights. The graphic below outlines the steps to obtain permission to reuse RSC materials, where required:

I am the author of the material I wish to reuse

I wish to reproduce my own material (figures, images, schemes, graphical abstract, blurbs)
- in a **thesis** or **dissertation**
- in **RSC** or **non-RSC books or journals**
- **in any other type of publication** (website, marketing, presentations)

→ **No permissions request needed**

I wish to reproduce my own book chapter or article in full
- in a **thesis** or **dissertation**
- in a **non-RSC book or journal**
  - my material is **Open Access**
    - under a **CC-BY licence**
    - under a **CC-BY-NC licence**
  - my material is **NOT Open Access**
- **in any other type of publication** (website, marketing, presentation)
  - my material is **NOT Open Access**
    - **20% of the material** has been **rewritten**
    - my material is **unaltered**
  - my material is **Open Access**

→ Fill in the **RSC permissions form**.

→ Submit request via the **Copyright Clearance Center.** See details here.

→ **Not allowed** unless 20% of the content is different to the original.

The correct **acknowledgement** must be included. More details can be found here.

195